Universidade de Aveiro Departamento de Engenharia Mecânica
2008

Victor Fernando Santos Neto

Revestimentos de base carbónica na indústria de plásticos

"Carbon-based coatings for the modern plastics industry"

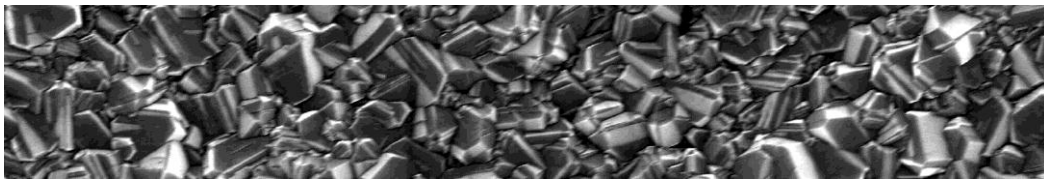

Universidade de Aveiro Departamento de Engenharia Mecânica
2008

Victor Fernando Santos Neto

Revestimentos de base carbónica na indústria de plásticos

"Carbon-based coatings for the modern plastics industry"

Tese apresentada à Universidade de Aveiro para cumprimento dos requisitos necessários à obtenção do grau de Doutor em Engenharia Mecânica, realizada sob a orientação científica da Doutora Mónica Sandra Abrantes de Oliveira Correia, Professora Auxiliar do Departamento de Engenharia Mecânica da Universidade de Aveiro e do Doutor Nasar Ali, Director da Divisão de Investigação e Desenvolvimento da CNC Coating (UK)

"Deixe o mundo um pouco melhor do que encontrou."
in: Última Mensagem de Baden-Powell (1945)
Fundador do movimento Escutista

“Leave this world a little better than you found it.”
in: Baden-Powell's Last Message (1945)
Founder of the Scouting movement

À minha família

o júri

presidente

Prof. Doutor Carlos Fernandes da Silva
professor catedrático do Departamento de Ciências de Educação da Universidade de Aveiro

Prof. Doutor António Sérgio Pouzada
professor catedrático da Escola de Engenharia da Universidade do Minho

Prof. Doutor Waqar Ahmed
professor of the Department of Technology of the University of Central Lancashire (UK)

Prof. Doutor José Joaquim de Almeida Grácio
professor catedrático do Departamento de Engenharia Mecânica da Universidade de Aveiro

Prof.ª Doutora Mónica Sandra Abrantes de Oliveira Correia
professora auxiliar do Departamento de Engenharia Mecânica da Universidade de Aveiro

Doutor Nasar Ali
director da Divisão de Investigação e Desenvolvimento da CNC Coating (UK)

agradecimentos

O autor agradece de forma reconhecida:

- Aos seus orientadores, a Prof.ª Doutora Mónica Oliveira e o Doutor Nasar Ali;
- À Universidade de Aveiro pelo financiamento da sua bolsa de doutoramento;
- À Fundação para a Ciência e Tecnologia pelo financiamento do projecto POCTI/EME/60816/2004;
- Ao Professor Doutor José Grácio, responsável cientifico pelo projecto acima referido e que permitiu a utilização de recursos fundamentais para o desenrolar deste doutoramento;
- Ao Eng. Gil Costa e à F. Ramada (Ovar, Portugal) pelo fornecimento dos aços utilizados neste trabalho;
- Ao Eng. António Festas, do Departamento de Engenharia Mecânica da Universidade de Aveiro, pela maquinação das amostras metálicas;
- Aos Eng. Luís Godinho, Eng. Rui Pimenta e Eng. Henrique Dias, da Prirev (Vagos, Portugal), pela produção dos "*interlayers*" de nitreto de crómio;
- À Professora Doutora Fátima Cerqueira, da Universidade do Minho, pela produção dos "*interlayers*" de silício;
- À Dr. Elisa Ubeda e à Galol, S.A. (Valência, Espanha) pela produção dos "*interlayers*" de titânio;
- À Eng.ª Marta Ferro, do Departamento de Cerâmica e Vidro da Universidade de Aveiro, pelo apoio na Microscopia Electrónica;
- Ao Doutor Jorge Soares, do Departamento de Física da Universidade de Aveiro, pela ajuda na aquisição dos espectros de Raman a 514 nm;
- À Eng.ª Maria Celeste Azevedo, do Departamento de Química da Universidade de Aveiro, pela ajuda na aquisição dos espectros de Raman a 1064 nm;
- À Doutora Rosário Soares, do Laboratório Central de Analises da Universidade de Aveiro, pela ajuda na aquisição dos espectros de DRX;
- Ao Professor Doutor Orlando Teodoro e ao Doutor C. Ghumman, da Universidade Nova de Lisboa, pela ajuda na aquisição dos espectros de SIMS;
- Ao Sr. Victor Marques e à MoldAveiro (Aveiro, Portugal), pela adaptação da placa moldante para receber os insertos revestidos;
- À Eng.ª Tatiana Zhil'tsova e ao Eng. João Teles, do Departamento de Engenharia Mecânica da Universidade de Aveiro, pelo apoio na operação da máquina de injecção de termoplástico;
- Ao Sr. Ricardo Beja, do Departamento de Engenharia Mecânica da Universidade de Aveiro, pela ajuda na operação da máquina de medição por coordenadas;
- À Mestre Raquel Vaz pela colaboração e ajuda nos revestimento de diamante e respectiva caracterização.

palavras-chave

Moldes de injecção de plástico, micromoldação, engenharia de superfícies, revestimentos, diamante, deposição química a partir da fase de vapor.

resumo

Em Portugal, uma das indústrias com maior expressão e competitividade é, sem dúvida, a indústria de moldes. A aposta em produtos de maior valor acrescentado e em nichos de mercado tem sido fomentada e extremamente valorizada.

É neste contexto que surge a micromoldação. Uma tecnologia de produção, também cíclica, com todas as vantagens da moldação por injecção, que abre novos mercados, mas que requer conhecimento tecnológico especifico nas diferentes vertentes: equipamento, processo, ferramentas. Neste contexto, para as ferramentas de moldação urge solucionar problemas tecnológicos que se prendem com questões processuais intrínsecas à micromoldação, nomeadamente dificuldades de escoamento em micro-canais, desmoldação, etc. No que concerne a interface fluído/ferramenta moldante, deve referir-se que esta deve promover um mínimo de adesão, por forma a não comprometer a frente de enchimento e a operação de desmoldação. As ferramentas de moldação devem portanto ser de materiais com alta dureza, baixo coeficiente de atrito e uma condutividade térmica elevada. Uma forma de obter tais características é utilizar revestimentos duros, tais como revestimentos de diamante, que possuem um conjunto de propriedades físicas excepcionais, podendo minimizar substancialmente a necessidade de manutenção no molde. Tais propriedades são ainda de importância crucial de forma a garantir a qualidade final das peças.

O presente trabalho visa apresentar uma solução para alguns dos problemas acima apontados, bem como estabelecer a metodologia de operação e os limites de validade e ou viabilidade da aplicação de filmes finos de diamante em ferramentas micro-estruturadas para a industria de moldes.

keywords

Plastic injection molds, micromolding, surface engineering, coatings, diamond, chemical vapor deposition.

abstract

Molds industry in Portugal is one of the most dynamic sectors in the national economy. For that reason, its competitiveness is of utmost importance and requires further insight into the development of high value products and new markets. The latter has been pointed out, quite often, as a gateway to improve the sectors performance.

Micromolding is, within this context, seen as an area of great potential. Nevertheless, when such a dimensional reduction is considered, the tools are also subjected to problems due to melt flow characteristics on micro-channels. In what concerns the melt flow/molding tool interface it's worth referring the requirements for minimum adhesion to avoid compromising the flow front advancement or demolding operations. Molding tools have therefore strict requisites in what concerns high hardness, low friction coefficients and high thermal conductivity materials. In order to attain the above, the use of hard coatings, such as diamond, which display outstanding physical properties, may minimize substantially the need for mold intervention. The latter is required to reestablish the surface finish to guarantee part quality.

The present work has as its fundamental objective to evaluate the viability and the added value of the diamond coatings on molding tools for thermoplastic micromolding.

Table of contents

List of figures

List of tables

List of symbols

Abbreviations

3D	Three-dimensional
AISI	American Iron and Steel Institute
CVD	Chemical Vapor Deposition
DIN	Deutsches Institut für Normung e.V. (German Institute for Standardization)
EDS	Energy Dispersive X-ray Spectroscopy
F	Helmholtz free energy
HB	Brinell hardness number
HFCVD	Hot-filament Chemical Vapor Deposition
HR	Rockwell hardness number
HV	Vickers hardness number
I	Raman intensity
N	Number of particles
n	Number of atoms or molecules
OM	Optical Microscopy
P_c	crystal pressure
P_v	Vapor pressure
Q	Quality factor
S	Crystal surface
SEM	Scanning Electron Microscopy
SIMS	Secondary Ion Mass Spectrometry
T	Temperature
TMCVD	Time-modulated Chemical Vapor Deposition
V	Volume
XRD	X-ray Diffraction Spectroscopy
Y	Young's modulus

Chemical Compounds

Ar	Argon
CH_3	Methyl
CH_4	Methane
Cr	Chromium
CrN	Chromium Nitride
Fe	Iron
H	Atomic hydrogen
H_2	Hydrogen
Ni	Nickel
Si	Silicon
Ta	Tantalum
TaC	Tantalum Carbide
Ti	Titanium

Greek letters

ω	Frequency
φ	Raman peak/band center
σ	Stress
ν	Poisson's ratio
α	Coefficients of thermal expansion
α_P	Molecule polarizability
σ_t	Surface tension
μ	Chemical potential
λ	Wavelength

Unit conversions

Energy	1 eV = 1.6022 x 10^{-19}J 1 cm^{-1} ≈ 8 meV
Flow	1 sccm = 1 ml/min (milliliter/minute)
Force	1 kgf = 9.807 N (Newton)
Length	1 Å = 0.1 nm (nanometer) = 1×10^{-10} m (meter)
Pressure	1 Torr = 133.3224 Pa (Pascal) 1 Torr = 1.333224 mbar (milibar) 1 kgf/mm^2 = 9.807x10^6 Pa
Temperature	0° C (degrees Celsius) = 273.15 K (Kelvin)

Chapter 1

Introduction

1 Thermoplastic injection molding and tools

Injection molding is a manufacturing technique to produce parts, as the ones showed in figure 1, from thermoplastic and thermosetting polymers. It consists of a cyclic process in which a melted (plasticized) polymer is injected into a mold cavity or cavities (impression), where it is held under pressure until it is removed in a solid state, thus duplicating the impression of the mold. [1]

Typically, polymers or plastics (as they are commonly named) are defined as materials which can be molded or shaped into different forms under the influence of pressure and heat. Chemically, polymers are substances composed of long chains of repeating molecules, called monomers, made up predominantly of carbon and hydrogen atoms, which under the desirable conditions, connect together to form chain structures. In addition to carbon and hydrogen, oxygen, nitrogen, chlorine, and other elements may be found in some polymers. [2]

The main difference between thermoplastics and thermosetting polymers is that the first ones may become soft, remoldable and weldable when heated. Thermosetting polymers however cannot be welded or remolded when heated.

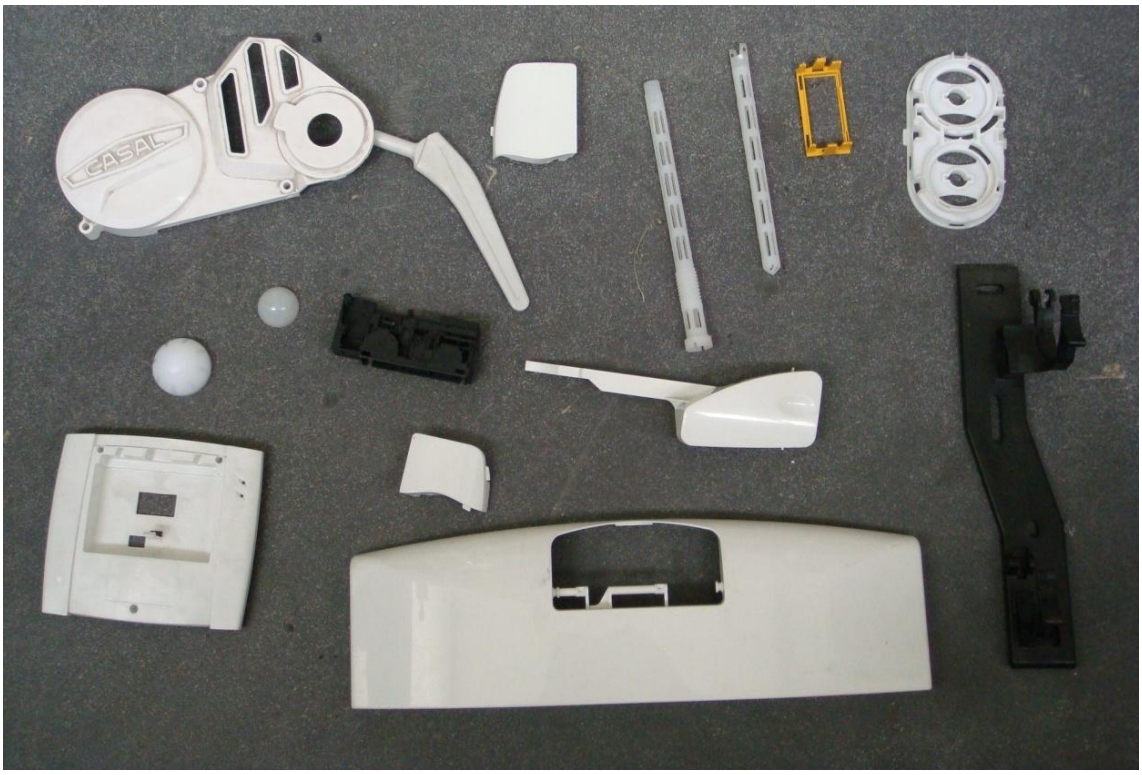

Figure 1 - Plastic molded objects

Three basic operations take place in the thermoplastic injection molding process: (i) heating the thermoplastic in the injection or plasticizing unit, so that it will flow under pressure; (ii) allowing the thermoplastic melt to solidify in the mold cavity or cavities; and (iii) opening of the mold to extract the molded product. These three steps are the operations in which the mechanical and thermal inputs of the injection equipment must be coordinated with the fundamental properties and behavior of the thermoplastic being processed. Figure 2 presents a picture of an Inauton D65 injection molding machine and figure 3 some mold tools for thermoplastic molding.

Different thermoplastics may display different characteristics, performances and will carry a different cost. The characteristics and performance are influenced by factors such as molecular size and weight, molecular distribution, and shapes or structures of individual molecules. Properties and behavior are also influenced by compounding of different amounts and combinations of additives (colorants, flame retardants, heat and light stabilizers, etc.), fillers (calcium carbonate, etc.), and reinforcements (glass fibers, glass flakes, graphite fibers, whiskers, etc.) that are used with plastics. Compounding also embraces the mixing (alloying, blending, etc.) of two or more plastics that may be miscible or immiscible, with or without additives.

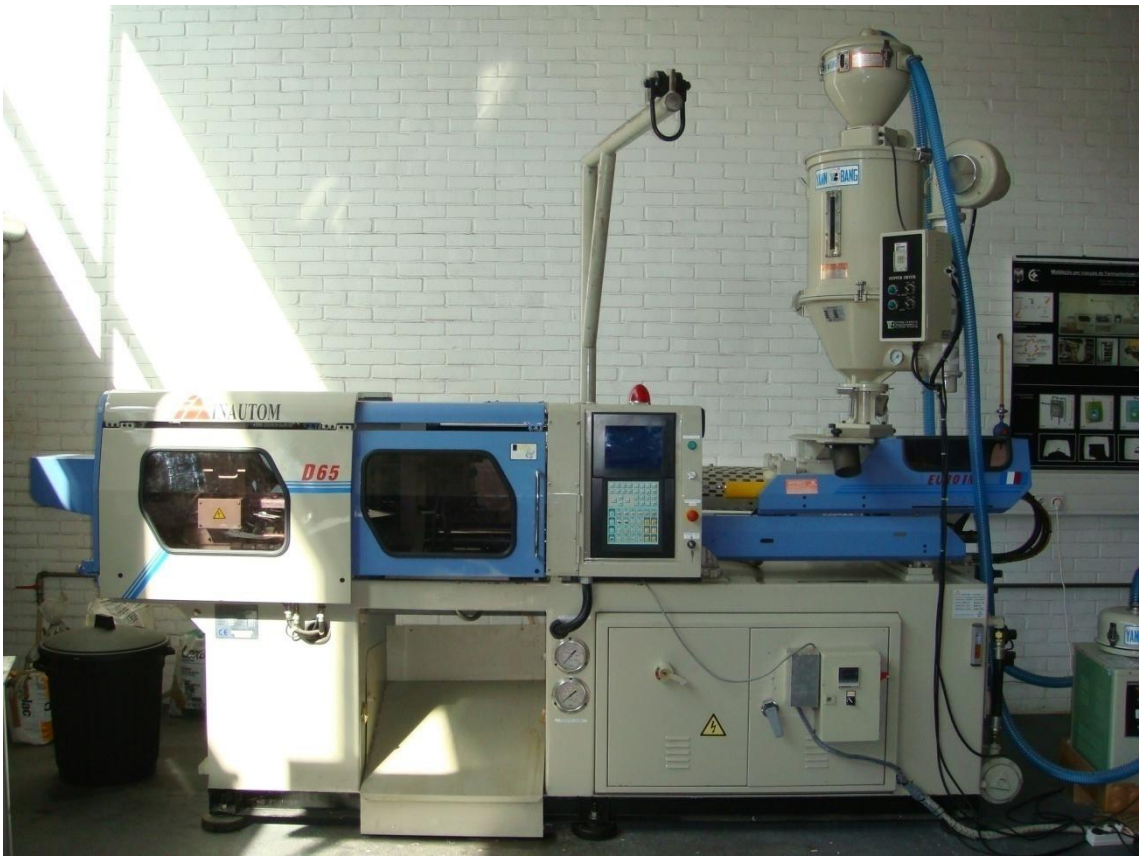

Figure 2 - Inauton D65 injection molding machine

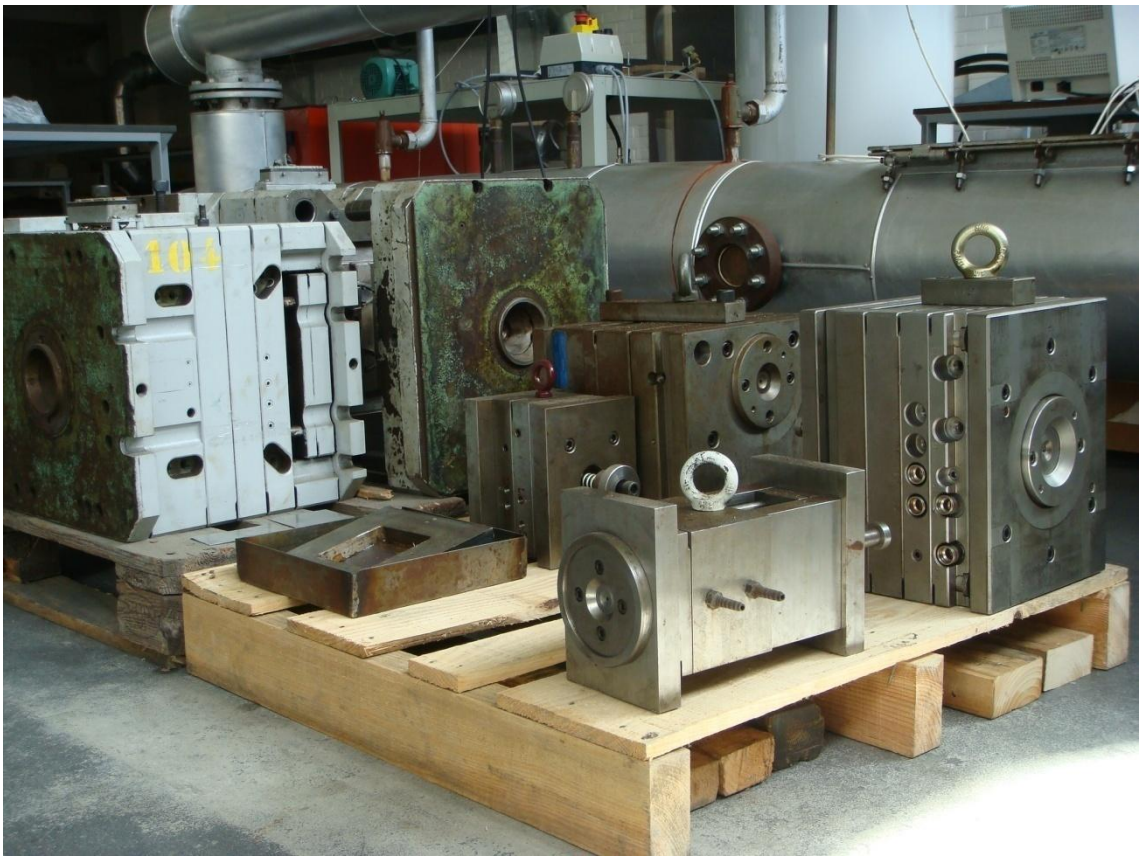

Figure 3 - Molds for thermoplastic molding

Molding tools or molds are the production tools used to produce polymer parts in injection molding. The mold is probably the most important part of the injection molding process. It is a controllable, complex and expensive device. If it is not properly designed, operated, handled, and maintained its operation will be costly and highly inefficient.

Under pressure, hot melt moves rapidly through the mold. During the injection into the mold, air in the cavity or cavities is released to prevent melt burning and the formation of voids in the product. Temperature-controlled cooling media (i.e. water, oil, etc.) circulates in the mold to remove heat.

The mold basically consists of a sprue, a runner, a cavity gate, and a cavity (impression). The sprue is the channel located in the stationary platen that transports the melt from the plasticator nozzle to the runner. In turn, melt flows through the runner and gate and into the cavity. With a single-cavity mold, usually no runner is used, so melt goes from the sprue to the gate. Different runner systems are in use to meet different processing requirements. The most popular are cold and hot runners. With a cold runner, the melt flowing from the sprue to the gate solidifies by the cooling action of the mold as the melt in the cavity or cavities solidifies. With a hot runner the sprue to the gate is insulated from the chilled cavity or cavities and remains hot, so that the melt never cools; the next shot starts from the gate, rather than from the nozzle as in a cold runner.

Molds are provided with different means, such as sliders, unscrewing devices, undercuts and extraction systems to eject products as well as solidified runners at the proper time. These basic operations require control of various parameters such as fill time and hold pressure.

Molds are typically constructed from hardened steel, pre-hardened steel, aluminium, and/or beryllium-copper alloy.

2 The worldwide molds industry – an overview

Plastics can be divided into natural, semi-natural and synthetic plastics. Natural plastics include amber, horn, tortoiseshell and bitumen, and were used in the most ancient civilizations. The ancient Egyptians molded amber into items such as jewelry. [2]

John Wesley Hyatt, an American inventor, was the first to inject hot celluloid (a semi-natural polymer) into a mold, using an injection molding machine, producing billiard balls, in 1868. He and his brother Isaiah, patented an injection molding machine that used a plunger in 1872. The first screw injection molding machine was built on 1946 by James Hendry, revolutionizing the

plastics industry. Roughly 95% of all molding machines now use screws to efficiently heat, mix, and inject plastic into molds. [3]

The use of polymers to produce manufactured goods boosted since the boom appearance of synthetic polymers and with the end of the Second World War. The British plastic industry passed from selling 50 000 tons in 1939, to 160 000 in 1950, and to 550 000 tons in 1960, and have continued to grow since. [2]

Portugal is an international leader in the molds industry. It is the eighth-largest producer of dies and molds in the world and it exports to more than 70 countries. Portugal is also one of the world's principal producers of precision molds for the plastics industry. Many multinational corporations recognize the industry's excellence and increasingly choose Portuguese suppliers for their molding requirements due to their experience, skills, delivery times and pioneering use of advanced technologies. The industry has more than 500 companies active in Portugal, working in different specialized areas with specific molds techniques, from simple services to highly complex molds production. [4-6]

In the late 18th century an Englishman named William Stephens opened a glass-making plant in the town of Marinha Grande, the Fábrica Escola Irmãos Stephens, employing artisans from Genoa and Lisbon. The skill of the town's glassworkers came to rival the best in the world and the town still remains today the "glass capital" of Portugal. [7]

At the beginning of the 20th century, Marinha Grande began producing molds for glassware, having previously imported them from Germany and Austria. This was the foundation for the growth of the plastics molds industry. Aníbal H. Abrantes, a partner and lathe-worker in the first pressed glass molds plant in Marinha Grande, established the first molds plant for Bakelite products in 1944. Two years later Abrantes produced Portugal's first plastic injection mold. Other plastics mold companies began to open in Marinha Grande and in the northern town of Oliveira de Azeméis, another traditional glassmaking centre. The industry developed with the importation of foreign technology. Exports began in 1955 with the sale of the first Portuguese mold to Britain. By 1980, in the Marinha Grande area alone 64 companies employing 2000 people were operational. [7]

Today, the molds sector in Portugal employees about 7500 people, in more than 500 companies, most of them in the Marinha Grande area. Most of these companies are small to medium-sized, employing an average of 30 workers. [4, 6, 7]

The dynamism and commercial drive of Portuguese molding industry are recognized internationally for its competitiveness in quality, delivery times, technological capacity and

price. This worldwide reputation has enabled Portuguese mold makers to establish a presence in more than 70 countries. [7]

The industry exports about 90% of its production. These exports earned around € 369 million in 2006. In this year, and maintaining the trend of the last 3 years, the main exports destinations were France, Spain, Germany, United Kingdom and the United States of America, as it can be seen in figure 4. Automobile industry sector by itself accounted for approximately 78% of the molds produced. Other relevant sectors are electrical domestic appliances, packing, and domestic tools, as presented in figure 5. [4]

Nevertheless, the Portuguese mold making industry, as the European, is coming under increasing economic pressure from the Pacific Rim countries, which can supply tooling more cheaply. To slow down or reverse the decline in the Small and Medium based EU tooling industry, processes that offer mold makers a competitive advantage over non-EU imports are required.

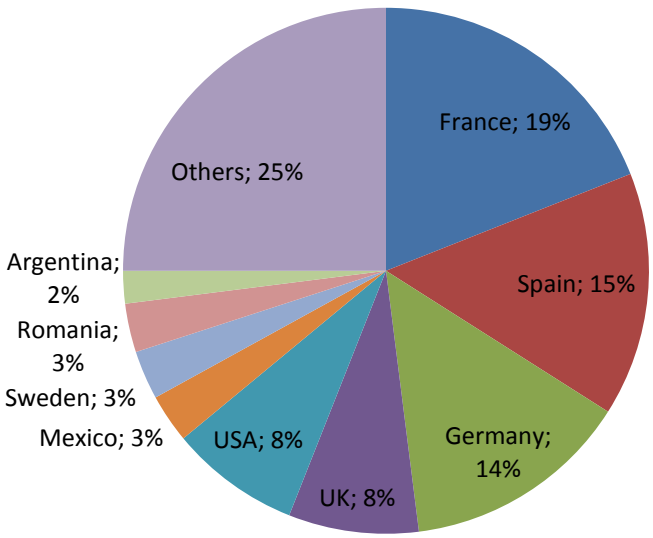

Figure 4 - Main export destinations of Portuguese molds in 2006 [4]

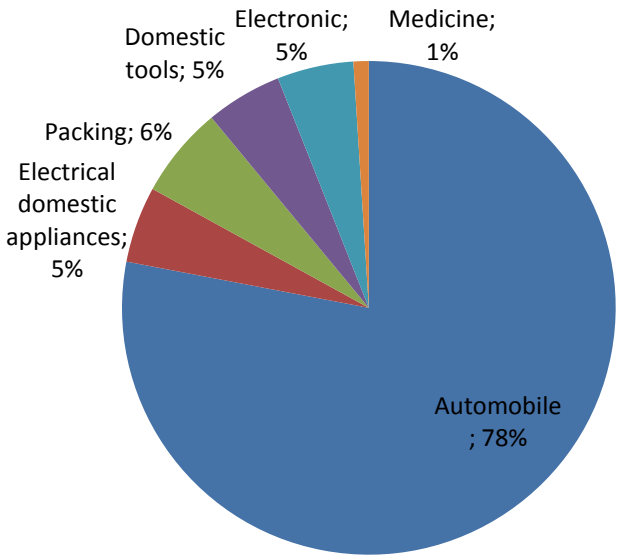

Figure 5 - Main industries supplied in 2006 [4]

An American report on Competitive Conditions in the United States and Selected Foreign Markets of Tools, Dies, and Industrial Molds by the United States International Trade Commission (United States International Trade Commission, 2002) pointed out that the Portuguese mold making unique industry characteristic to be composed of small industry dedicated almost exclusively to exporting. The same report also highlighted the strengths to be: specialist training colleges; quick lead times (time required to produce a die or mold), technological capability, price, and low labor costs; quality, technology, service, skilled in producing high precision and complex dies and molds. And the weaknesses: small domestic market with lowest productivity indicators (sales per worker) among International Special Tooling and Machining Association members; lacks modern automotive and aerospace industries to stimulate technological advancement; and many die and mold producers tend to be small companies with limited financial and management resources.

New value strategies are being proposed and carried out [8, 9]. The integration of the mold tool in a high-tech engineering chain, that is not limited to the mold tool production, but assists from its conception to the end of its service, enlarges the intervention period of the molding system provider, reducing the importance of the mold production cost. A different or complementary business strategy is the specialization in high complexity mold with top pioneering and engineering solutions.

In both strategies, the technology knowledge must be enlarged and network partnerships between complementary enterprises, R&D institutions and prime clients must be considered.

Increased tool functionality and productivity during component processing, decreased tool cost, wider range of tool application, reduced environmental, health and safety impact during both tool and component manufacture, and extended tool longevity and reduced maintenance times are key parameters for future strategies. [8, 9]

3 Industry challenge

As pointed in the previous section, the implementation of new value strategies implies challenges for the mold making industry, namely the improvement of technology comprehension. One of the main goals of the present doctoral thesis is to modestly contribute to the latter.

Microsystems-based products will be an important contributor to the industrial and economic future, as a key value adding element for many sectors of industry — and the predicted nanotechnology future will also be largely delivered by microtechnologies. The 21st century will most surely adopt micro and nano manufacturing technologies making use of a variety of materials, components and knowledge based technologies that provide functionality and intelligence to highly miniaturised systems. [10]

Machining has been the only feasible manufacturing alternative for manufacturers sourcing low to moderate quantities of micro components. The process of micro molding has been in existence for over 20 years, but because of the modest volumes or the complexity of the components it has often been avoided. However, in the last five years, with the advances in materials, processing and measurement techniques, micro molding can offer a range of cost-effective alternatives for components that are miniatures, complex and require high precision tolerances. [11, 12]

Machining places limitations on the material selection process where high-cost ceramics or engineered metallic materials are commonly used. As a result, sourcing low to moderate volume micro components has been a costly challenge for manufacturers. Advances in material science and plastic injection molding equipment permit complex machined micro components to be injection molded in metal, plastic, or plastic with metal or ceramic filler. Molded micro-switch plungers are shown in figure 6. There are a number of cost and design advantages that can be obtained by converting to injection molding. Engineers looking to decrease the overall size of their product, to incorporate complex features, to reduce the

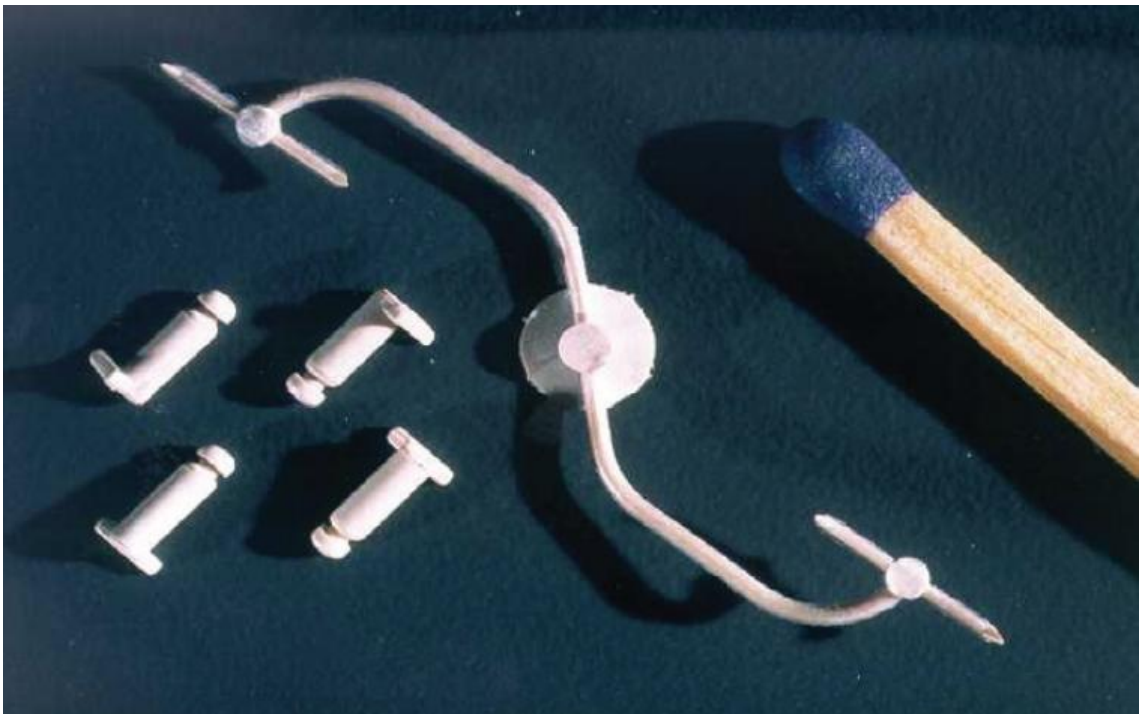

Figure 6 - Mini Micro-switch Plunger [11]

number of components, or to reduce costs should consider micro molding as an alternative to machining. [12]

Plastic microinjection molding tools can clearly be seen as an added value strategy specialization, with a high complexity and top pioneering and engineering solutions requirements.

There are a number of benefits that can be achieved by converting to micro molding. One advantage is that the amount of time it takes to mold a component is a fraction of what it takes to machine a component. Another is particle contamination. Designers do not want to have the possibility of foreign matter being introduced into their fluid-carrying medical devices, for example. Micro molding eliminates the potential failure mode of having particulates left after machining and enables better surface finishing. Micro molding also gives more freedom to designers to place intricate features in products thereby enhancing their ability to create more innovative products. As the trend for smaller components becomes greater, it might become more difficult to machine complex geometries making micro molding the only option. In addition, micro molding also offers a dimensionally stable production process and improvement of mechanical and/or electrical properties using alternative resins or fillers. [12]

Although the advances acquired in the past couple of years in the microinjection molding technology process, there are still some problems on the downstream that must be overcome. Micro moldings may become statically charged and tend to adhere to surfaces around the molding area, making free fall extraction difficult or even impossible.

In the conventional thermoplastic injection molding, the wear of molding tools is known to be one of the main sources of breakdown failures, resulting in production losses [13]. In microinjection of thermoplastic parts, molds for components that are miniature, complex and require high precision tolerances are not wear free, on the contrary, the cavity wear can be even much more critical than in conventional molding [11, 12].

Issues such as aspect ratio have to be considered carefully, as fine details that can approach micron levels of dimension must be capable of withstanding cavity pressures created during the injection phase. The wear out of the molding tools creates demolding problems, compromising the polymeric parts finishing quality, speeding up the corrosion of the tools, and result in maintenance stops. Most of the mold tools have complex geometries and complex moving parts which favor the corrosion and wear mechanisms. Polymer abrasion, adhesion and corrosion are the catalyzers of these mechanisms. Furthermore, the increasing usage of polymers reinforced with glass fibers, minerals, or even carbon nanotubes, enhance the abrasive power of polymers. [14]

In terms of mold design, new materials are being developed with high coefficients of thermal conductivity, and coatings can be applied to assist part removal without damage.

Hard chrome and nickel plating are currently the most commonly employed method of treating the surface of conventional mold tools to improve durability. Although plating is an effective technique it does suffer from a number of attendant problems. Most significantly, all commercial chromium plating baths utilize Cr^{VI}, which is highly toxic and is hazardous to the environment and the user, requiring careful monitoring and legislated control. Nickel plating, although not as hazardous as Cr plating, still releases significant emissions into the environment. From a technical standpoint electrodeposited Cr coatings are inherently micro-cracked, resulting in poor corrosion resistance and spalling. Two further hard coating techniques of note are Physical Vapor Deposition and the Thermal Diffusion process and its variants. Both are used to deposit nitrides onto tools (particular TiN, CrN and NbN) but again these processes are severely limited by the size of the application cell. [14]

Chemical Vapor Deposition of polycrystalline diamond, in microcrystalline or nanocrystalline morphology, detains a number of extreme properties that point it as a technology suitable for

exploitation in numerous industrial applications. It possesses an extreme mechanical hardness and wear resistance, one of the highest bulk modulus, the lowest compressibility, the highest room temperature thermal conductivity, a very low thermal expansion coefficient at room temperature and is very resistant to chemical corrosion (see table 3). Most of these properties are attractive for cavities and molding tools.

The application and evaluation of CVD diamond thin films as a surface engineering to improve operation and durability of mold tools will be the prime objective of this doctoral thesis.

Chapter 2

Diamond CVD coatings

1. Introduction

Diamond is considered an ideal material for many applications due to its extreme properties. It is a metastable carbon polymorph at room temperature and atmospheric pressure. Its crystal structure belongs to the space group[1] O_h^7 (F4, /d 32/m) with two atoms per primitive Bravais cell. Its structure can be viewed as two interpenetrating face centered cubic lattices shifted along the body diagonal by $\left(\frac{1}{4},\frac{1}{4},\frac{1}{4}\right)a$ [2], where a is the dimension of the cubic (mineralogical) unit cell, as shown in figure 7. Each carbon atom has a tetrahedral configuration consisting of sp^3 hybrid atomic orbitals[3]. The $\{111\}$ [4] crystallographic plane comprises 6-atom hexagonal rings arranged so that the adjacent atoms are alternately dislocated upward and downward from the plane. The stacking sequence in the $\langle 111\rangle$ [5] direction is ABCABCABC. The lattice constant is 3.56 Å and the bond length is 1.54 Å. Natural diamond consists of 98.9% ^{12}C and 1.1% ^{13}C. The characteristic Raman spectroscopic signals for diamond are 1332 cm^{-1} for ^{12}C and

[1] The space group of a crystal or crystallographic group is a mathematical description of the symmetry inherent in the structure.

[2] The notation (lmn) denote planes orthogonal to a direction (l,m,n) in the basis of the reciprocal lattice vectors. l, m and n are the Miller indices that are a notation system in crystallography for planes and directions in crystal (Bravais) lattices.

[3] Hybridization, in chemistry, is the concept of mixing atomic orbitals to form new hybrid orbitals suitable for the qualitative description of atomic bonding properties. The hybridization theory was promoted by chemist Linus Pauling in order to explain the shape of molecular orbitals for molecules.

[4] The notation $\{lmn\}$ denotes all planes that are equivalent to (lmn) by the symmetry of the crystal.

[5] The notation $\langle lmn\rangle$ denotes all directions that are equivalent to $[lmn]$ by symmetry. $[lmn]$ denotes a direction in the basis of the direct lattice vectors instead of the reciprocal lattice.

1284 cm^{-1} for ^{13}C. A typical unit cell for the diamond cubic crystal structure can be seen in figure 7. [15, 16]

Carbon has two isomers. The first isomer is lonsdaleite found in meteorites. The positioning of atoms in each plane of the structure of lonsdaleite is the same as that in the cubic structure. However, the planes are linked in a manner which results in a stacking sequence of ABABAB. Consequently, the atoms experience closer chemical bonding, with lattice constants in the *a* and *c* directions of 2.52 and 4.12 Å, respectively. The distance between adjacent atoms is 1.52 Å. The corresponding Raman peak is in the range of 1315–1325 cm^{-1}. Another isomer is graphite, the most common form of carbon. Each carbon atom has a sp^2 atomic configuration and therefore, three in-plane sigma bonds. The remaining valence electron forms π bonds using a p_z atomic orbital. Thus, the trigonally bonded 6-carbon rings are situated in a flat plane instead of being in alternate order plaited as in diamond. The planes are layered in an ABABAB sequence. The lattice constant in the basal plane between repeating layers is 6.707 Å, and the in-plane, nearest neighbor spacing is 1.42 Å. The signature Raman peak of the in-plane layers is 1580 cm^{-1}. [15]

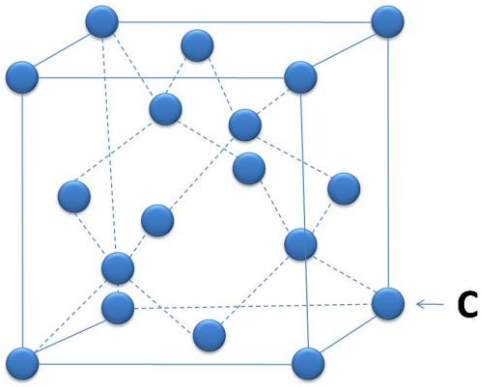

Figure 7 - Unit cell for the diamond cubic crystal structure

2. History and developments

The modern use of impregnated tools, which consume the vast majority of the industrial diamond used today, is probably a century old, and most of the growth witnessed by the industry has taken place in the last fifty years. However, diamond has been recognized as being a unique material for several centuries. Originally recognized for its spectacular cosmetic properties and found in southern India, its early use as an industrial tool was confined to that of engraving. Asian references to the cutting of the very hard jade stone can be traced back to

300 BC and possibly further. In the 18th century French philosopher Diderot described the use of a hand-held diamond tool for drilling stone. By the mid 1800s this had developed considerably, and diamond rock drills were powered by machines.

The very early developments in diamond tools took place relatively slowly, as presented in table 1. When only natural diamond was available, the development of new applications using diamond was largely self-defeating, since the more material they consumed, the less feasible they were in terms of world supply due to shortage of raw material.

The scenario changed noticeably in the 1950s when innovation changed to invention and synthetic diamond became a commercial reality. Large presses simulate the conditions of high pressures and temperatures that created natural diamond deep within the crust of the earth and through the application.

The first CVD diamond growth under low pressures was reported by Spitsyn and Deryagin from the Physics and Chemistry Institute of Moscow, in 1956 and by Eversole from the Union Carbide Corporation (USA), in 1962. Their method consisted of a cyclic pyrolysis, where diamond was used as a substrate and diamond growth occurred homoepitaxially. This method was further expanded by Angus et al. and Derjaguin et al. in the early 1970s. However, since

Table 1 - Chronology of diamond utilization [17, 18]

Date	Event
340 BC	Aristotle describes the use of diamond tipped drills in Greece.
1000s	Pliny describes the use of diamond splinters in handles of iron to form an engraving tool in Italy. Reports describe the use of a diamond engraving tool called jade cutter knife in China.
1400s	Crushed diamond powder used for polishing diamond.
1500s	Leonardo da Vinci reports the use of diamond tools for glass cutting.
1600s	Report on the first diamond drilling tool.
1700s	Ramsden reports the first single diamond turning tool for application in metal working. Smith-Tennant reports diamond to be composed solely of carbon.
1800s	Diamond grinding wheels are being used by Pritchard in England to shape lenses. France grants a patent for a diamond core drill for use in the French stone industry. Use of diamond as a wire drawing die. Diamond drills for dentistry are introduced in the USA by Desau.
1900s	Wheel for glass grinding developed by Carl Zeiss Jena. First description of grinding tungsten carbide with diamond. First successful diamond synthesis via High Pressure, High Temperature by ASEA, Sweden (February 16th, 1953). Shockwave sintering of diamond reported. Natural diamond used as heat spreaders for semiconductors. First large synthetic diamond crystals grown up to 0.25 cts in weight. Polycrystalline diamond launched commercially. Growth of diamond crystals via low pressure CVD on non-diamond substrates announced in the Soviet Union. Sales by volume of synthetic diamond products exceeds natural diamond for the first time.
2000s	Development of high quality single crystal CVD diamond for electronic applications. Polycrystalline CVD diamond dome used as tweeter in loudspeaker application.

cyclic, hydrocarbon pyrolysis had a very slow diamond deposition rate (1 - 10 nm/h) and required a diamond grit substrate, its application was unrealistic. [15, 19]

In 1982, Matsumoto et al. made a breakthrough in CVD diamond technology. They used hot filaments (at 2000 °C) to directly activate hydrogen and hydrocarbon which were passed through the hot filament. The diamond film was then deposited onto a non-diamond substrate located 10 mm away from the filament. Graphite was etched simultaneously by atomic hydrogen during deposition which rendered the cycling of deposition and etching unnecessary and therefore led to a higher growth rate (1 μm/h). [20]

Thermodynamically, the crystal growth process is a matter of chemical potential equilibrium between two systems: the environment in the reactor chamber and the crystallites. Chemical potential governs the flow of particles between the systems. If two systems have different chemical potential, particles will flow from the system at the higher chemical potential to the system at lower chemical potential. Chemical potential, μ, is a function of the system temperature, T, volume, V, and number of particles, N, and is defined as:

$$\mu(T,V,N) \equiv \left(\frac{dF}{dN}\right)_{T,V} \quad (1)$$

where F is the Helmholtz free energy. [21-23]

Applying the chemical potential concept [23], with the Laplace equation:

$$P_C - P_V = 2\frac{\sigma_t}{r} \quad (2)$$

where σ_t is the surface tension of the crystal and r is the body radius (considering a crystal with a shape similar to a droplet) and the product $\frac{2\,\sigma_t}{r}$ is known as the Laplace pressure, and with the Thomson-Gibbs equation:

$$\mu_V - \mu_C = 2\frac{\sigma_t V_C}{r} \quad (3)$$

it can be supposed that volume, V_c, is gained when transferring n atoms or molecules from the supersaturated ambient phase (vapor), with higher chemical potential, μ_v, to the crystal phase with lower bulk chemical potential, μ_c:

$$(P_C - P_V)V_C = n(\mu_V - \mu_C) \quad (4)$$

where P_v is the vapor pressure and P_c is the crystal pressure.

Nevertheless, to be able to promote the crystal growth it is required the appearance of small clusters of building units (atoms or molecules) in the volume of the supersaturated ambient phase (nucleation sites).

The crystal shape is due to the equilibrium of a small crystal with its ambient phase, that leads to the formation of a particular shape which is the most favorable from a thermodynamic point of view, this is, when the work to form such crystal is at a minimum [23].

The surface requires a work equal to $\sigma_t S$, where S is the crystal surface, to create a new phase-dividing surface.

The volume part depends on the crystal volume or the atoms transferred. At a constant volume, the surface part depends only on the crystal shape, tending for a minimum of surface energy or an equilibrium shape. Then the conditions for a minimum Gibbs free energy changes with the crystal formation at a constant volume.

If instead of a crystal, there is a liquid droplet, the equilibrium shape would be evidently a sphere. In the case of a crystal, equilibrium shape is not that simple, due to the different crystallographic orientations and different specific surface energies. The latter meaning that the surface energy depends on the crystallographic orientation and in that sense it is anisotropic.

The growth of a polycrystalline diamond film starts from distinct nucleation sites. As individual randomly oriented nuclei grow larger, its diameters equal the average distance between the nucleation sites and start to form a continuous film. The subsequent film growth is dominated by competitive growth between randomly oriented grains. With increasing film thickness, more and more grains are overgrown and buried by adjacent grains. Only those crystals with the direction of fastest growth perpendicular to the surface will survive.

As mentioned above, thermal or plasma energy is the key factor to promote the fluctuations of the density to achieve small aggregates and to promote the thermodynamic environment to lead to crystal growth. Nevertheless, it has been gradually recognized that the superequilibrium concentration of atomic hydrogen has also an important role on diamond growth. [19]

It is presently accepted that the growth of diamond crystals at CVD conditions, does not occur only due to a simple step process, but due to several stages and phenomena as presented in table 2 and figure 8.

Table 2 - Cyclic reactions leading to the diamond deposition

Stage	Event
1st	Activation of the gas mixture
2nd	Transport of the active gas mixture to the substrate
3rd	sp^2 and sp^3 simultaneous deposition
4th	Dissolution of the deposited sp^2 carbon in the gas phase (etching) or its conversion to sp^3

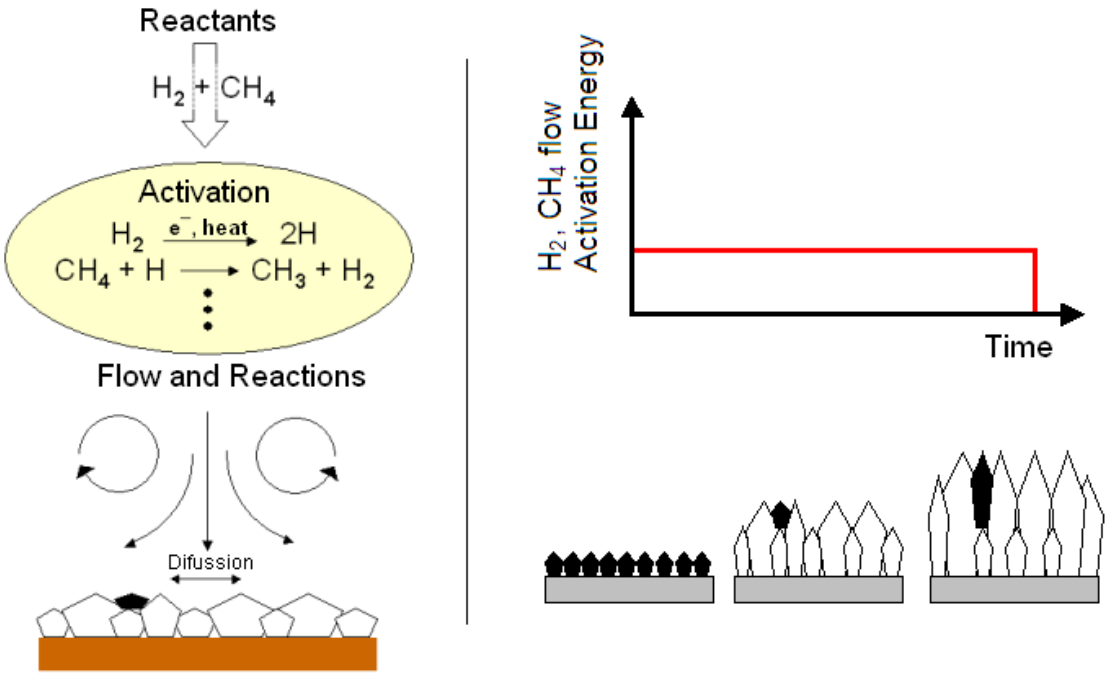

Figure 8 - Reactions taking place inside the CVD chamber during diamond growth

Various activating methods for diamond CVD such as DC-plasma, RF-plasma, microwave plasma, electron cyclotron resonance-microwave plasma CVD, and their modifications were developed.

A method also worthy of mention is the pyrolysis of fluorocarbons, such as CF_4, that could produce epitaxial diamond growth. OH radicals, O_2, O, F_2, and F as graphite etchants are even better than atomic hydrogen.

Besides CVD, physical vapor deposition methods were also attempted and were expected to deposit diamond at low temperatures. Recent work has demonstrated that diamond nanocrystals in the matrix of amorphous carbon could be produced by direct low-energy ion bombardment using a mixture of CH_4/H_2/Ar ions. [15]

3. Properties and applications

Diamond exhibits a number of exceptional properties, as presented in table 3, which individually or in combination with other materials, makes it the potential application material for a range of industrial applications.

The strength of the carbon-carbon bond is the source of the exceptional mechanical properties of diamond. Dislocation of the atoms is difficult and consequently diamond is the hardest known substance.

It is chemically inert and due to the high strength of the covalent bonds it is highly resistant to chemical attack by acids or other chemical reagents. The only exceptions are materials that at high temperatures act as oxidizing agents - these provide the only effective way to attack diamond at normal pressures and temperatures (below about 1000 °C). Salts, such as sodium nitrate, are known to attack diamond when in the molten state at temperatures as low as 450 °C and, in oxygen itself, diamond starts to be oxidized at around 650 °C. The only other possible form of chemical attack is by two groups of metals. The members of the first group are strong carbide formers, and include tungsten, tantalum, titanium and zirconium. At very high temperatures, these will react chemically with diamond to form their respective carbides. The second group of metals includes iron, cobalt, manganese, nickel and chromium (and also the platinum group of metals). In the molten state these metals are true solvents for carbon. [17]

Table 3 - Mechanical and thermal properties of diamond [17, 19, 24]

	Natural	Synthetic	Polycrystalline	Thin Film
Density (g/cc)	3.51 - 3.52	3.20 - 3.52	3.00 - 4.00	2.65
Volume Compressibility (x 10-10 m²/N)	18.0	--	--	--
Coefficient of friction (dynamic)	0.03	0.03		
Hardness, Knoop	8000	--	--	--
Microhardness, Knoop (GPa)	56.0 – 102 (001) face 58.0 - 88.0 (110),(111) face	54.0 - 84.0	49 - 78	65.0
Vickers Microhardness (GPa)	88.0 – 147 (001) face 98.0 (111) face	88.0 - 108 Type Ib 108 – 145 Type IIa	25.0 - 98.0	29.0 - 118
Hardness, Mohs	10.0	--	--	--
Abrasive Hardness	140000	--	--	--
Modulus of Elasticity (GPa)	700 - 1200	800 - 925	749 - 953	536 - 1035
Compressive Yield Strength (MPa)	8680 - 16530	4500 - 5800	1900 - 6900	--
Poisson Ratio	0.100 - 0.290	0.200	0.0700 - 0.200	--
Fracture Toughness (MPa-m½)	3.40	6.00 - 10.7	6.00 - 8.80	--
Thermal Expansion Coef., linear (µm/m-°C)	1.18	--	1.50 - 3.80	0.8 (at RT) 4.5 (at 800 °C)
Specific Heat Capacity (J/g-°C)	0.4715	--	--	2.76 - 3.49
Thermal Conductivity (W/m-°C)	2000	2000	1200 - 1800	--
Melting Point (°C)	4027	--	--	--
Heat of Formation (kJ/mol)	714.4	--	--	--
Debye Temperature (°C)	2067	--	--	--

Diamond has always been considered to be a highly suitable material for the fabrication of active electronic devices for the most demanding high power and high frequency applications. However, until recently it has not been available in sufficient quality or purity. The theoretical figure-of-merit comparisons indicate that CVD diamond should offer a substantially higher level of performance than other established electronic materials, such as silicon or gallium arsenide. Due to its large bandgap and material purity, diamond is an excellent electrical insulator. Doping of CVD diamond however, makes it possible to create materials that can conduct (semiconductors). [17, 19]

The use of the electrical properties of diamond is receiving growing interest from the scientific community, however diamond-based electronic devices could possibly include high-voltage switching in future generation power distribution networks and high power, high frequency communication systems.

It is unmatched in being transparent from near the ultra-violet cut-off at 225 nm to beyond a wavelength of 100 µm, including the atmospheric infrared transmission bands. [18, 25]

The use of diamond materials in optical applications such as infrared laser windows, was, for a long time, restricted by the size and cost of natural diamond. The use of CVD diamond is an economic alternative to zinc selenide (ZnSe) because of its hardness and high thermal conductivity.

Diamond's strong covalent bonds and rigid lattice result in high stress wave (phonon) velocity. This in turn gives diamond a high thermal conductivity, about five times that of copper at room temperature. The first natural diamond heat sink for a microwave diode was manufactured in 1967 and since then, this material has been used for the thermal management for microwave and laser diode devices.

Diamond can be used for many different applications because of its unique properties and because it is available in various forms. This versatility is mainly due to the different synthesis techniques that are presently employed which enable a diamond product to be tailored to match a specific application. High Pressure High Temperature synthesis produces diamond grit particles in sizes and characteristics that cater for many different abrasive applications - grinding, sawing and drilling. Polycrystalline diamond discs are also synthesized with this method to provide the raw material for cutting tools and drill products. As an industrial abrasive, diamond is involved in a wide range of industries including stone, construction, metalworking, glass, electronics, wood-working and oil and gas drilling. [19]

CVD synthesis produces coated and free standing diamond products in the most complex of shapes and in specific grades to exploit diamond's optical, thermal or electrical properties. This newer technology is expanding the use of diamond within the non-abrasive fields, where the range is also very diverse and includes components for usage such as optical windows, thermal devices, high performance electronic parts and medical instrumentation.

Diamond is now one of the most versatile materials used across all industries. From kitchen furniture to electric light bulbs; granite and ceramic tiles to silicon chips; aluminium alloy wheels to medical scalpels; car windows to face cream; space probes to oil and gas drilling. [17-19, 25-28]

4. Diamond CVD on Steel substrates review

Diamond films deposited on surfaces of non-diamond materials is termed as heteroepitaxial growth. Such thin films and surface coatings can be deposited onto a variety of materials, which can be classified into the following three groups:

- strong carbide-forming materials, including Si, Ti, Cr, W and SiC.
- strong carbon-dissolving materials, including Fe, Co and Ni.
- small or non-carbon affinity materials, such as Cu and Au.

The synthesis of diamond on carbide-forming materials usually leads to the production of adherent diamond coatings. Silicon is a widely used material for depositing diamond films using CVD processes. This is because silicon has a sufficiently high melting point (1683 K), it forms a localized carbide layer and it has a comparatively low thermal expansion coefficient.

On the other hand, diamond grown directly on strong carbon-dissolving materials, such as steel, or on non-carbon affinity materials, such as copper, yields poor adhesion. [29-34]

The application of diamond coatings on steel substrates would be of great importance for numerous industrial applications. The diamond coating can improve steel tool properties, such as hardness, wear resistance, chemical inertness and thermal conductivity.

As stated above, steel is a carbon-dissolving material, especially at diamond CVD conditions (1.3 wt.% C at 900°C). Therefore, during diamond CVD, the carbon swiftly diffuses into the steel substrate, forming a soot composed of graphite, Fe_3C and other carbides, thus leaving behind relatively little carbon precursor at the steel surface, to initiate the formation of

carbon–carbon sp^3 bonds, typically found in the diamond lattice. This normally results in poor diamond nucleation densities, film growth and diamond adhesion to the steel substrates.

Nevertheless, this is not the only problem that hinders the successful deposition of diamond coatings on steel using vapor-assisted deposition processes. Iron (Fe) is known to have a high vapor pressure (2.53×10^{-8} mbar), so it expectedly diffuses out from the bulk steel material towards the substrate surface during the growth process [35]. Iron is known to catalyze the growth of sp^2 carbon bonds found in graphite and also in carbon nanotubes. Furthermore, the difference in the thermal expansion coefficients of diamond (see table 3) and steel (11 µm/m.°C at room temperature to 13.2 µm/m.°C at 800 °C [36]) is sufficiently large, which results in the incorporation of residual stresses in the deposited diamond films and influences the adhesion in a negative way (weakens the adhesion strength at the diamond/steel interface).

Figure 9 shows the schematic of some of the key processes taking place during diamond growth from the vapor phase.

Direct diamond growth on as-received (no pre-treatments) bare steel substrates results in the formation of a diamond-based film, which delaminates from the substrate during post-deposition cooling. Primarily, a graphite layer is deposited on the steel, which acts as a precursor for subsequent non-adherent diamond growth. Figure 10 shows the Raman spectra representing the front and the reverse sides of a diamond film deposited directly on steel using microwave plasma CVD by Fan et al. [34]. The peaks for the reverse side of the film show that graphite is present.

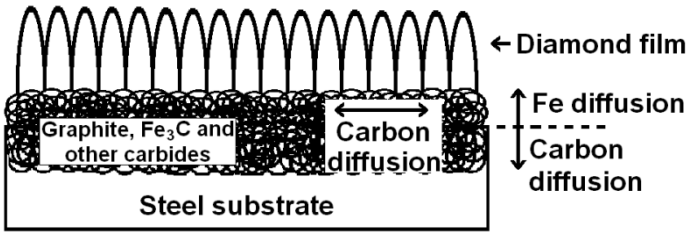

Figure 9 - Schematic of the critical processes taking place in and on the steel substrate during diamond synthesis from the vapour phase

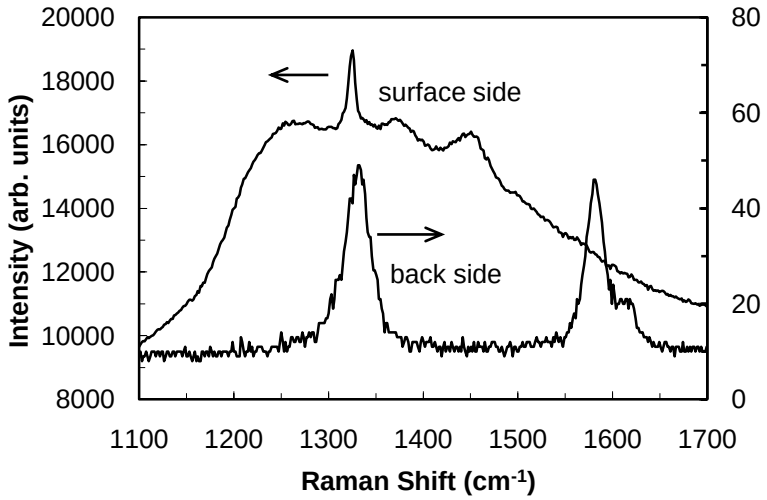

Figure 10 - Raman spectra from the front and the reverse sides of an as-deposited diamond film on a steel substrate [34]

Interlayer route

A possible solution to overcome the problems addressed above is to use an interlayer or an interlayer system, consisting of several intermediate sandwiched layers that block both inward carbon and outward Fe vapor diffusions. An ideal interlayer material should detain the following characteristics:

- refractory material that can tolerate the high CVD temperature used for diamond synthesis (usually 700 – 900 °C);
- good chemical compatibility with carbon (carbide former);
- good adhesion to the substrate material;
- thermally stable – structurally and geometrically – when submitted to typical temperatures of the CVD process;
- accommodate thermal-induced stresses developed during the growth and ramp down processes, due to thermal expansion coefficient mismatch;
- promote an effective barrier for carbon diffusion in Fe and outward diffusion of Fe vapor;
- goog control of film thickness and surface morphology;
- should be competitively priced.

Good adhesion requires both substrate/interlayer mutual diffusion and interlayer/carbon affinity (carbide formation). Hence, in order to obtain a strong coupling between the substrate and the interlayer, Fe must diffuse adequately into the interlayer material. Iron is known to have low diffusion in W, Ta and Cr; medium diffusion in Cu, Ag and Au and high diffusion in Ti [37]. Among these materials, Cu, Au and Ag do not form carbides, therefore, those are not best suited for diamond deposition. However, carbon has a high diffusion in Ti, medium in Cr and Ta and weak in W. Diffusion depth calculations by Fan et al. [37] show that W, Cr and Ta are excellent diffusion barriers against Fe, while Ti and Si need to be much thicker to be just as effective.

Table 4 presents a summary of the interlayers and interlayer systems used for diamond deposition on steels. The table also provides information on the diamond film quality, coating adhesion and the coating process used to deposit the interlayer(s).

Chen et al. [38] reported the use of Si interlayer for the growth of diamond films on steel. They have obtained well-adhered diamond films. Silicon and diamond have similar thermal expansion coefficients and also similar structure arrangement. A multilayer structure based on refractory metals and silver has also been used [29]. This multilayer was effective in relieving the stress of the film, so that the CVD diamond displayed good adhesion [29].

Ion-implanted Si was used by Fenker et al. [39] with relative success. A very thin chemical vapor deposited silicon interlayer (75 nm) was employed by Buijnsters et al. [40], which gave very good results, in terms of diamond film quality and coating adhesion strength.

Cubic silicon carbide 3C–SiC was used by Klages et al. [41]. In this paper, the authors also reported the use of metal–diamond-type interlayer that resulted in good adhesion to the steel substrate and a push-button-like connection to the CVD diamond coating. Reasonable adhesion results for diamond films on steel substrates were achieved using Ni–diamond composites. This is possibly due to the additional compensation of thermal stresses by plastic deformation of the metal matrix.

Schäfer et al. [42] used SiC interlayer to produce well-facetted diamond films with good crystallinity. However, there was complete delamination of the coatings after post-deposition cooling to room temperature. The delamination was found to occur at the SiC–steel interface.

Diamond films have been successfully grown on steel substrates with intermediate tungsten layers, using a d.c. arc plasma system with a CH_4/H_2 gas mixture, by Ralchenko et al. [36]. Although the Rockwell indentation tests revealed good adhesion of the diamond film, Raman spectroscopy have shown that the films were under high compressive stress.

Table 4 - Summary of interlayers used for diamond deposition on steels

Interlayer(s)	Interlayer thickness (μm)	Diamond quality[6]	Diamond adhesion[7]	Interlayer coating process	Reference
CrNi	5	No film	-	-	[35]
TiN	5	No film	-	-	[35]
Ti(C,N)	5	No film	-	-	[35]
(Ti,Al)N	5	No film	-	-	[35]
CrN	5	No film	-	-	[35]
WC/C	5	No film	-	-	[35]
Ti	2	Good	Good	Sputtering	[37, 43, 44]
Si	-	Good	Good	-	[38]
Mo/Ag/Nb	0.02/2–25/0.02	Medium	Good	Sputtering	[29]
Si	0.026	Medium	Medium	Ion Implantation	[39]
Si	0.075	Very good	Good	Hot-filament	[40]
3C-SiC	-	-	-	CVD	[41]
Metal-diamond composite	-	-	Good	Electrodeposition	[41]
SiC	0.3	Good	Very weak	Plasma activated CVD	[42]
Ni-diamond composite	15	Good	Good	Electroplated	[42]
Cr-diamond composite	15	Good	Good	Electroplated	[42]
W	25	Good	Good	Hot-wall reactor	[36]
TiN	3	Medium	Weak	Electron-beam evaporated	[45]
TiN	2.2–3.0	Medium	Weak	PVD and cathodic arc evaporation	[46]
Cr	0.8	Good	Good	Electroplated	[47]
Cr	1.0	Medium	Good	Sputtered	[47]
Ti	1.8	Good	Good	Sputtered	[47]
ZrN	10	Very good	Very weak	Reactive cathodic arc	[48]
ZrC	10	Very good	Weak	Reactive cathodic arc	[48]
TiC/Ti(C,N)/TiN	10	Very good	Very weak	Reactive cathodic arc	[48]
TiC	10	Good	Good	Reactive cathodic arc	[48]
Ni	-	Good	Good	Electroplated	[49]
Ni/Ni-diamond composite	0.5–1/18–20	Good	-	Nitridation/Watts type electroplating bath	[50]
N	-	Good	Good	Ion beam	[51]
N (CrN)	-	Good	Good	Ion nitriding	[52]
Cr	20 – 25	Good	Good	Chromising	[53]
CrC	10 – 15	Good	Good	Chromising	[54, 55]
CrN	10	Good	Good	Electrochemical deposition and nitridation	[56]
CrN	20	Medium	Good	Electrochemical deposition and nitridation	[57-59]
CrN	20	Medium	Good	Electrochemical deposition and nitridation	[60]
CrN	2.5	Good	Good	Arc-plated	[61, 62]
B	40	Good	Medium	Boriding	[61, 62]
Ni/Cu/Ti	3–4/32–36/0.5–2.5	Very good	Very weak	Ni and Cu – electroplated; Ti – PVD	[63, 64]
Ni/diamond embedded crystallites/Cu	7/32/26	Good	Medium	Ni and Cu – electroplated	[65]

[6] Diamond quality depends on uniformity; Raman quality; crystalline and film stress.
[7] Diamond adhesion qualification is based on hardness, wear and other tests.

TiN was employed by several researchers [35, 45, 46], however, the results were not very impressive. Similar observations were made when using other Ti-based ceramics, such as Ti(C, N) and (Ti,Al)N [35]. Nevertheless, Ti and TiC produced good results and show good potential for use as intermediate layers in diamond growth on steel substrates. Sputtered Ti, with approximately 2 µm thickness, was successfully employed by Fan et al. [34, 44] and Silva et al. [47] as a promising interlayer.

More recently, a 10-µm TiC was employed by Polini et al. [48]. They produced adherent polycrystalline diamond films after three hours of deposition. However, with six hours of deposition, the diamond films delaminated from the steel substrates.

Lin and Kuo [49] reported high adhesion and produced good-quality diamond films on steel substrate using electroplated Ni interlayer. The nickel–carbon–hydrogen alloy system can effectively enhance diamond nucleation density and subsequent film growth and form a high retention force. Similar results were obtained by Sikder et al. [50], who initially nitrided the steel and then coated it with a Ni–diamond composite using Watts-type electroplating bath, thus forming a multilayer system. A similar Ni–diamond composite interlayer was also used by Schäfer et al. [42]. In their work, they reported the use of Cr–diamond composite. Both metal diamond composites produced well-faceted diamond films. The deposited diamond coatings displayed good adhesion. The impressive results obtained using this interlayer system was due to the toughness of the metal matrix–steel interfaces and of the diamond–metal composite interface. The possible factors contributing to the adhesion of diamond to the metal composite interlayers could possibly include the following:

- the partial compensation of the thermally induced stress by plastic deformation of the metal matrix;
- the reduction of interface stresses due to the additional interfaces;
- the presence of carbide phases with intermediate thermal expansion coefficients;
- the bonding of the growing diamond film to the incorporated diamond particles;
- and, the formation of the carbide layer during the deposition process.

Shang et al. [51] reported the influence of ion beam nitriding on diamond nucleation and growth on steel substrates. This effectively prevented carbon diffusion in steel and provided suitable nucleation sites, which resulted in the nucleation and growth of reasonably good-quality and adherent diamond coatings.

A slightly different approach adopted by Borges et al. [52] also produced good results. They employed stainless-steel 304 substrates for diamond deposition, which consists of high Cr content (Cr 18 wt.%). By nitriding the substrates, the amount of CrN increased on the substrate surface layer and, during the initial stages of diamond deposition, carburisation of the substrate surface occurred, resulting in the formation of chromium carbide at close vicinity to the substrate surface.

Chromium and chromium composites are widely used interlayers for producing adherent diamond coatings on steel. Silva et al. [47] carried out a comparative study using electroplated Cr and sputtered Cr interlayers for improving diamond coating adhesion. They found electroplated Cr to produce comparatively more adherent coatings.

Bareiβ et al. [53] reported the production of adherent diamond coatings by using a thick Cr layer produced by chromating. A thick chromated CrC layer employed by Schwarz et al. [54, 55] also displayed good adhesion results.

The use of CrN as an interlayer has been extensively studied by Fayer et al. [56], Glozman and Hoffman [59], Avigal et al. [60] and Glozman et al. [57, 58], Buijnsters et al. [61, 62] and more recently by Haubner and Lux [35].

Fayer et al. [56] used a chromium film on steel deposited by electrochemical synthesis method, followed by a nitridation process, to produce mixed CrN and Cr_2N crystalline phases. On this mixed of approximately 10 µm interlayer they deposited approximately 2 µm thick homogeneous diamond film, which displayed good crystallinity and homogeneity and did not show any indication of film delamination up to a load of 1000 N.

In another work by the same group [57-59], the researchers evaluated the diamond coating adhesion at different deposition times on a 20 µm thick nitrided chromium interlayer. They used deposition times ranging from 15 minutes to 180 minutes and obtained a continuous film after 60 minutes.

The Raman spectroscopic analysis revealed a dominant peak centered at 1334 cm^{-1}, which is representation of diamond. After continuous diamond films were obtained, the Raman diamond peak was observed to split and shift to 1345 cm^{-1}. With increasing deposition time, the Raman diamond peak shifted to even higher wave numbers, having a maximum shift of the peak on the 180 minutes sample (1360 cm^{-1}). The splitting and shifting of the Raman diamond peak is due to the increased magnitude of biaxial stress in the deposited films. The films deposited for growth times of less than 120 minutes did not delaminate from the substrates

up to 1000 N loading using Rockwell indenter. Further wear testing results, namely fretting wear, were reported later by Kreines et al. [66].

With the aim to improve the tribological performance, namely the friction coefficient, Avigal et al. [60] deposited (100) textured diamond crystals on steel substrates, with the addition of N_2 in the precursor gas mixture. The as-deposited diamond coatings displayed good homogeneity, uniformity, crystallinity and adhesion.

Buijnsters et al. [61, 62] employed arc-plated CrN coatings with a thickness of 2.5 µm to produce adherent and good-quality diamond coatings on steel. The same group carried out experiments using boron as an interlayer material [40, 62]. These samples presented improved hardness values, increased wear resistance and better fatigue properties and enhanced corrosion resistance compared to nitriding and carburising (deposition of diamond directly to the steel substrate) samples. In the absence of FeB phase, having only Fe_2B phase, continuous and adherent diamond films with low residual stress were obtained. Nevertheless, the presence of FeB on the surface of the borided steel resulted in very high thermal stresses and, consequently, delamination of the diamond film occurred.

Haubner and Lux [35] used a 5 µm CrN interlayer, not being able to achieve a considerable nucleation density, to successfully grow diamond coatings on steel substrates. Similar results were obtained when using CrNi and WC/C interlayers.

Zirconium compounds, such as ZrC and ZrN, were employed by Polini et al. [48], who produced good quality diamond films but with weak and very weak coating adhesion, respectively.

Some authors have also used multilayer systems, such as Ni/Cu/Ti [63, 64], Ni/diamond embedded crystallites/Cu [65] and TiC/Ti(C,N)/TiN [48] to improve diamond adhesion on steel.

The Ni/Cu/Ti interlayer system [63, 64] enabled the growth of good quality diamond films, with good adhesion being confirmed by a 200 N load indentation using a Rockwell indenter. The interfaces, constituted by smooth and continuous electroplated Ni and Cu layers, were stated to allow adequate plastic deformation during the CVD thermal cycle. The Ti layer was to promote diamond nucleation and strengthen coating adhesion of diamond films. The multilayer systems consisting of Ni/diamond embedded crystallites/Cu [65] and TiC/Ti(C,N)/TiN [48] were successful in initiating diamond nucleation and diamond crystal growth.

Although a number of researchers have presented reasonably good results using the interlayer route to improve coating adhesion (see table 4), there are still few reports attempting direct diamond deposition on bare steel substrates, such as the report by Gowri et al. [67]. In this

recent paper, the authors report direct deposition of diamond films on steel, using a three-step growth process. This three-step growth process consisted of:

- deposition under high CH_4 concentration;
- ultrasonication of samples in diamond slurry to improve the nucleation density;
- diamond growth under optimized conditions.

The process produced films consisting of a mixture of diamond crystals, graphite and amorphous carbon phases, as shown by Raman spectroscopy and SEM analysis. Also different grades of steel were used by the workers to deposit the diamond coatings.

In this doctoral thesis, the presented results will be adapted to the application that is intended in this work and to the existing conditions at the research unit.

In the next chapter, the experimental techniques and methodologies that will be used in the development of the diamond CVD coatings on steel substrates, and the evaluation performance of the diamond coated mold tools.

Chapter 3

Experimental techniques

1. Introduction

The current chapter gives detailed information about the experimental techniques and methodologies used to develop diamond CVD coatings on steel substrates which will be presented in chapter 4. Moreover, this chapter will also describe the techniques used to assess the performance of the diamond coated tools, whose results will be presented and discussed in chapter 5.

The overall experimental procedure may be summarized in five main stages: a) substrate/mold inserts material selection and preparation; b) diamond deposition; c) diamond coatings evaluation; d) thermoplastic injection molding; and e) thermoplastic parts evaluation.

The substrate/molding inserts preparation consists of the manufacturing of samples; of the interlayers deposition (in most of the steel samples); and of the pre-deposition treatments. Diamond depositions were carried out in a hot-filament CVD system, using different deposition conditions. The deposited diamond films were evaluated and characterized by Scanning Electron Microscopy (SEM); Energy Dispersive X-ray Spectroscopy (EDS); Optical Microscopy (OM); Raman Spectroscopy; X-ray Diffraction Spectroscopy (XRD); Secondary Ion Mass Spectrometry (SIMS), indentation hardness techniques and surface profilometery. The thermoplastic injection molding was performed with the assistance of an adapted mold tool, in a conventional 65 tons injection molding machine. Finally, the thermoplastic parts evaluation

was performed by simple eye observation; optical microscopy; and the dimensions of three dimensional features on a coordinate measuring machine.

2. Substrate/molding inserts selection and preparation

The steel substrates and the inserts for mold tools were obtained from block material by different saw cutting, milling and polishing procedures. The polishing of the steel samples was performed with Silicon Carbide paper till a grid of 2000, which are composed of particles with a size of ~10 μm.

Four different steels, supplied by *F. Ramada, Aços e Indústrias, S.A.* [68], have been used: AISI P20 modified (*F. Ramada, Aços e Indústrias, S.A.* trade name is PM300); AISI 304; AISI 310; and AISI 316. AISI P20 modified is a pre-treated steel typically used in the production of mold tools. AISI 304, AISI 310, and AISI 316 are refractory stainless steels. [69]

Flat silicon substrates 5.0 x 5.0 x 0.5, with a mirror polished surface, were also used.

In order to block the diffusion of carbon to the steel and of iron to the growth layer, different interlayers were tested, based on the literature review and presented in table 4 (previous chapter). Silicon (Si), Titanium (Ti) and Chromium Nitride (CrN) were tested. Si films were deposited by reactive radio frequency magnetron sputtering in a reactive atmosphere [70] on AISI P20 modified, at the Department of Physics of the University of Minho, Portugal. Ti was deposited using a commercial PVD system, also on AISI P20 modified, at GALOL (Valencia, Spain) [71]. CrN was deposited also using a commercial PVD system, at Prirev (Vagos, Portugal) [72], on AISI P20 modified, AISI 304, AISI 310 and AISI 316.

Prior to the deposition of diamond coatings, all samples were submitted to a pre-deposition treatment to enhance the nucleation of the diamond crystals. Nucleation is the first and critical step of CVD diamond growth. The control of nucleation is essential for optimizing the diamond properties such as grain size, orientation, transparency, adhesion, and roughness that are necessary for targeted applications. [15]

When in 1982 Matsumoto made a breakthrough in growing diamond on non-diamond substrates without using diamond seeds, he achieved a very low nucleation density and a continuous film could not be formed. In 1987 Mitsuda found that scratching substrate surfaces with diamond powder could greatly enhance the nucleation density. Since then, substrate scratching has become the most common and powerful method for achieving nucleation that can form diamond with a high nucleation density and fine uniform grain size. [15]

The reason why scratching enhances diamond nucleation is not clear. One possible reason may be that, during scratching with diamond, c-BN, or a-SiC powder, the residual powder or fragments are unavoidably left in the scratched groove and act as seeds for diamond growth. Another opinion is that scratching with powder merely creates a change in the surface morphology, such as edges, steps, dislocations, and other surface defects. These kind of defects are labeled chemically active sites, which prefer to adsorb diamond precursors together due to enhanced bonding at high energy intersecting surfaces with a high density of unsaturated bonds and low coordination numbers. [15, 25]

Several authors have reported the bias-enhanced nucleation method, applying a negative bias to the substrate, at the beginning of the process. This is believed to accelerate carbon-containing ions onto the substrate, causing it to plant beneath the surface and create a carbon-rich layer in the topmost few layers of the substrate, leading to a higher initial nucleation density. [15, 25]

Recently, other methods for enhancing diamond nucleation have been reported. One method is the nucleation enhancement under very low gas pressures (0.1 to 1.0 Torr) [15]. The addition to diamond slurry of various hard material particles (such as alumina, silica, boron-carbide or silicon-carbide), enhances the nucleation, if compared with pure diamond slurry [73]. Recently, a modified New Nucleation Process (NNP), initially proposed by Shlomo S. Rotter [74], was suggested. The process consists of two steps. The first step, referred to as the “plasma pretreatment”, involves exposure of the substrate to the diamond growth environment in the deposition chamber for a short period of time using standard diamond growth parameters, except for a higher methane concentration. In the second step, termed the “seeding” step, the substrate is taken out of the deposition reactor and subjected to ultrasonic treatment in an alcohol solution with diamond powder. The seeded substrate is then returned to the deposition chamber and diamond growth is initiated. [75]

With regards to the mechanical abrasion of the substrate, the method used in the present work, it is known that the nucleation density is proportional to the scratching time, and the morphology changes, from large isolated crystals for short scratching times, to smaller, high number density crystals with increasing scratching time. The grit size of the diamond powder used for scratching also influences the nucleation density. A grit size of 0.25 μm is the most effective for scratching by hand and a 40 to 50 μm powder is the best for scratching in an ultrasonic bath using a grit suspension. [15]

Both hand and ultrasonic bath processes where used in the present work, with grit of 0.25, 2 and 4 µm, with times going from 2 minutes when abrading by hand to 3 hour of ultrasonic bath scratching.

3. Diamond deposition

The diamond depositions performed during the present work were carried out in a hot-filament CVD (HFCVD) system. The latter is the earliest used method for the growth of diamond under low pressures and it is also the most popular [15, 20, 25]. The HFCVD method is relatively cheap and easy to operate and produces reasonable quality polycrystalline diamond films at a rate of 1 to 10 $\mu m.h^{-1}$, depending upon the exact deposition conditions [25]. Despite suffering from a number of disadvantages, namely its sensitivity to oxidizing or corrosive gases, which limits the variety of gas mixtures that can be employed and the difficulty to avoid contamination of the diamond film with filament material, it is a suitable method for the mechanical application being tested in this work. The experimental setup is presented in figure 11.

Figure 11 - Hot-filament reactor used

Hot-filament CVD uses a vacuum chamber continuously evacuated using a rotary pump, while process gases are metered, at carefully controlled rates, through mass flow controllers (a total flow rate of 200 sccm (200 ml/min) was used in this work). Throttle valves maintain the pressure in the chamber at 30 Torr (39.99672 mbar or 3999.672 Pa). The substrate to be coated is placed on a holder, a few millimeters (4 to 10 mm) beneath a filament, which is electrically heated to temperatures in excess of 2000 °C. At this temperature, as H_2 passed over the hot filament, atomic hydrogen is produced. A schematic of the HFCVD system used to deposit the diamond films is presented in figure 12.

The filament is made of metal that is able to survive the deposition conditions and not react significantly with the process gases. Metals such as tungsten and tantalum are most often used, although they react with the carbon-containing gases and carburize to form the metal carbide. This, changes their resistivity and makes them brittle, reducing their lifetime and hence the maximum deposition time that can be performed in one run [25]. Rhenium can also be used, with the great advantage of not reacting with the carbon-containing gases and as a result are more durable than tungsten or tantalum, but it is much more metal contaminant than W and Ta [20, 76], and it is a much more expensive material than the former two. Tungsten filaments carburize faster than Ta filaments, and deform to a higher degree during carburization. Tungsten carbide (WC) and tantalum carbide (TaC) filaments break easily, however, TaC filaments tend to have a longer life and can be reliably operated to a higher temperature than tungsten carbide [76]. Carbide-forming refractory metals should be first carburized before starting the deposition of diamond films, in order to deform before the sample to be coated is introduced into the reactor and the filament-substrate distance is set.

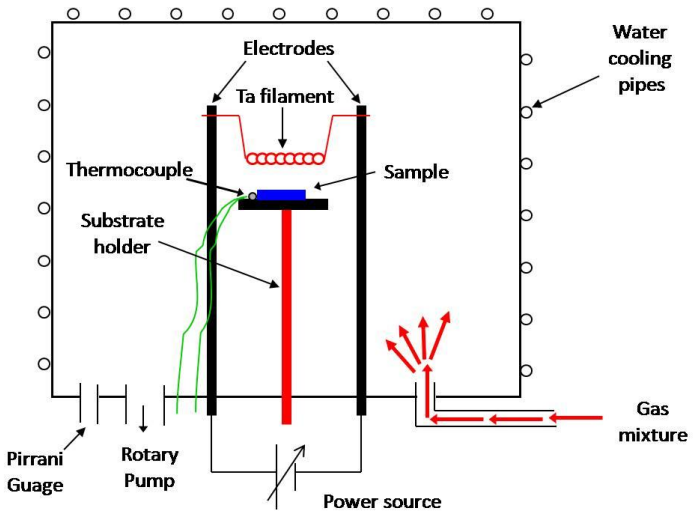

Figure 12 - Schematic of the HFCVD system used to deposit the diamond films

Tantalum wire, with 0.4 mm of diameter, was selected to perform the diamond depositions reported here. The Ta wire was rolled up to form a spiral, with a diameter of 4 mm, normally with 5 to 7 coils, depending on the size of the sample to be coated. Also depending on the size of the sample to be coated, one or three springs were used. One of the filament setups, inside the CVD reactor, is presented in figure 13.

The carburization process was normally conducted for 30 minutes in a gas mixture of 200 sccm of H_2 and 6 sccm of CH_4 (3% CH_4/H_2 rate), at a pressure of 30 Torr and a filament temperature in excess of 2000 °C.

It is known that with tantalum, carburization proceeds in the sequence of Ta, Ta_2C and TaC from the outer surface to the center, forming concentric circular carbide layers in cross-section. The literature also highlights [77], that at these conditions, 30 minutes will ensure the formation of TaC.

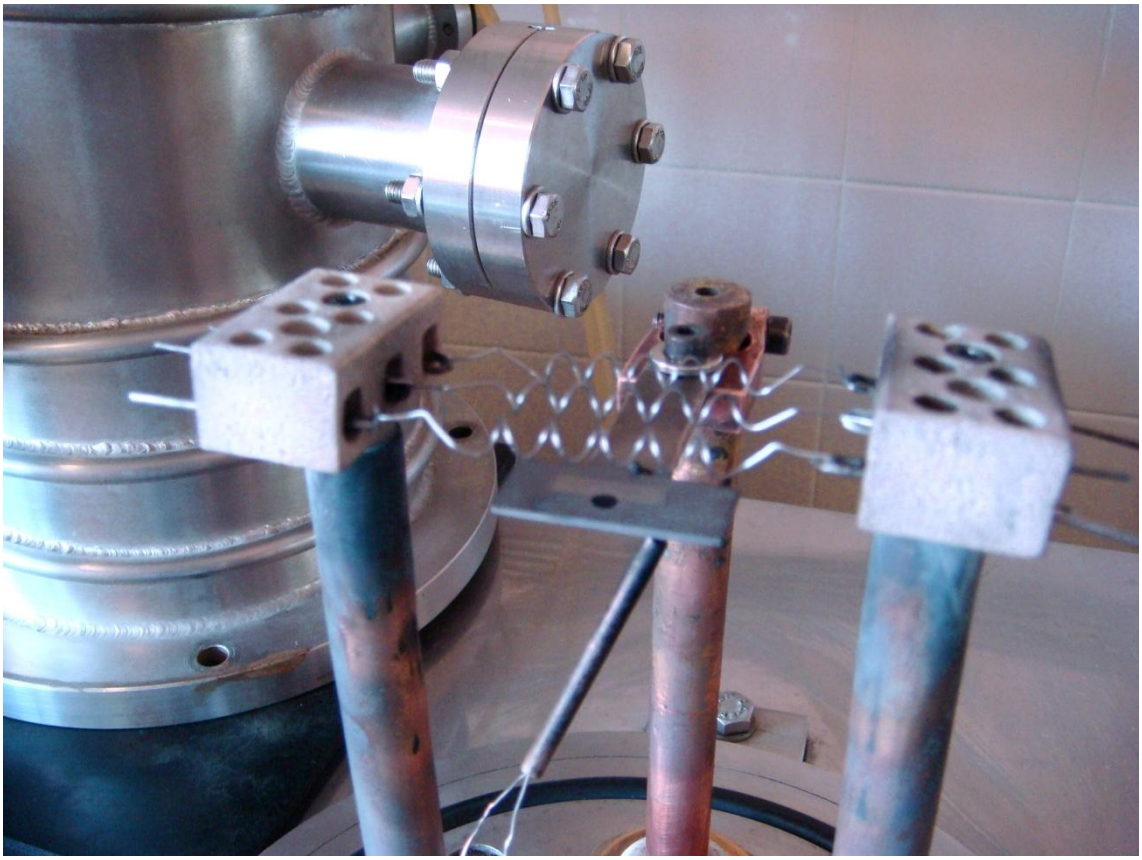

Figure 13 - Filament setup inside the CVD reactor

The substrate temperature was measured using a K type (chromel[8]–alumel[9]) thermocouple in direct contact with the molybdenum substrate holder. The temperature range of a K type thermocouple goes from 0 to +1100 °C. In these depositions, no substrate heater was used. Substrate temperature accuracy depends upon the thermocouple calibration, but it is also greatly influenced by the relative position of the sample and of the filament. The accuracy of the substrate temperatures here presented, were determined to be ± 50 °C.

The filament temperature was acquired by an IMPAC IS140 infrared pyrometer, with a focusable optics for a spot size of 0.35 mm, and a working range from 749 to 2500 °C. The instrument has an adjustable emissivity, which depends on the material being measured. For the TaC filament, it was used an emissivity of 0.23%. The temperature accuracy of the pyrometer, on its technical specifications, is of about 0.5%, for the temperatures in the order of 2000 °C. Nevertheless, errors can arise from the deformation of the filament (the spot of the photoelectric current source moves away from the filament) and from variations on the filament surface composition, leading to incorrect emissivity values. To guarantee that the atomic hydrogen is formed, the filament must have a temperature above 2000 °C. Considering that there may be an inaccuracy of ± 50 °C, it was normally used a filament temperature settled to 2100 °C.

The gas mixture used to grow the diamond films was composed of H_2 mixed with small amounts of CH_4. In most of the depositions carried out, it was used a recently developed time-modulated CVD (TMCVD) process [78-83]. TMCVD consists on the modulation of the CH_4 gas flow during the deposition time, as schematically represented in figure 14. The high pulses of CH_4 enriches the reactor atmosphere with methyl specimens, which at the nucleation stage enables a higher nucleation density and during the growth process it is believed to inhibit further growth of diamond crystallites and promote a new nucleation site on top of the growing crystals [80]. Higher CH_4 content in the diamond CVD reactor leads to the incorporation of nondiamond carbon phases in the film, such as graphite and amorphous carbon, and degrades the global quality of the deposited film [43]. Therefore, the higher CH_4 pulse duration must be kept short, relative to the lower CH_4 pulse. It was also found out that the concentration of CH_4 has influence on the system temperature. Filament temperature is directly proportional to the CH_4 concentration. On the other hand, substrate temperature is inversely proportional to the CH_4 concentration.

[8] Chromel is an alloy consisting of approximately 90% nickel and 10% chromium.
[9] Alumel is an alloy consisting of approximately 95% nickel, 2% manganese, 2% aluminium and 1% silicon.

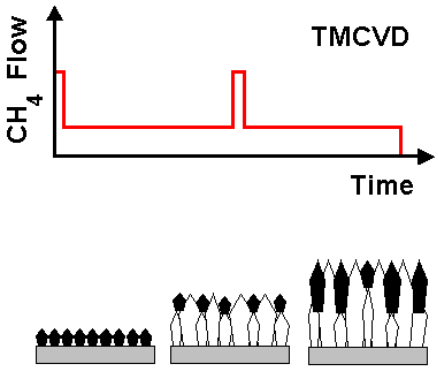

Figure 14 - Schematic representation of the time-modulated CVD process

Thus, the duration, value and number of cycles of the high and low CH_4 flow must be tailored according to the coating desired characteristics, such as crystal size and film thickness. In the majority of the depositions conducted, the objective was to achieve high quality (high purity diamond), smooth surface, low intrinsic stress and adherent thin films of diamond coatings.

Typically, it was used high CH_4 flows of 3 to 4%, for approximately 10 to 15 minutes, and low flows of 1 to 2%, for 45 to 120 minutes.

4. Diamond evaluation

The deposited diamond films were evaluated and characterized by using Scanning Electron Microscopy (SEM) and Energy Dispersive X-ray Spectroscopy (EDS); Optical Microscopy (OM); Raman spectroscopy; X-ray Diffraction Spectroscopy (XRD); Secondary Ion Mass Spectrometry (SIMS); indentation hardness, namely Vickers micro-hardness, Rockwell C and Brinell hardness; and surface profilometery.

Scanning Electron Microscopy and Energy Dispersive X-ray Spectroscopy

Electron microscopy analyzing techniques are normally employed for high magnification characterization of samples. The scanning of the top surface and cross-section surface of coated samples with high magnification techniques allows the observation of the coating morphology, crystal size, size and shape of the grown film, and qualitative cohesion and adhesion of the film to the substrate.

Electronic microscopy is a result of the bombardment of specimens with high-energy beam and the interaction of the beam with the specimens matter [84-86]. In a general way, it consists in scanning a focused electron beam over a material surface, which will penetrate the sample, resulting on a number of interactions that can produce the emission of electrons or photons from or through, the surface, as it is represented in figure 15. The detection of the resulting signals allows the acquisition of images, giving information about the topography and crystalline structure, but also chemical composition, among other information.

During the present work, the goal was to examine the diamond nucleation, the diamond coatings and the elemental distribution. In its primary detection mode, secondary electron imaging, the SEM has a wide range of magnifications (commonly from about 25 times to 250 000 times), producing very high-resolution images of a sample surface, revealing details on the nano-scale. SEM micrographs have also a very large depth of focus yielding a characteristic three-dimensional appearance useful for understanding the surface structure of a sample. X-rays are emitted when the electron beam removes an inner shell electron from the sample, causing a higher energy electron to fill the shell and give off energy. These characteristic x-rays are used to identify the elemental composition of the sample, and may be detected in a SEM equipped for energy-dispersive X-ray spectroscopy.

Two SEM equipments were used: a Hitachi S-4100 SEM; and a Hitachi SU-70 UHR Schottky FE-SEM system. Both instruments are equipped with energy dispersive X-ray spectroscopy (EDS), but the SU-70 is a more recent equipment, with superior capabilities. For that reason, the X-ray maps and profiles were assessed with a Bruker AXS Microanalysis GmbH system associated to the SU-70 microscope, due to its high performance and faster acquisition.

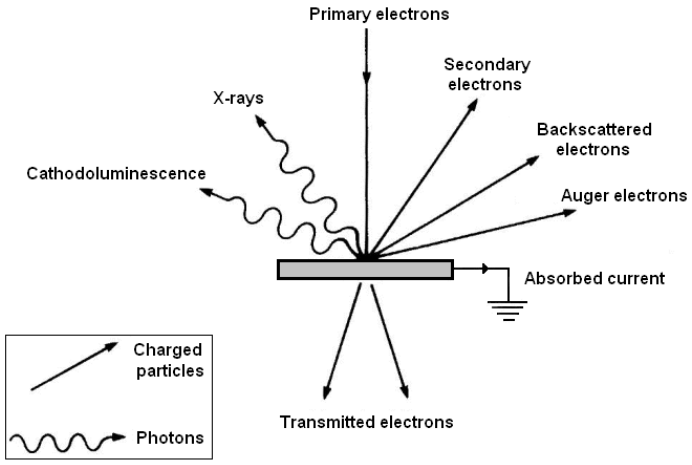

Figure 15 - Emission of electrons and photons as a result of the bombardment of a sample with an electron beam (Adapted from[85])

Due to the electron conducting requirements of the process, whenever the substrate was not metallic or if it was mounted in cold-setting epoxy resin, the samples were coated with a thin carbon conducting layer. When the samples were embedded in resin, before the conducting layer was deposited, the sample was polished to a mirror-like finish.

Optical Microscopy

Optical microscopy is a magnification equipment that allows the observation of samples with a magnification strength of approximately 2000 times. Although it has not the magnification range of SEM, nor the depth of focus, it is a very fast preliminary step for the observation of the coatings. [87]

Optical or light microscopes are a type of equipments that uses visible light and a system of lenses to magnify images of small samples.

By using light, the maximum resolution is limited (resolving power of a microscope), this is, the ability of the microscope to reveal adjacent structural detail as distinct and separate. After this limit, point objects are seen as fuzzy discs surrounded by diffraction rings, called Airy disks. The extent and magnitude of the diffraction patterns are affected by the wavelength of light (λ), the refractive materials used to manufacture the objective lens and the numerical aperture (A_N) of the objective lens. Assuming that optical aberrations in the whole optical set-up are negligible, the resolution d_r, is given by:

$$d_r = \frac{\lambda}{2A_N} \quad (5)$$

If it is assumed that λ is 550 nm (green light). With air as medium, the highest practical A_N is 0.95, so d is around 0.29 µm.

Optical microscopes are composed of the eyepiece or an image acquisition system, the objective lens, which collect light from the sample, the platform which supports the specimen being viewed and the illumination source that is focused through the condenser, with diaphragms and filters available to manage the quality and intensity of the light. Different filters or accessories may be used to enhance or reveal details not seen in direct illumination (bright field). Dark field apparatus blocks the directly transmitted light from being collected and just the scattered light enters the objective lens and produces the image.

While the dark field image may first appear to be a negative of the bright field image, different effects are visible in each. In bright field microscopy, features are visible where either a

shadow is cast on the surface by the incident light, or part of the surface is less reflective. Raised features that are too smooth to cast shadows will not appear in bright field images, but the light that reflects off the sides of the feature will be visible in the dark field images. This is the case of a smooth polycrystalline diamond film.

Another useful accessory is the differential interference contrast (DIC), also known as Nomarski Interference Contrast, used to enhance the contrast. DIC works with interferometry to gain information about the optical density of the sample, giving the appearance of a three-dimensional physical relief corresponding to the variation of optical density of the sample, emphasizing lines and edges though not providing a topographically accurate image. [88]

The three optical imaging techniques (bright field, dark field and DIC), available in the Department's Nikon Eclipse LV150 microscope, were used to evaluate the as deposited diamond films, in a preliminary evaluation of the coating.

Optical microscopy was also used to analyze the thermoplastic injected parts, as it will be referred later.

Raman spectroscopy

Raman spectroscopy is a technique based on the light dispersion phenomenon [84, 89, 90], valuable for coating composition evaluation and stress assessment.

Raman spectroscopy relies on inelastic (or Raman) scattering of monochromatic light, from a laser, to study vibrational, rotational, or other low-frequency modes in a system. The illumination of a sample with monochromatic light results in Rayleigh and Raman dispersion, due to elastic and inelastic collisions, respectively, as illustrated in figure 16.

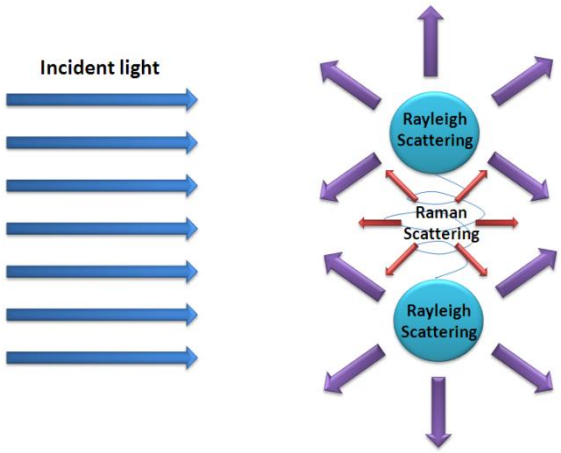

Figure 16 - Rayleigh and Raman scattering as a result of the interaction of light with a molecule (Adapted from [89])

The scattered light from the illuminated spot is collected with a lens and sent through a monochromator. Wavelengths close to the laser line, due to elastic Rayleigh scattering, are filtered out, while the rest of the collected light is directed onto a detector.

A complementary way to understand the Raman effect is by a quantum energy scheme, as shown in figure 17. The exchange of energy from the incident phonons to the molecule is not large enough to transport the system to the excited state, so a virtual state "quasi-excited", between the fundamental and excited state is formed, giving place in the decay to the Stoke or anti-Stokes emission.

If an electromagnetic wave:

$$E = E_0 \cos(\omega_0 t) \tag{6}$$

illuminates a diatomic molecule, it will create a vibration on the molecule, inducing a dipolar momentum, μ_e, in the form:

$$\mu_e = \alpha_P E_0 \cos(\omega_0 t) \tag{7}$$

where α_P is the molecule polarizability and in general is a function of the atomic separation.

If x is the extra dislocation of the molecule atoms, the polarizability can be expanded by a Taylor expansion development, around x_0

$$\alpha_P(x) = \alpha_{P_0} + \left(\frac{\partial \alpha_P}{\partial x}\right) x + \cdots \tag{8}$$

where α_{p0} is the polarizability in the average x position. The molecule will vibrate also in its natural resonant frequency, ω_m, then:

$$x = a \cos(\omega_m t) \tag{9}$$

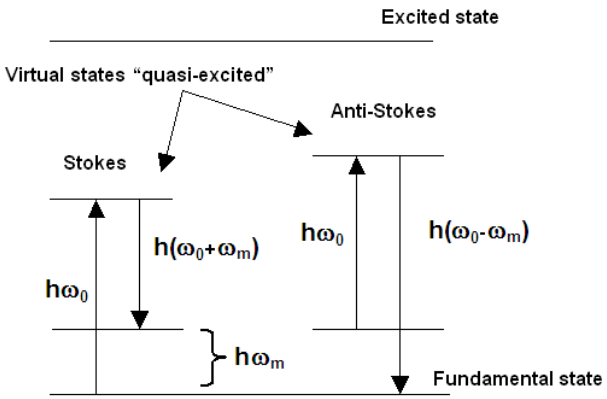

Figure 17 - Quantum representation of energy exchange in the non-resonant Raman phenomenon (Adapted from [89])

Combining equations (7), (8) and (9):

$$\mu_e = \alpha_{P_0} E_0 \cos(\omega_0 t) + \left(\frac{d\alpha_P}{dx}\right).(a\cos(\omega_m t)).E_0 \cos(\omega_0 t) + \cdots$$

$$= \alpha_{P_0} E_0 \cos(\omega_0 t) +$$

$$+ \frac{1}{2}\left(\frac{d\alpha_P}{dx}\right) a E_0 \{\cos((\omega_0 - \omega_m)t) + \cos((\omega_0 + \omega_m)t)\} + \cdots \qquad (10)$$

The dipolar momentum presents the emission of three different frequencies: the Rayleigh emission with a frequency of ω_0; the Raman Stokes emission with a frequency of ω_0-ω_m; and Raman anti-Stokes emission with a frequency of ω_0+ω_m.

The inelastic shift of energy is therefore dependent upon the natural resonant frequency, ω_m, of each material. Knowing the natural resonant frequency or frequencies of a material (molecule) it is possible to identify it in an unknown sample, by identifying the scattered peaks or bands.

It is known that pure crystalline materials present well defined resonant frequency, so the scattering is a perfect peak, tending to a Kronecker delta. As the crystallinity, this is the degree of structural order in the solid, is reduced, instead of having a Kronecker delta, the peak will tend to a Lorentzian one. As the material becomes amorphous, the Raman scattering will be represented by a Gaussian band.

The list of scattering peak and band for different materials, has been elaborated since the first usage of the spectroscopic technique. The list is not finished, nor the discussion about the accurate identification of the scattering source. Table 5 presents a list of Raman scattering peaks and bands due to different carbon species.

By the identification of the Raman peaks or bands, the composition of the material can be achieved. Nevertheless, most of the materials, as it is the case of diamond coatings, are not composed of one single scattering source, but a mixture of sources. In CVD polycrystalline diamond films, associated to the diamond crystals, graphite and amorphous carbon are most often also present. In these cases, the Raman spectrum will be a convolution of the different sources of Raman dispersion, and disconvolution can be useful to understand the acquired spectrum. Disconvolution is normally possible by Lorentzian and Gaussian functions. Several commercial software's offer this possibility.

Table 5 - Raman scattering of carbon materials

Scattering Center (cm^{-1})	Peak/Band	Scattering source	Ref.
1140	Peak	Nanocrystalline diamond	[91]
1140	Band	Diamond precursors (sp^2 disordered carbon)	[92]
1150	Peak	Nanocrystalline diamond	[93]
1200	Band	Graphite phonons from the K zone boundary	[93]
1200	Band	Amorphous glassy Carbon	[94]
1280	Band	Disordered graphitic Carbon	[94]
1300	Band	Amorphous glassy Carbon	[94]
1326	Peak	Hexagonal diamond	[93]
1331	Peak	Natural Diamond	[93]
1333	Peak	Polycrystalline diamond	[93]
1350	Peak	Microcrystalline graphite	[93]
1350	Band	Carbon with a high disordered order	[93]
1350	Band	Microcrystalline graphite (D band)	[93]
1355	Band	Diamond Like Carbon (DLC)	[93]
1357	Peak	Polycrystalline graphite	[93]
1357	Band	Vitreous carbon	[93]
1360	Band	Disordered graphite	[93]
1360	Band	Graphite D band	[94]
1380	Band	CH_3 group phase deformation vibrations	[93]
1400	Band	CH_2 group anti-phase deformation vibrations	[93]
1415	Peak	Luminescence peak	[94]
1450	Band	Amorphous carbon or DLC	[93]
1470	Band	CH_3 group anti-phase deformation vibrations	[93]
1470	Peak	Nanocrystalline diamond	[93]
1480	Band	sp^2 amorphous phase structures	[95]
1490	Band	Diamond precursors (sp^2 disordered carbon)	[93]
1500	Band	Amorphous carbon	[93]
1500	Band	Polyacetylene (PA)	[94]
1510	Band	Bridged graphite or diamond	[93]
1530	Band	Amorphous Carbon	[94]
1530	Band	sp^2 bonded carbon	[93]
1550	Band	Amorphous carbon or DLC	[93]
1550	Band	DLC	[94]
1550	Band	Carbon without no diamond structure	[93]
1560	Band	Bridged graphite or diamond	[93]
1560	Band	Graphite (G band)	[93]
1560	Band	Carbon phases with inclusions of structures similar to graphite (graphite like carbon)	[93]
1560	Band	Amorphous carbon duplet	[93]
1580	Peak	Microcrystalline graphite	[93]
1580	Peak	Graphite (crystalline, hexagonal crystalline and natural)	[93]
1580	Band	Vitreous carbon	[93]
1580	Band	Diamond Like Carbon (DLC)	[93]
1580	Band	Graphite G band	[94]
1581	Peak	Graphite (crystalline and hexagonal crystalline)	[93]
1590	Band	Microcrystalline graphite (G bands)	[93]
1600	Band	Carbon with a high disordered order	[93]
1610	Band	Amorphous carbon duplet	[93]
1610	Peak	Microcrystalline graphite (D band)	[96, 97]
1620	Peak	Microcrystalline graphite	[93]
1690	Band	Tetrahedral amorphous Carbon	[94]

In diamond films, Kulisch et al. [98] presented a semi-quantitative measurement (see equation 11) of the quality of the films from the ratio between diamond phases and non-diamond phases, obtained from the disconvoluted data.

$$Q = \frac{I_{diamond}}{I_{diamond} + \sum I_{non-diamond}} \quad (11)$$

where Q is the quality factor of the diamond film, $I_{diamond}$ is the intensity of the Raman diamond peak (at 1333 cm^{-1}), and $I_{non\text{-}diamond}$ is the intensity of the non-diamond peaks or bands. It is worth noting that pure crystalline diamond has a quality factor of 1.

Other authors, such as Silva et al. [99], use a similar equation, but instead of the intensity of the peaks or bands, they use the area of the diamond peak and the sum of the areas of the non-diamond peaks or bands. Other approaches have been listed in the literature [100]. In what concerns the study here reported, the quality factor is determined as presented in equation 11.

Materials are often subjected to stress of diverse sources. In the case of diamond coatings, the films residual stress, this is the stress that remains after the original cause of the stresses has been removed, results from the sum of three main sources: the thermal stress, originated by the difference in thermal expansion coefficients between diamond and the substrate material; the intrinsic stress, which rises from the presence of different types of defects, grain boundaries, and impurities in the film; and the lattice mismatch stress, due to the difference in lattice parameter of the substrate and the film. From the three, thermal stress is found to be the dominant one [94].

The materials stress affects natural resonant frequency, creating deviation of it center. So the Raman shift of a known scattering center may then give an idea of the material stress.

Ager and Drory [95] first, and Ralchenko et al. [36] later, presented a quantification process for an experimental estimation of the coatings stress, from the shift of the diamond typical Raman peak positions.

Ager and Drory [95] proposed that when the diamond peak is divided in two, due to the singlet phonon and doublet phonon, the experimental estimation of the coatings stress, σ, measured in GPa, may be determined by:

$$\sigma = -1.08(\varphi_s - \varphi_0), \text{ for singlet phonon} \quad (12)$$

$$\sigma = -0.384(\varphi_s - \varphi_0), \text{ for doublet phonon} \quad (13)$$

Where φ_0 is the polycrystalline typical peak center, φ_s is the observed maximum of the singlet in the spectrum, and φ_d the maximum of the doublet.

Since most of the times the split of the Raman line due to singlet and doublet is not obvious, Ralchenko et al. [36] proposed that the observed peak position, φ_m, is located at the center between the singlet, φ_s, and the doublet scattering energy, φ_d, this is:

$$\varphi_m = \frac{1}{2}(\varphi_s + \varphi_d) \tag{14}$$

Combining equations 12, 13 and 14:

$$\sigma = -0.567(\varphi_m - \varphi_0) \tag{15}$$

The experimental estimation of the coatings stress can be, to some extent, compared to theoretical estimated values. The theoretical total stress, σ_T, present in the film can then be expressed as:

$$\sigma_T = \sigma_{th} + \sigma_{in} + \sigma_{lm} \tag{16}$$

where $\sigma_{th}$is the theoretical thermal stress, σ_{in} is the theoretical intrinsic stress and σ_{lm} is the theoretical lattice mismatch stress.

The presence of lattice mismatch stress (expected to be tensile) is rarely observed and it is negligible when compared to the thermal and intrinsic stress. [94]

The theoretical thermal stress, σ_{th}, originated by the difference in thermal expansion coefficients between diamond and the substrate material can be obtained by:

$$\sigma_{th} = \left[\frac{Y_d}{(1-\nu_d)}\right] \int_{T1}^{T2} (\alpha_s - \alpha_f) dT \tag{17}$$

where Y_d is diamond Young's modulus and ν_d is the Poisson's ratio of diamond α_s and α_f are the coefficients of thermal expansion of the substrate and film, respectively, and T1 and T2 are the room temperature and deposition temperature, respectively. [36, 94, 95]

Although the intrinsic stresses are due to impurities, structural defects, and grain boundaries, the grain boundaries have been identified as the dominant source of intrinsic stresses in diamond films [94].

$$\sigma_{in} \approx \left[\frac{Y_d}{(1-\nu_d)}\right] \frac{\delta}{d} \tag{18}$$

where δ is the constrained relaxation of the lattice constant of diamond (0.077 nm) and d is the average grain diameter of the diamond film. [94]

Typical diamond coatings, produced during this study, σ_{in} is at least 10% inferior than σ_{th}.

Slightly different approaches to determine the coatings stress can be found in the literature, some of them even more elaborated such as the method presented by Rats et al. [101]. For the present research work, the model presented by Ralchenko et al. [36] (see equation 15) was used.

The Raman scattering of the samples presented in this work, was assessed by a Raman ISA JOBIN YVON-SPEX T6400 spectrometer, at room temperature, equipped with an Ar ion laser with a wavenumber of 514.5 nm. Appropriate filter for spectrum acquisition was selected and it was used an acquisition time of 30 s. It was also used a Bruckner RFS 100/S FT-Raman spectrometer system equipped with an Nd:YAG ion laser with a wavenumber of 1064 nm, at room temperature, for carbon diffusion into steel experiments.

X-ray Diffraction Spectroscopy

X-ray Diffraction Spectroscopy (XRD) is a non-destructive analytical technique, based on the observation of the scattered intensity of an X-ray beam hitting a sample as a function of incident and scattered angle, polarization, and wavelength or energy, which reveal information about the crystallographic structure (crystallite size and preferred orientation in polycrystalline samples, such as CVD diamond [102]), chemical composition, and physical properties of materials and thin films. [103]

When a monochromatic X-ray beam, with precise wavelength, is projected onto a crystalline material at certain angle, diffraction occurs only when the distance traveled by the rays reflected from successive planes, differs by a complete number of wavelengths. By varying the projected angle, the Bragg's Law conditions are satisfied by different d-spacings in polycrystalline materials:

$$n\lambda = 2d\sin\theta \tag{19}$$

where n is an integer determined by the order given, λ is the wavelength of the X-ray, d is the spacing between the planes in the atomic lattice, and θ is the angle between the incident ray and the scattering planes.

Plotting the angular positions and intensities of the resultant diffracted peaks of radiation produces a pattern, which is characteristic of the sample. If the sample is not monocrystalline, a mixture of different phases is present, the resultant diffractogram is formed by the addition of the individual patterns.

The obtained diffracted peaks can be compared with the database of crystallographic diffraction data, maintained by International Centre for Diffraction Data (ICDD), and so the composition of the sample being studied may be determined. Table 6 presents the crystallographic XRD data for diamond, CrN and FeCr.

The letters h, k, and l of table 6, represent the Miller Indices, a set of numbers which quantify the intercepts and thus may be used to uniquely identify the plane or surface, and in the present case, represent the crystallographic orientation of the material being studied. It should be noted that (220) equivalent to (110), (222) equivalent to (111) and (400) equivalent to (100).

In the scope of the work developed and presented here, X-ray diffraction was used for crystallinity characterization and morphology modification of the steel substrates.

The X-ray diffraction spectroscopy of the samples presented in this work, was performed by a Philips XPERT-MPD (now PANalytical), and the phase identification was assessed with the assistance of the search-match algorithm X'Pert HighScore software (PANalytical).

Table 6 - Diamond, CrN and FeCr crystallographic database [104]

	2θ	d (Å)	Int (%)	h	k	l
Diamond	43.9154	2.60000	100	1	1	1
	75.3018	1.261000	25	2	2	0
	91.4952	1.075400	16	3	1	1
	119.5215	0.891600	8	4	0	0
	140.587	0.818200	16	3	3	1
CrN	37.526	2.39480	84.2	1	1	1
	43.605	2.07400	100.0	2	0	0
	63.372	1.46650	44.0	2	2	0
	76.034	1.25070	18.3	3	1	1
	80.078	1.19740	10.9	2	2	2
FeCr	44.485	2.03500	100	1	1	0
	64.779	1.43800	20	2	0	0
	81.986	1.17430	50	2	1	1
	98.475	1.01700	18	2	2	0
	115.763	0.90950	30	3	1	0
	136.204	0.83020	12	2	2	2

Secondary Ion Mass Spectrometry

Secondary Ion Mass Spectrometry (SIMS) is a technique used to analyze the composition of solid surfaces and thin films by sputtering the surface of the specimen with a focused primary

ion beam and collecting and analyzing ejected secondary ions. These secondary ions are measured with a mass spectrometer to determine the elemental, isotopic, or molecular composition of the surface. [105]

SIMS is a very sensitive surface analysis technique, being able to detect elements present in the parts per billion range.

Dependent on the SIMS type, there are three basic mass analyzers available: sector, quadrupole, and time-of-flight. For the measurements done in the scope of this thesis, it was used a time of flight mass analyzer. The time of flight mass analyzer separates the ions in a field-free drift path according to their kinetic energy. It requires pulsed secondary ion generation using either a pulsed primary ion gun or a pulsed secondary ion extraction. It is the only analyzer type able to detect all generated secondary ions simultaneously and is the standard analyzer for static SIMS instruments.

The time-of-flight SIMS was performed for the acquisition of the depth profile of the samples being studied. It was accomplished by a VG ToF-SIMS (IX23LS) instrument. This system is based on Poschenrieder time-of-flight mass analyzer, equipped with a gallium pulsed-metal ion source (analysis) and duoplasmatron ion source for etching. Full positive SIMS spectra were acquired over a mass range m/z of 0-100 using a pulsed (5 kHz) 12kV Ga+ primary ion beam by rastering it over the etched area well in the crater spot. The duoplasmatron ion source was used at 8kV ion energy delivering sample current of approximately 500nA of oxygen ions.

Figure 18 presents a schematic representation of the spectroscopy techniques used in this work.

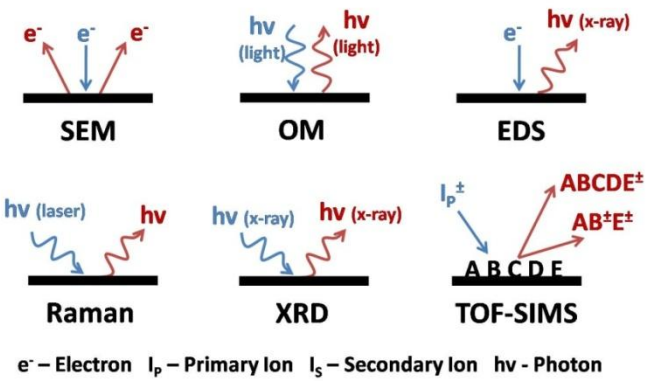

Figure 18 - Schematic representation of the spectroscopy techniques used. Adapted from [105]

Indentation Hardness

Hardness is a measure of a material's resistance to localized plastic deformation, such as a small dent or a scratch [16]. To perform a hardness measurement, an indenter is forced into the surface of the material to be tested, under controlled conditions of load and rate of application. The depth or size of the resulting indentation is measured, which in turn is related to a hardness number. The softer the material, the larger and deeper is the indentation, and the lower the hardness index number.

Solids generally have three responses to force, depending on the amount of force and the type of material: they exhibit elasticity (the ability to temporarily change shape, but return to the original shape when the pressure is removed); plasticity (the ability to permanently change shape in response to the force, but remain in one piece); and fracture (split into two or more pieces). Indentation hardness tests should be done with a load that goes to the plastic region of the material to give rise to a permanent deformation in the sample being tested.

Hardness measurement can be defined as macro-, micro- or nano- scale according to the forces applied and displacements obtained.

Measurement of the macro-hardness of materials is a quick and simple method of obtaining mechanical property data for the bulk material from a small sample. It is also widely used for the quality control of surface treatments processes. However, when concerned with coatings and surface properties of importance to friction and wear processes for instance, the macro-indentation depth would be too large relative to the surface-scale features. Where materials have a fine microstructure, are multi-phase, non-homogeneous or load can lead to the fracture region, macro-hardness measurements will be highly variable and will not identify individual surface features. It is here that micro-hardness measurements are appropriate. [16, 106]

Microhardness is the hardness of a material as determined by forcing an indenter such as a Vickers or Knoop indenter into the surface of the material under load inferior than 1000 gf. Microhardness is capable of determining hardness of different microconstituents within a structure, or measuring steep hardness gradients.

There are three major types of tests used with accuracy by the metals industry: Brinell hardness test; Rockwell hardness test; and Vickers hardness test.

Brinell hardness [16, 106, 107] is determined by forcing a hard steel or carbide sphere of a specified diameter under a specified load into the surface of a material and measuring the

diameter of the indentation left after the test. The Brinell hardness number (HB) is obtained as presented in equation 20:

$$HB = \frac{2P}{\pi D\left[D-\sqrt{D^2-d^2}\right]} \quad (20)$$

Where P is the applied load in kgf (1 kgf = 9.80665 N), D is the ball diameter and d is the indentation diameter, both in millimeters.

The depth, h, in mm, of a Brinell indentation can also be calculated from equation 21 [108]:

$$h = \frac{P}{\pi D[HB]} \quad (21)$$

Depth calculation is useful to determine the minimum sample thickness for a particular HB value. The sample thickness should be at least ten times the depth of the indentation. [108]

The Brinell hardness experiments performed during this study, were done according to DIN[10] 50351. According to this latter, the load $\frac{P}{D^2}$ must be such that the indentation mark d must be between 0.2 and 0.7 of D. Extensive tables can be found relating directly d to HB, in accordance with the standard sphere diameter.

The Rockwell hardness test [16, 106, 107] method consists of indenting the test material with a diamond cone or hardened steel ball indenter, depending on the scale being used (A, B, C, …). The indenter is forced into the test material under a preliminary minor load. When equilibrium has been reached, an indicating device, which follows the movements of the indenter and so responds to changes in depth of penetration of the indenter, is set to a reference position. While the preliminary minor load is still applied, an additional major load is applied with resulting increase in penetration. When equilibrium is again reached, the additional major load is removed but the preliminary minor load is still maintained. Removal of the additional major load allows a partial recovery, so reducing the depth of penetration. The permanent increase in depth of penetration, resulting from the application and removal of the additional major load, is used to calculate the Rockwell hardness number (HR):

$$HR = E - e \quad (22)$$

Where E is a constant depending on form of indenter: 100 units for diamond indenter, 130 units for steel ball indenter and e is the permanent increase in depth of penetration due to major load, measured in units of 0.002 mm. Rockwell Hardness numbers have no units and are commonly given with reference to the used scale.

[10] German Institute for Standardization

The procedure followed was according to DIN 50351 and the scale used was HRC. Table 7 presents the particular details of the used Rockwell indentation test scales.

Advantages of the Rockwell hardness method include the direct Rockwell hardness number readout and rapid testing time. Disadvantages include many arbitrary non-related scales and possible effects from the specimen support.

The Vickers hardness test [16, 106, 107] method consists of indenting the test material with a diamond indenter, in the form of a right pyramid with a square base and an angle of 136° between opposite faces subjected to a load of 1 to 100 kgf, in macro-indentation, and 15 to 1000 gf, in micro-indentation. The full load is normally applied for 10 to 15 seconds. The two diagonals of the indentation left in the surface of the material after removal of the load are measured using a microscope and their average calculated. The Vickers hardness is then given by:

$$HV = \frac{2P \sin\frac{136^\circ}{2}}{D^2} = 1.854\ \frac{P}{D^2} \quad (23)$$

Where P is the applied load in kgf, and D is the arithmetic average of the two diagonals, in mm. The Vickers hardness should be reported like AAA HV/BB, which means a Vickers hardness of AAA, obtained using a BB kgf force. Nevertheless, Vickers hardness can be expressed in$[kgf/mm^2]$, and hence converted to $Pascal$ by multiplying by 9.807×10^6.

Several different loading settings give practically identical hardness numbers on uniform material, which is much better than the arbitrary changing of scale with the other hardness testing methods. The advantages of the Vickers hardness test are that extremely accurate readings can be taken, and just one type of indenter is used for all types of metals and surface treatments.

Vickers microindentation test is carried out in a similar manner to the Vickers macroindentation tests, using the same pyramid but lower indentation loads, as stated above.

Table 7 - Particular details of HRA, HRB and HRC Rockwell scales [107]

Scale	Penetration Die	Initial Force	Total testing force	Main application range
HRA	Diamond cone with cone angle of 120°	98 N	588 N	Cemented carbides, thin steel and shallow case hardened steel
HRB	Ball with diameter of 1/16''	98 N	980 N	Copper alloys, soft steels, aluminium alloys, malleable irons, etc.
HRC	Diamond cone with cone angle of 120°	98 N	1471 N	Steel, hard cast irons, case hardened steel and other materials harder than 100 HRB

It must be noted that micro-indentation techniques require low roughness surface to achieve accurate results. To increase the results accuracy, it must be known that for any given load, the hardness increases rapidly at low diagonal lengths, with the effect becoming more pronounced as the load decreases. Thus at low loads, small measurement errors will produce large hardness deviations. Thus it should always be used the highest possible load in any test. Also, in the vertical portion of the curves, small measurement errors will produce large hardness deviations.

When micro-indenting polycrystalline diamond is concerned, it should not be ignored that although a diamond coating is only a couple of microns thick, it has the same nature than the indentation tip. To achieve good reproducibility, the degradation of the diamond indention tip should be regularly checked. Also, proper considerations must be given to the contributions from the film and the substrate material, when testing thin surface coatings [109].

During the present work, indentation hardness was used for the substrate and system (substrate, interlayer and film) hardness assessment, but also to evaluate the adhesion of the diamond films to the substrates.

The deformation imposed to the coated substrates may lead to the appearance of spalling or cracking around the indentation craters in the diamond film. The load/deformation that imposes the initial appearance of such features can give an indication of the adhesion of the diamond film to the substrate. [110-119]

As it can be depicted from figure 19, the load imposed to the film-substrate system can lead to the appearance of concentric ring cracks, lateral cracks and radial cracks. The concentric ring cracks are the first one appearing, due to the material dislocation under the indenter. The lateral cracks appear after some degree of deformation and give an indication of the level of adhesion of the film to the substrate. The lateral cracks may depend on the fracture resistance

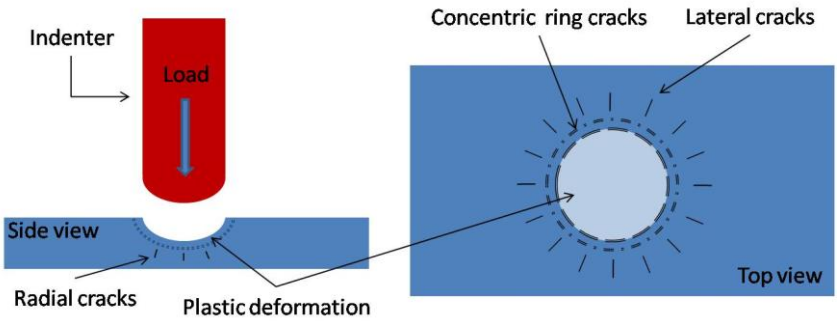

Figure 19 - Indentation and the appearance of cracks

and strength. The fracture resistance depends on the bonding across the interface and is a fundamental measurement of the adhesion. Strength is determined by the combined influences of the fracture resistance, defects and films residual stresses.

In the present study, an evaluation of diamond coatings adhesion was done by indentation testing employing a Brinell indenter. A range of indentation loads between 50 and 187.5 kgf where employed. SEM and Raman spectroscopy were used as a complement of the indentation tests. SEM to visually evaluate the cracks at high magnification and the Raman to evaluate stress levels. As the coating is released from the substrate, the stress due to the connections between the film and the substrate fade.

All the macro-indentation tests were performed in a Frank hardness tester Frankoskop 38180, with the appropriated indenters. The micro-Vickers indentations were achieved in a Shimadzu micro-hardness tester HMV-2000.

Surface profilometery

Surface profilometery is used to measure the surfaces profile, in order to quantify its roughness, by direct contact between a diamond stylus and a sample, as shown in figure 20. Roughness is the arithmetic average of the absolute values of the measured profile height deviations taken within the sampling length and, ensured from the graphical centerline.

The diamond stylus type profilometers are designed to respond only to irregularity spacing less than a given value, called the cutoff. In other words, all irregularities having a spacing less than the value of the cutoff are included in a measurement.

Surface profilometery was conducted in a Hommelwerke T1000 (Japan) surface profilometer.

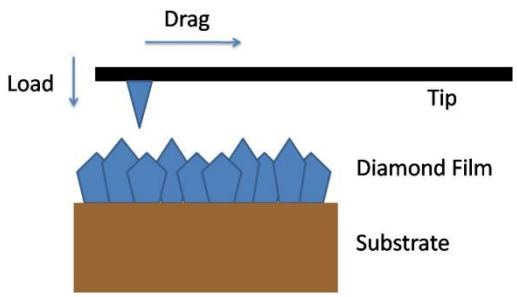

Figure 20 - Films roughness measurement principal

5. Thermoplastic injection molding

An important stage of the carbon-based coatings study for the modern plastics industry was the assessment of the diamond coated inserts suitability for thermoplastic injection molding.

Thermoplastic injection molding was performed in a EURO INJ D065, by Lien Yu Machinery Co LTD, injection molding machine. The latter has an intensification factor of the hydraulic pressure at the nozzle equal to 12.7. Further characteristics of the machine include: a screw diameter of 32 mm, maximum injection rate of 65 g/s, maximum injection pressure of 1777 bar, maximum injection stroke of 160 mm and maximum locking force of 65 ton.

The mold tool that accommodates the microstructured coated inserts was an already existing multi-cavity mold tool, where one of the cavities houses a 50 × 50 × 5 mm steel sheet in which appropriated holes were open to accommodate the testing samples, as it is illustrated in figure 21. This cavity allows for the testing of all the samples being evaluated in each injection cycle and thus at the same processing conditions.

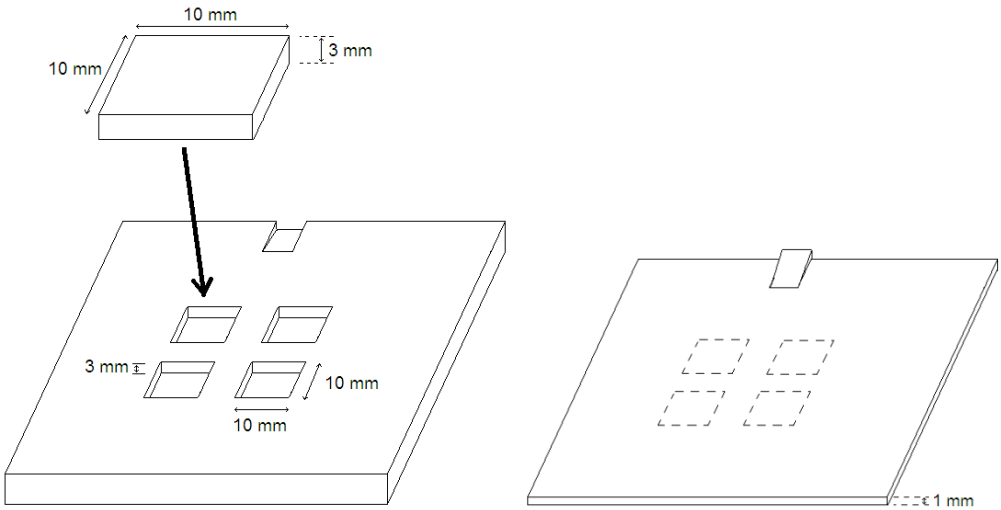

Figure 21 - Schematic drawings of the adapted mold tool (left) and the molded polimeric part (right)

The injection material selected for the experiments was High Density Polyethylene (HDPE) "Politeno HDPE IA-59 U3" (Braskem, Brasil). It offers high stiffness and impact strength, combined with good processability and low warpage. The characteristics were a density of 0.96 g/cm^3 (ASTM D-792), melt mass-flow rate (MFR) (190 °C/5 kg) at 7.3 g/10 minutes (ASTM D1238), a tensile strength at break of 25 MPa (ASTM D-638), a tensile strength at yield of 28 MPa (ASTM D-638), an izod impact resistance of 73 J/m (ASTM D 256) and a heat deflection temperature (HDT) of 81 °C at 0.45 MPa (ASTM D-648).

The HDPE injection temperature and pressure throughout this project was kept at 200 °C and 50 bar, respectively. A holding pressure was used for 5 s followed by a cooling time of 22 s, before the samples were extracted, as shown in table 8.

Table 8 - Cycle injection molding processing conditions

Parameter	Value
Injection pressure	50 bar
Melt temperature	200 °C
Hold pressure time	5 s
Cooling time	22 s

6. Thermoplastic parts evaluation

The polymeric samples molded by the diamond coated inserts and by other non-coated reference inserts were analyzed at naked eye, optical microscopy and the dimensions of three microstructured features were acquired using a coordinate measuring machine.

The naked eye observation provides a first evaluation of the piece being molded. Optical quality, such as brightness of the object, may be obtained in this way.

Further visualization was performed using optical microscopy, where both bright and dark field observations techniques were used, as described in previously in this chapter.

The optical microscopic images of the thermoplastic injected samples enabled the evaluation of the homogeneity of the surfaces and allowed for the comparison of the surfaces molded by the different coated and non-coated inserts.

Some 3-dimensional featured inserts were also tested in order to evaluate the diamond coating performance in a non-flat surface. For the dimensional stability evaluation of the microstructured features it was used a coordinate measuring machine.

Dimensional measurements

The dimensional stability of the molding insert and of the polymeric object is of utmost importance, in order to guaranty the molded parts quality and to comply with customer requisites.

A coordinate measuring machine is a device for dimensional measuring. It is an equipment where the movement of a measuring probe enables to monitor the coordinates of points on an object surface, assessing the dimensions of the object.

The machine uses an X-Y-Z grid to determine its position on a worktable. As the probe touches different spots on the part being measured, the X,Y,Z coordinates of each of these points are determined, and the dimensional details are recorded.

In the present work, it was used an Aberlink 3D MAXIM CNC with a Renishaw TP8 probe (1 mm ruby ball), control by Aberlink 3D control and measurement software. The dimensional trend was only measured for the polymeric injected objects, because it was not feasible to periodically measure the inserts. Nevertheless, the dimensional stability of the molding insert and of the polymeric objects are directly related to one another.

In the next chapter, it will be presented experimental work on the development of the diamond CVD coatings on steel substrates, which will provide tuned data to be used on the production of coated inserts to evaluate their performance as mold tools.

Chapter 4

Diamond CVD on steel substrates

1. Introduction

Diamond CVD on steel substrates has been discussed and its techniques and applications extensively reviewed. This chapter presents the work carried out in order to accomplish the objectives of this study. The experimental work and the techniques used will be fully described.

The first approach carried out was the direct deposition onto steel substrates. Diamond was deposited directly onto the steel substrates, only if enough deposition time was given in order to saturate the ferrous substrate with carbon, and then form the diamond crystallites. The resulting diamond coating exhibited very poor adhesion to the substrate.

The direct deposition on steel substrates was followed by the investigation of different interlayers, namely chromium nitride (CrN), titanium (Ti) and silicon (Si). The best performance was attained with CrN coating. The effect of the film thickness was also investigated and results achieved are presented.

It was also performed some depositions onto non-ferrous substrates materials, such as silicon wafers, in order to evaluate the suitability of this type of material to produce injection molding microstructured inserts.

2. Direct deposition on steel substrates

A first set of deposition experiments were performed directly onto AISI P20 modified steel, under different growth regimes and times, using both conventional and time modulated Chemical Vapor Deposition (CVD) processes. Conventional CVD means, in the context of the present work, a fixed flow rate of CH_4. The depositions were carried out in the hot filament CVD system, with a three filament setup.

The Time Modulated Chemical Vapor Deposition (TMCVD) was carried out for 2h00, at 5 and 2% CH_4/H_2 rates, with high pulses of 10 minutes and low pulses of 50 minutes, as presented in figure 22.

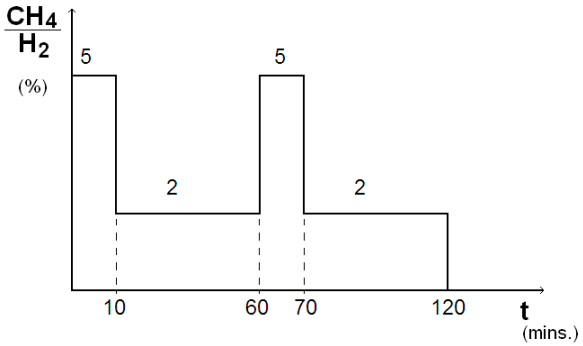

Figure 22 - TMCVD deposition conditions used

The conventional deposition was performed at 2% CH_4/H_2 rate, for 2h00. The common parameters for this set of experiments are presented in table 9. The substrate temperature was kept around 700 °C, in order to prevent important steel structural modifications.

Table 9 - Deposition conditions

Parameter	Value
H_2 flow (sccm)	150
CH_4 flow (sccm)	3 – 7.5
Base pressure (Torr)	2 x 10-2
Deposition pressure (Torr)	30
Substrate temperature (°C)	700
Filament power (W)	600
Filament-substrate distance (mm)	8

Prior to the deposition stage, samples were abraded in a polishing machine for 2 minutes, using 0.25 µm diamond paste, and then inserted in an ultrasonic bath composed of 10 ml isopropyl alcohol with 2 g of polycrystalline diamond powder (2–4 µm crystallite size) for 2h30. An additional cleaning was done with acetone, using an ultrasonic bath for 1 minute, to remove any non-adherent particles. Inside the CVD reactor, prior to the deposition stage,

samples were exposed for 5 minutes to hydrogen plasma, to enhance cleaning and remove any native oxide layers.

As expected, the direct diamond deposition onto steel did not produce a diamond coating, as it can be depicted from figure 23. Both deposition techniques (conventional CVD and TMCVD) produced an amorphous carbon layer.

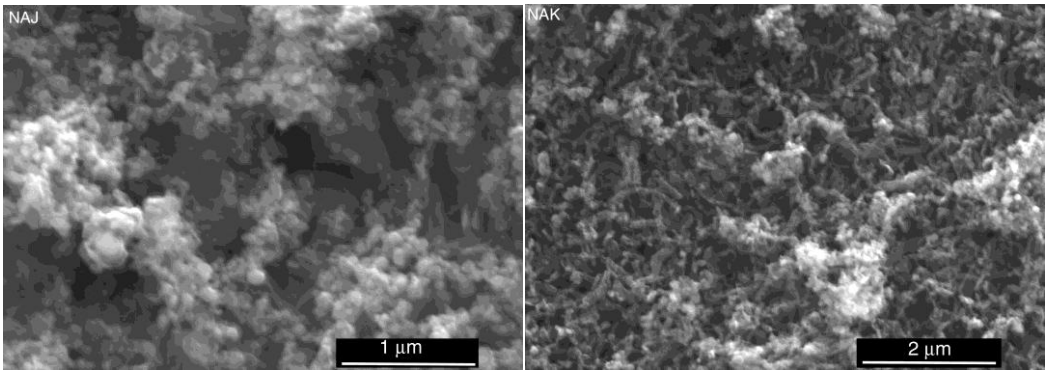

Figure 23 - SEM images of direct diamond deposition onto steel using conventional CVD (left) and TMCVD (right)

A third deposition was performed at a substrate temperature around 650 °C, using a 3% CH_4/H_2 gas rate for 10 minutes, followed by 16h50 deposition at 2% CH_4/H_2 rate. This sample was polished with diamond powder (2–4 µm crystallite size) for 5 minutes (using acetone as lubricant), plus 1 minute in acetone using ultrasounds to obtain deeper cleaning. This pre-treatment led to the formation of an uniform layer of carbon on top of the steel substrate.

The long deposition carried out, resulted in good diamond crystals with an homogeneous size and distribution, as it can be seen in figure 24. It must be noted that although a diamond coating was achieved with long deposition time, it was not a completely coalesced and homogeneous film.

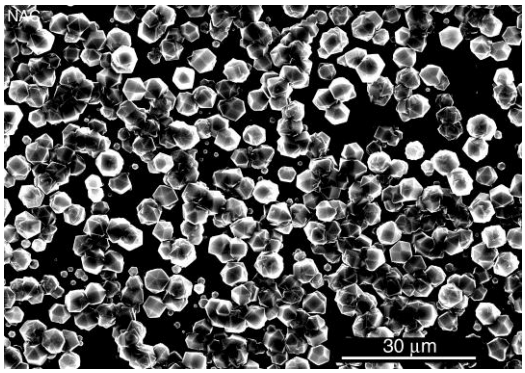

Figure 24 - SEM image of a 17h deposition directly into steel

Further experiments were performed in order to understand the diffusion mechanism of the direct deposition on steel.

Carbon diffusion into steel during diamond chemical vapor deposition

A new set of samples with no interlayer was prepared out of AISI P20 modified steel, with 10 x 10 x 2 mm. Prior to the deposition process, all samples were subjected to a grinding process with 500 and 1200 graded SiC paper, followed by 5 minutes cleaning in an ultrasonic bath with isopropyl alcohol.

The CVD general conditions can be seen in table 10 and the experimental details in table 11.

Table 10 - Deposition conditions

Parameter	Value
H2 flow (sccm)	200
CH4 flow (sccm)	4 – 6
Base pressure (Torr)	2 x 10-2
Deposition pressure (Torr)	30
Substrate temperature (°C)	700 – 850
Filament temperature (°C)	2100 – 2300
Filament-substrate distance (mm)	4

Table 11 - Experimental details

Sample	Deposition time (min)	Substrate temperature (°C)	$\frac{CH_4}{H_2}$ rate (%)
DCA01	30	700	2
DCA02	60	700	2
DCA03	120	700	2
DCA04	180	700	2
DCA05	120	850	2
DCA06	120	700	3

When analyzing the experimental samples, the diffusion depth can be measured, and the diffusion coefficient for this particular type of steel can be obtained.

According to the first law of diffusion [120], the transfer of solute atoms per unit area in a one-dimensional flow can be described by:

$$J = -D\frac{\partial C(x,t)}{\partial x} \tag{24}$$

where J is the particle flux, C is the concentration of the solute, D is the diffusion coefficient, x is the distance into the substrate, and t is the diffusion time. The negative sign indicates that the diffusing mass flows in the direction of the decreasing concentration. Combining equation

24 with the conservation of mass, the second law of diffusion can be derived (otherwise known as Fick's Law), which states:

$$\frac{\partial C}{\partial t} = D\frac{\partial^2 C}{\partial x^2} \tag{25}$$

In order to solve Fick's Law, initial and boundary conditions are required. Considering that this particular case can be represented by a semi-infinite medium, $x > 0$, where the boundary is kept at a constant concentration C_0 (the concentration of carbon in the surrounding atmosphere) and the initial concentration, C_0^{steel}, throughout the steel medium includes the carbon contents of the used steel, this is: $C_x = C_0^{steel}$ for $t = 0$ and $C_x = C_0$ for $x = 0$. Using the initial and boundary conditions and a Laplace transform, a solution of the following form may be obtained:

$$\frac{C_x - C_0}{C_0^{steel} - C_0} = erf\frac{x}{2\sqrt{Dt}} \tag{26}$$

where erf is the error function, a standard mathematical function with extensive look up tables available in literature, and D is the diffusion coefficient, that is dependent on the temperature and is determined by a typical Arrhenius equation, $D = D_0 exp\left(-\frac{Q}{RT}\right)$, where D_0, is the maximum diffusion coefficient (at infinite temperature) in $[m^2/s]$ unit; Q is the activation energy for diffusion in $[J/mol]$ unit; T is the absolute temperature in $[K]$ and R, is the universal gas constant $\left(8.314\ {}^{J}/_{mol.K}\right)$. Diffusivity data, as the values of D_0 and Q for different metallic systems are available in the literature [120].

From equation 26, an estimate can be obtained for the value for diffusion depth, h, the diffusion coefficient or the diffusion time, once the other two are known. Taking into consideration that $C_h = C_0$, then:

$$erf\frac{h}{2\sqrt{Dt}} = 1 \Longrightarrow \begin{cases} erf(z) = 1 \Leftrightarrow z = 0.8427 \\ z = \frac{h}{2\sqrt{Dt}} \Leftrightarrow h = 2z\sqrt{Dt} \end{cases} \Longrightarrow h = 1.6854\sqrt{Dt} \tag{27}$$

From figure 25 and table 12, the average diffusion depth per unit of time can be determined being approximately $21.1 \pm 5.6\ \mu m/hour$. Then using equation 27, the diffusion coefficient for the used steel can be calculated and the value of $6.03 \times 10^{-14} \pm 1.24 \times 10^{-14}\ m^2/s$ can be obtained. Sample DCA05 was not used for this calculations, as it will be explained ahead.

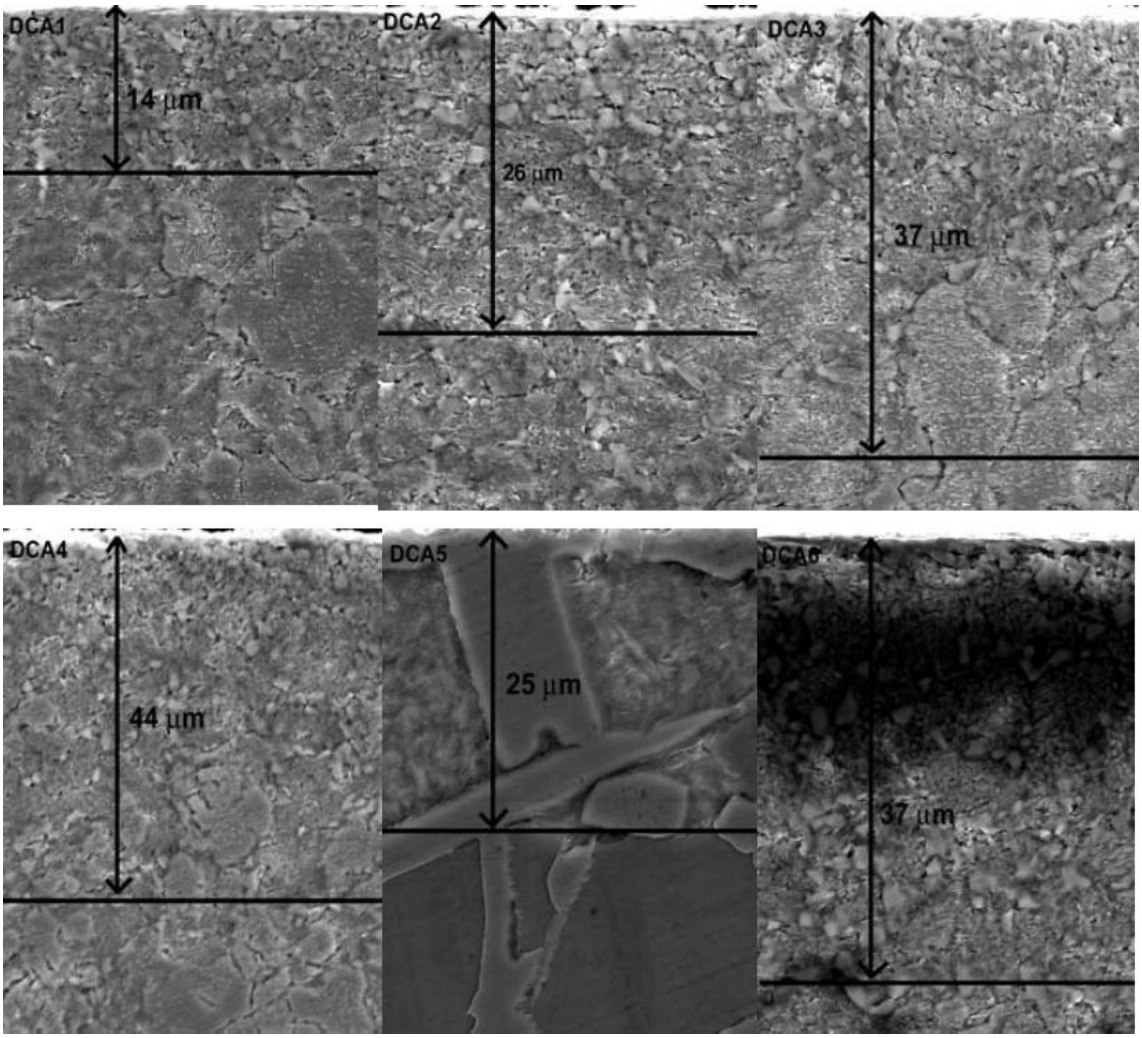

Figure 25 - SEM image of the carbon diffusion into the substrate of sample DCA01, DCA02, DCA03, DCA04, DCA05 and DCA06 after carbon CVD deposition

Table 12 - Measured mass increase and diffusion depth

Sample	Mass increase (g)	Diffusion depth (µm)
DCA01	0.0015	14
DCA02	0.0017	26
DCA03	0.0026	37
DCA04	0.0029	44
DCA05	0.0199	25
DCA06	0.0036	37

The diffusion depth can also be measured by surface analysis by SIMS with depth profiling. The relative ion emission was calculated from positive TOF-SIMS spectrums at each point. As it can be seen in figure 26 and in accordance with the SEM visual measurements, carbon diffusion depth increases with increasing time at constant temperature and C^+ and C_2^+ switch between each other with time at constant temperature. The incorporation of hydrogen in the diffusion

path cannot be neglected, having a considerable percentage in the sample with shorter deposition time.

The SEM image also reveals further information regarding the morphology of the steel. This particular AISI P20 modified steel (PM300 from *F. Ramada, Aços e Indústrias, S.A.* [68]) is delivered in a hardened and tempered to 290 – 330 HB (~65 – 68 HRA) condition. Even on the sample DCA04 submitted to 700 °C for three hours, no significant morphological changes were detected. However, in what concerns sample DCA05, submitted to 850 °C for two hours, martensite and bainite phases appear. Martensite is known to block the carbon diffusion, as it can be seen in figure 25 (sample DCA05) and as a result, a carbon layer is more rapidly formed on top of the substrate, this being the reason for the significant mass increase (see table 12). The morphological modification on this sample is also observable in the XRD spectrum, presented in figure 27. Sample DCA05 presents a $Fe_4Mn_{77}Si_{19}$ phase, not detectable in any other sample.

Raman spectroscopy of the tested samples, presented in figure 28, are, as expected, very similar to one another, presenting mainly three bands centered at 1280 cm^{-1}, 1580 cm^{-1} and 1605 cm^{-1}, as it can better be seen in the deconvoluted lines. The peak at 1280 cm^{-1} is not clearly assigned, but some authors consign it to a defect activated phonon absorption, which is observed in natural diamond [94, 95], the 1580 cm^{-1} is attributed to microcrystalline graphite, graphite or vitreous carbon [93] and the 1605 cm^{-1} to microcrystalline graphite (D' band) [96, 97].

The Raman scattering of this samples was assessed at room temperature using a Bruckner RFS 100/S FT-Raman system equipped with an Nd:YAG ion laser with 1064 nm of wavelength.

Vickers micro-hardness and Rockwell A hardness were conducted in order to complement the information on the morphological changes due to the treatment procedure. Vickers micro-hardness provides us information on the hardness of the first micrometers of the samples surface.

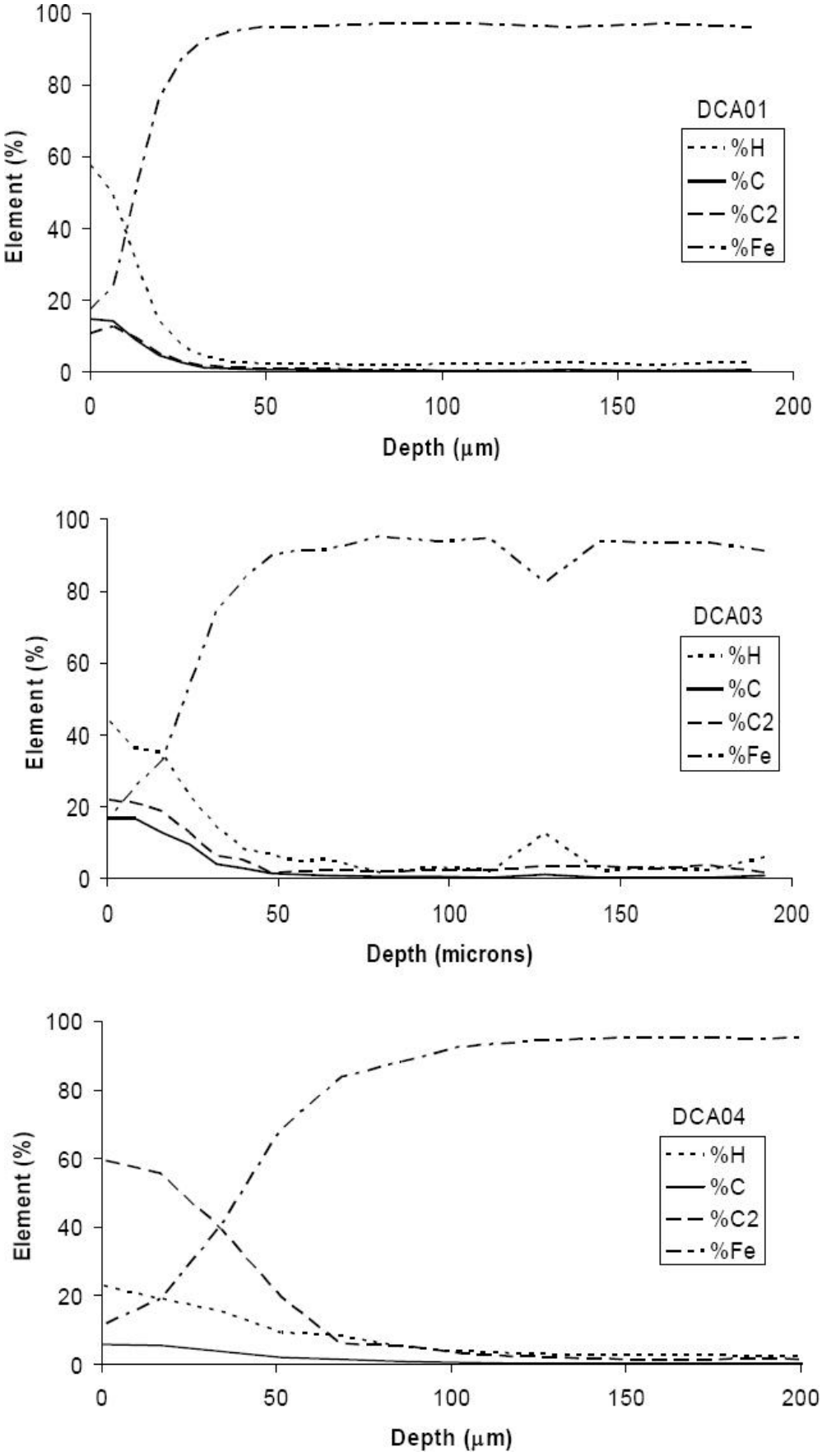

Figure 26 - Relative concentrations of hydrogen, carbon, C2 and Fe depth profile of samples DCA01, DCA03 and DCA04, by SIMS

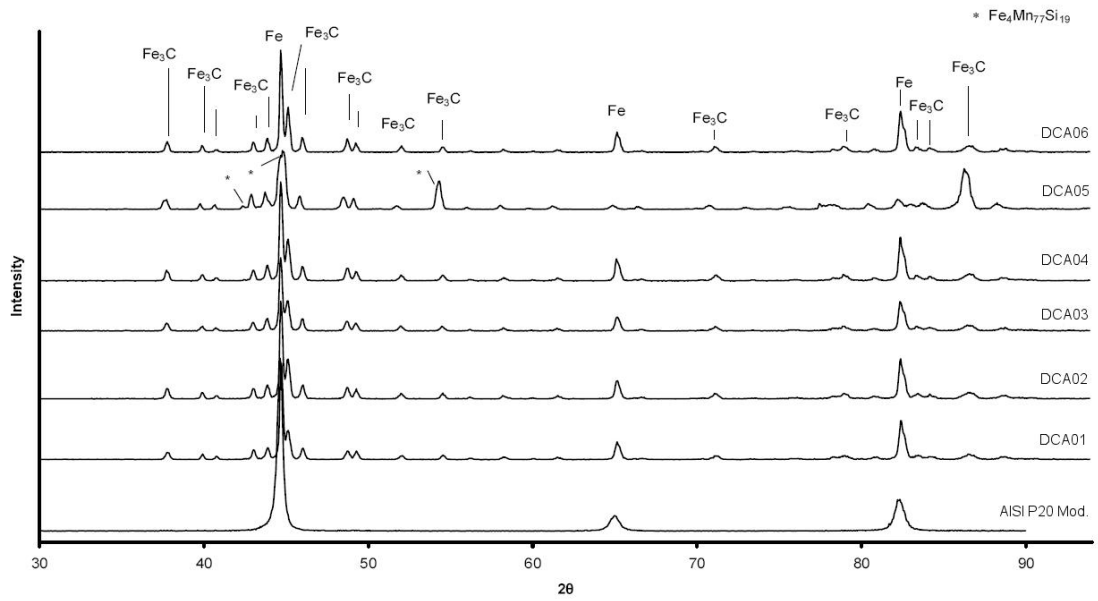

Figure 27 - X-ray diffraction of the diffusion samples

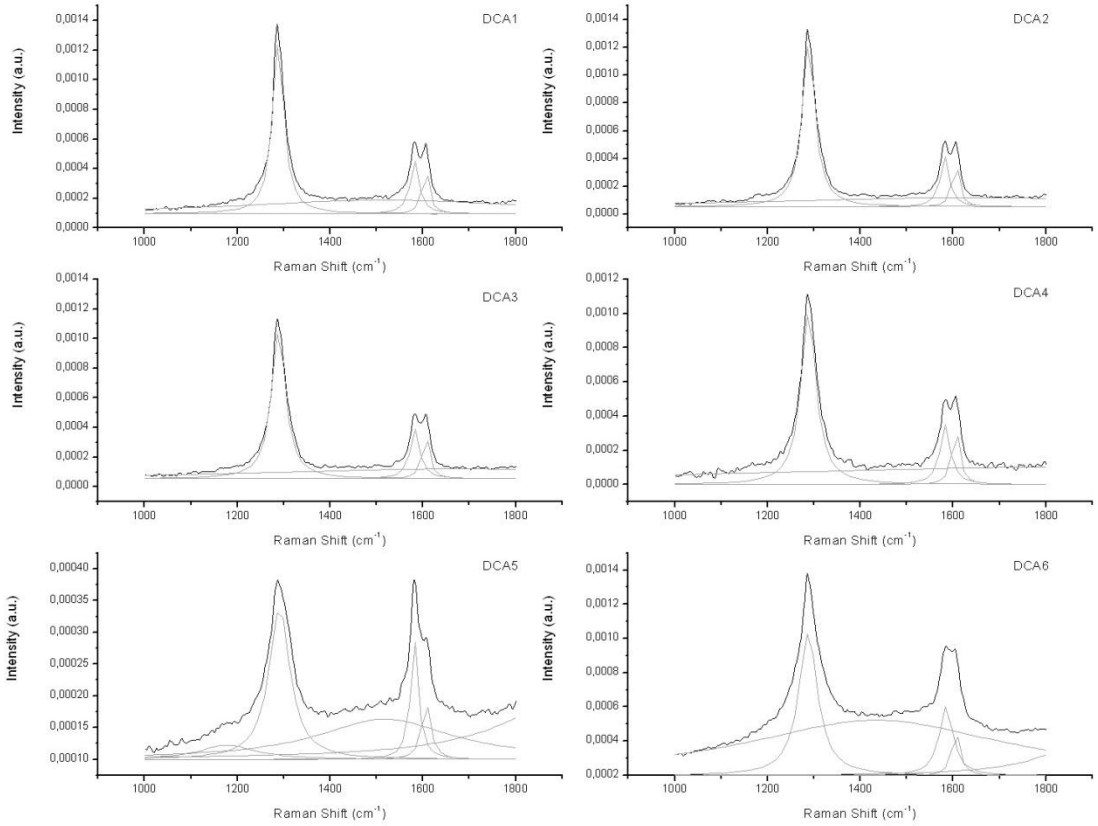

Figure 28 - Raman spectrum of the tests samples

Both Vickers micro-hardness (see figure 29) and Rockwell A hardness (see figure 30) show that the hardness of the samples subjected to the CVD process, increased from 225 HV (2207 MPa) to a minimum value of 339 HV (3325 MPa), in DCA01, and a maximum value of 457 HV (4482 MPa), in DCA04, and from 67.2 HRA (~1014 MPa) to a minimum value of 70.7 HRA (~1220 MPa), in DCA05, and a maximum value of 78.2 HRA, in DCA03(~1772 MPa), respectively.

In both the procedures, the hardness rised with the increased diffusion depth (increased CVD time). Due to the different amplitude of the test, DCA05 presents a high micro-hardness value and a low hardness value, confirming the observations referred above about this sample.

Vickers micro hardness measurements were made using a force of 200 gf and a holding time of 10 seconds. Rockwell A hardness was conducted using the HRA scale (cone-shaped diamond indenter of 120° cone angle, total force of 60 kgf).

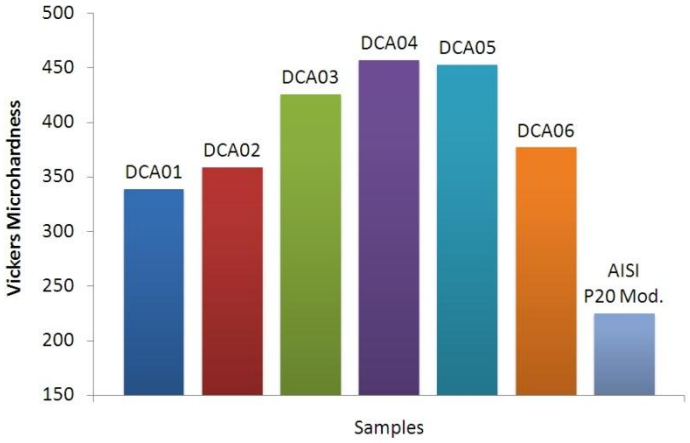

Figure 29 - Vickers micro-hardness

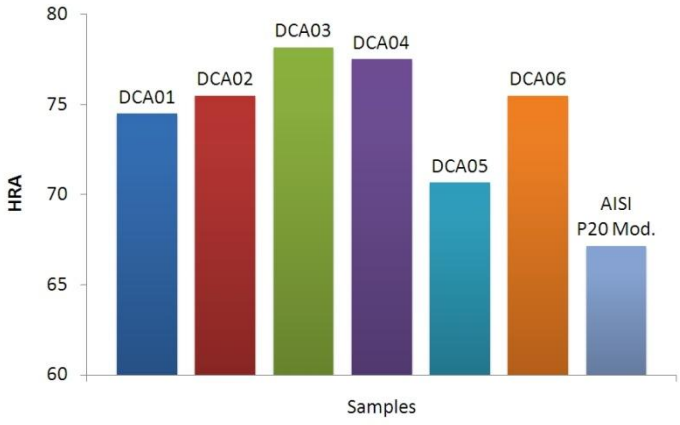

Figure 30 - Rockwell A hardness

The results clearly demonstrate that diffusion mechanism is the only process taking place in the sample substrate during the direct attempt to deposit CVD diamond. Therefore, during diamond CVD, the carbon diffuses into the steel substrate, forming a soot composed of graphite, Fe_3C and other carbides, leaving relatively little carbon precursor at the steel surface to initiate the diamond nucleation sites. When the substrate face layer is supersaturated, diamond nucleation may occur and eventually poor adhered diamond film may grow.

The literature reports the usage of interlayers to block the diffusion of carbon to the steel substrate and the Fe to the diamond coating. The following work addresses the issue and reports on the approach undertaken to investigate the use of interlayers for depositing diamond films on steel substrates.

3. Use of interlayers for the deposition on steel substrates

In a new group of AISI P20 modified steel samples, titanium (Ti) and chromium nitride (CrN) were deposited using a commercial PVD system, and silicon (Si) was deposited using a research CVD system. These coating materials were selected based upon the good resulted reported in the literature, and also due to its availability.

The interlayer coated samples were subjected to diamond deposition conditions, using both conventional and TMCVD processes, at the hot filament CVD system, with a three filament setup.

The TMCVD was carried out for 2h00, with 5 and 2% CH_4/H_2 rate, with high pulses of 10 minutes and low pulses of 50 minutes, as presented previously in figure 22. The conventional deposition was performed at 2% CH_4/H_2 rate, for 2h00. The common parameters for this set of experiments were presented previously in table 9. The substrate temperature was kept around 700 °C, in order to prevent important steel structural modifications.

Prior to the deposition stage, samples were abraded in a polishing machine for 2 minutes, using 0.25 µm diamond paste, and then inserted in a ultrasonic bath composed of 10 ml isopropyl alcohol with 2 g of polycrystalline diamond powder (2–4 µm crystallite size) for 2h30. An additional cleaning was done with acetone, using ultrasounds for 1 minute, to remove any non-adherent particles. Inside the CVD reactor, prior to the deposition stage, samples were exposed for 5 minutes to hydrogen plasma, to enhance cleaning and remove any native oxide layers.

The samples coated with silicon did not stand the deposition conditions. Silicon evaporated from the samples surface and they were abandoned. In what concerns the samples with Ti and CrN interlayers, diamond coatings were achieved with both the conventional and time-modulated processes.

In the insert of figure 31 (left) that corresponds to the Ti interlayer using conventional CVD, a diamond coating can be observed, and it can also be depicted the presence of amorphous carbon. In the time-modulated CVD sample, figure 31 (right), the morphology is completely different. From the lower magnification image, it becomes clear the appearance of secondary nucleation sites, on top of the previous diamond layer. From the high magnification insert, the typical hexagonal geometry diamond crystals that correspond to diamond (111) oriented crystals, can be observed.

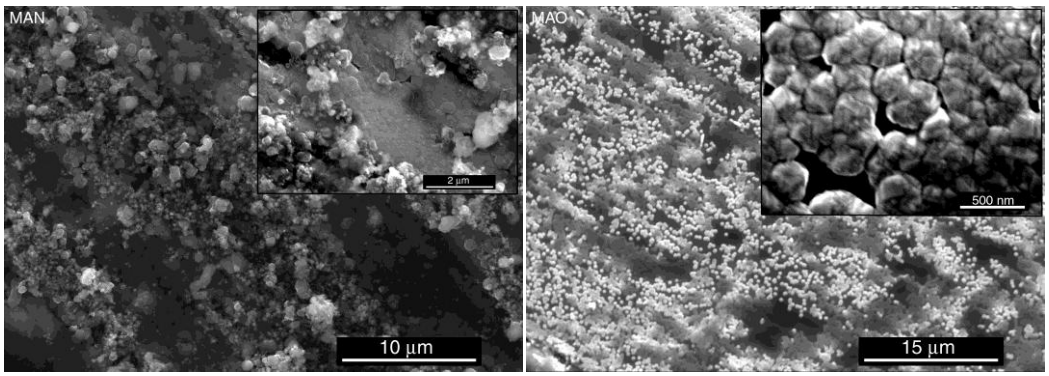

Figure 31 - SEM images of diamond deposition onto steel with titanium interlayer using conventional CVD (left) and TMCVD (right)

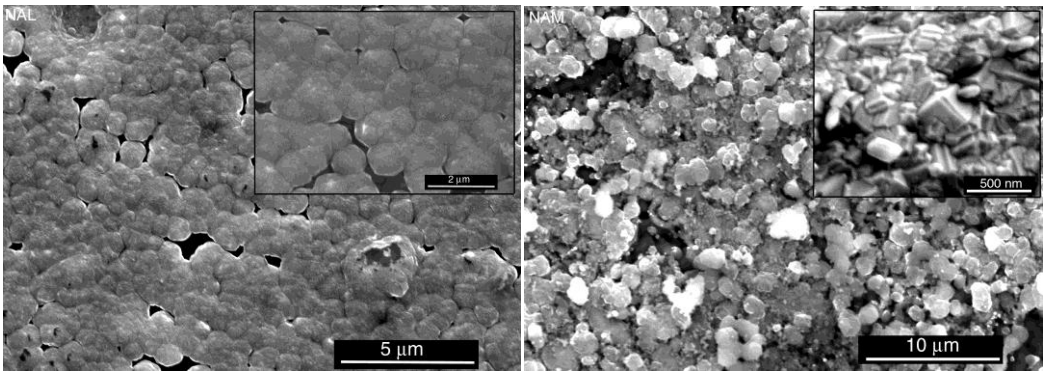

Figure 32 - SEM images of diamond deposition onto steel with chromium nitride interlayer using conventional CVD (left) and TMCVD (right)

From the results obtained during this study, it appears that the deposition on steel samples with CrN interlayer, via conventional or time-modulated CVD, presents better results than the ones obtained using Ti interlayers.

The conventional deposition on the sample with CrN, which can be seen in figure 32 (left), displays a continuous film coating, composed of diamond crystals of an average size of less than 1 µm. It is evident from figure 32 (left) that a ballas like structure is formed. It is most likely that the ballas consists of nano-sized diamond crystallites [121].

The time-modulated sample, as seen in figure 32 (right), exhibits an homogenous and continuous polycrystalline film coating. The polycrystalline film displays predominantly (111) crystal orientation.

Extensive studies of the CrN interlayers will be presented in the next sub-chapter.

4. Deposition using CrN interlayers

The literature has highlighted several successful attempts where chromium nitride (CrN) interlayers were used. A broader range of steel materials were tested and different surface treatments and interlayer thicknesses were evaluated.

The steel materials tested include the stainless steels – austenitic chromium-nickel alloys AISI 304, 310 and 316, and a common steel used for mold tool production – AISI P20 modified. All four different steels were supplied by *F. Ramada, Aços e Indústrias, S.A.* [68].

A set of samples with the dimensions of 10 x 10 x 3 mm was prepared. All samples were prepared from steel blocks, by cutting and machining processes until the appropriate dimensions were obtained, a methodology used for all the steel samples used in this doctoral work. After this stage, the samples were subjected to mechanical polishing with SiC papers, up to a 2000 mesh, followed by an ultrasonic cleaning of 5 minutes with isopropyl alcohol.

Prior to diamond deposition, a commercial PVD CrN interlayer was deposited on the samples. An industrial Microcoat PVD-arc system equipped with a random arc source [72] was used to deposit a layer of CrN with around 2 µm in thickness according to product specifications.

Before diamond deposition, the samples coated with CrN were ultrasonically abraded during 2h30 in a 0.25 µm diamond powder suspension for diamond nucleation seeding, followed by 2 to 3 minutes of ultrasonic cleaning in isopropyl alcohol.

The CVD diamond films were deposited, using the hot filament CVD system, described in figure 11. The deposition total time varied from 4h30 (270 minutes) in deposition conditions identified as DEP1 and DEP2, to 9h00 (540 minutes) in deposition condition DEP3. Deposition condition DEP4 had a deposition total time of 6h45 (405 minutes). The time-modulation deposition process used a high $CH_4/\ H_2$ rates, for 15 minutes, of 3% in deposition conditions DEP2, DEP3 and DEP4 and 4% in deposition condition DEP1 and low $CH_4/\ H_2$ rates of 1% for 120 minutes in all the deposition condition, as presented in figure 33. During deposition, the single filament was kept at a temperature around 2100 °C, in order to activate the process gases (CH_4 and H_2).

Prior to each deposition, the samples were submitted to 10 minutes at 0.5% $CH_4/\ H_2$. This period was used to increase the temperature gradually until it reached its desired value, and to promote some surface etching before the nucleation of the first diamond crystallites, without the filament degradation. At the end of the deposition, 0.5% $CH_4/\ H_2$ gas rate was again used for 10 minute, in order to gradually lower the temperature and to accomplish some etching of the amorphous contents of the deposited film.

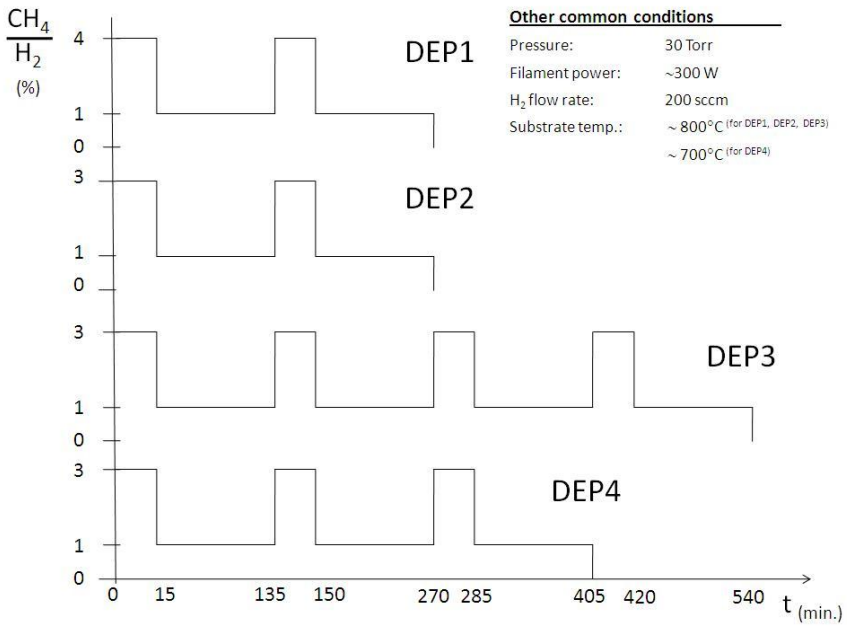

Figure 33 - Time-modulated CVD conditions used

Diamond deposition onto AISI 304 steel with CrN interlayer

In all the depositions carried out in AISI 304 steel with CrN interlayer, deposition times lower than 4h30 did not result in a fully closed and homogenous film. The latter were only obtained for more than 6h00 of deposition time. Figure 34 presents the SEM images of diamond deposition onto AISI 304 steel with chromium nitride interlayer using deposition conditions DEP1 and DEP4.

The SEM image of the diamond on AISI 304 steel with chromium nitride interlayer using DEP1 presents ~5 µm round crystals not fully covering the substrate. The (111) crystal orientation seems to be the preferential growth orientation.

The SEM image of the diamond on AISI 304 steel with chromium nitride interlayer using DEP4 presents an uniform surface, with an average crystal size of ~2 µm, with mainly (111) crystal orientation.

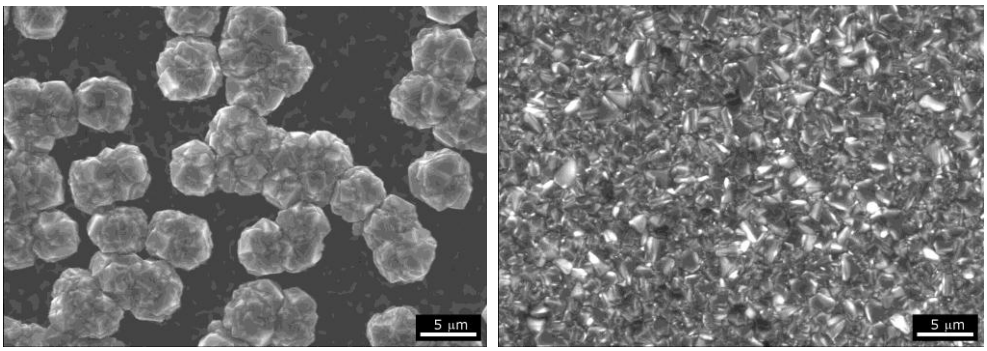

Figure 34 - SEM images of diamond deposition onto AISI 304 steel with chromium nitride interlayer using DEP1 (left) and DEP4 (right)

Diamond deposition onto AISI 310 and 316 steel with CrN interlayer

All the depositions carried out on AISI 310 and 316 steel with CrN interlayer result in a not properly closed film. Figure 35 presents SEM images of diamond deposition using DEP1 on AISI 310 steel and on AISI 316 steel with chromium nitride interlayer.

On these materials, not even the longer deposition conditions presented good results. Both substrates presented individual crystals similar to the ones presented by the AISI 304 steel with chromium nitride interlayer using DEP1.

AISI 310 and 316 steel samples did not present promising results for diamond growth, comparatively with the other tested materials. This may be due to their chemical composition

and properties, namely their high nickel (Ni) contents, as it can be seen in table 13. Nickel, such as iron and cobalt, is a strong carbon-dissolving material [29-34]. For the latter, those materials were abandoned.

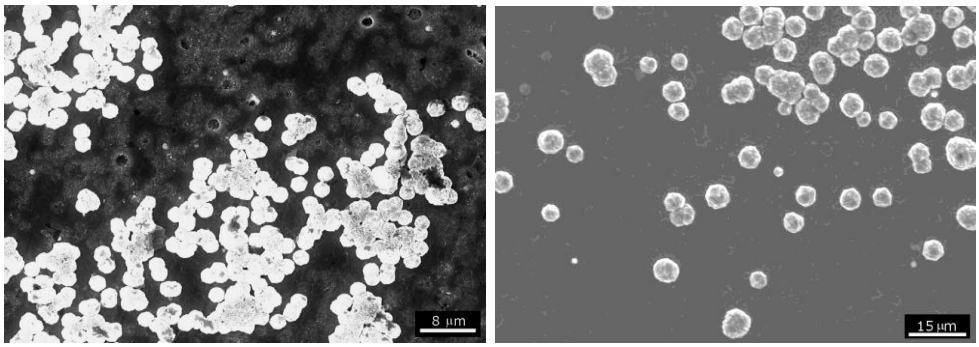

Figure 35 - SEM images of diamond deposition using DEP1 onto AISI 310 steel (left) and onto AISI 316 steel (right) with chromium nitride interlayer

Table 13 - Chemical composition of the AISI 310 and 316 steels [69]

Steel	C (%)	Si (%)	Mn (%)	Cr (%)	Mo (%)	Ni (%)	S (%)
AISI 310	0.20	1.50	2.00	25.00	-	20.50	-
AISI 316	0.08	1.00	2.00	17.50	2.50	12.00	-

Diamond deposition onto AISI P20 modified steel with CrN interlayer

Diamond deposition on AISI P20 modified steel with CrN interlayer almost always presented good results. As it can be seen from the SEM images presented in figure 36, all deposition conditions, from the shorter (DEP1 and DEP2) to the longer (DEP3), presented fully covered substrates with an uniform and homogeneous diamond film.

All the displayed films present an average crystal size of ~1 µm, with mainly (111) crystal orientation, although some (100) crystal may be found.

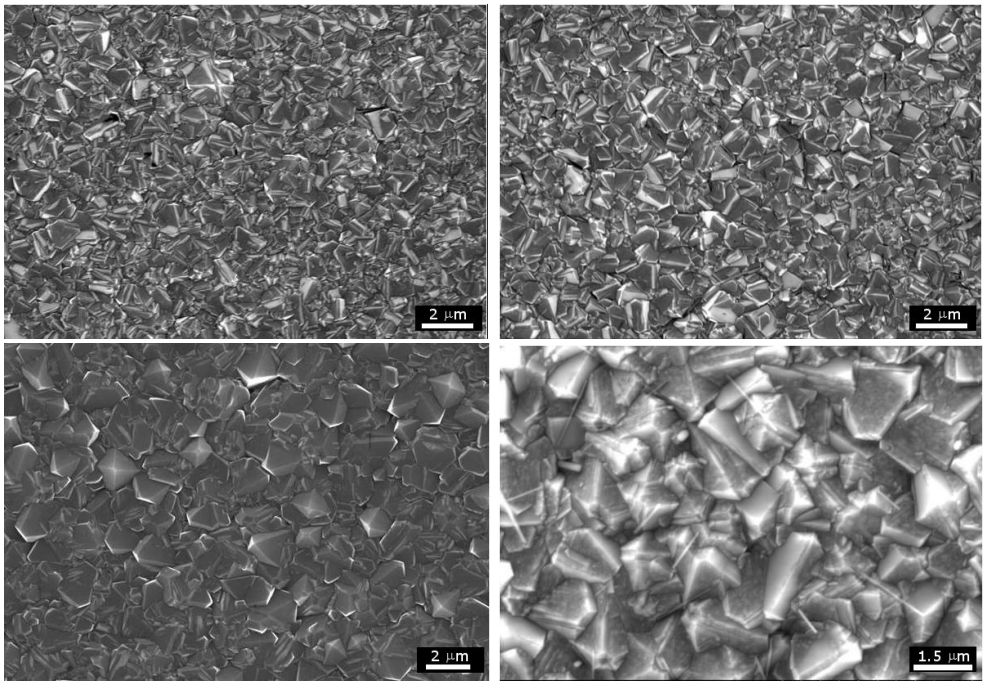

Figure 36 - SEM images of diamond deposition onto AISI P20 modified steel with chromium nitride interlayer using DEP1 (up-left), DEP2 (up-right), DEP3 (down-left), DEP4 (down-right)

Validation of the interlayer as a diffusion blocker

A bare CrN coated steel sample (without diamond deposition) was cut transversally to the surface and the cross-sections were analyzed in terms of elemental composition distribution on a section of around 6 µm, measured from the surface to the interior of the sample. Figure 37 shows the SEM and X-ray profile and map distribution of a AISI P20 modified steel sample with CrN. The profile represents an average of a measurement on 100 points. This number is a characteristic of the acquisition system. As illustrated, there are well defined layers that define the substrate and the interlayer.

The high iron (Fe) presence in the bottom of the CrN layer is a signal of inter-diffusion, which means a good bonding between CrN and the substrate, in a comparable process as the one reported by Bareiβ et al. [122] for TiBN-steel.

The effectiveness of the interlayer during the deposition is shown in figure 38, which presents the SEM cross-section image and the EDS map of an AISI 304 sample system after the deposition cycle DEP4 and an AISI P20 modified sample system after the deposition cycle DEP1. The samples were cut transversally to the surface and mounted in a cold-setting epoxy resin with the cut face to the top and polished with SiC paper to a mirror finishing.

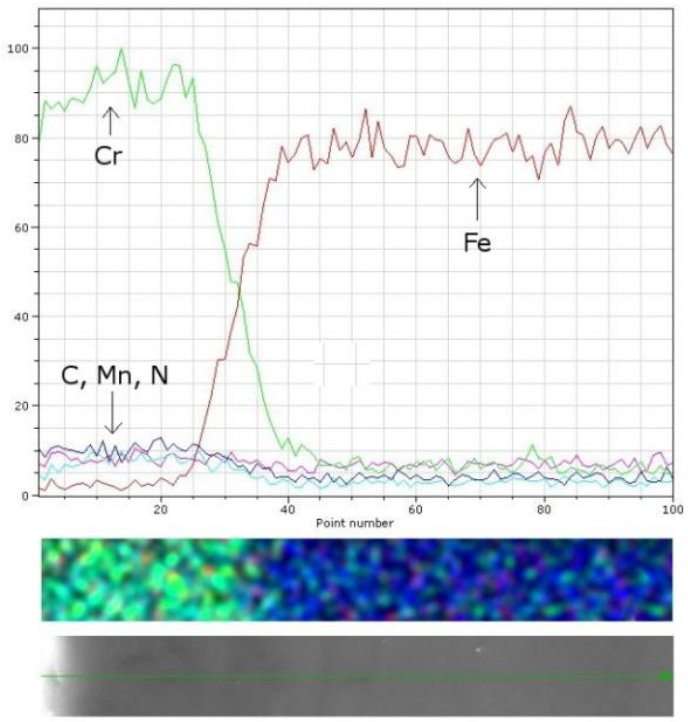

Figure 37 - SEM and X-ray profile and map of a P20 modified steel sample with a CrN interlayer

In all the studied samples, the Fe concentration decreases rapidly at the steel/CrN interface when Cr and N increase. At the diamond/CrN interface Fe is scarcely detectable. These data show that the CrN interlayer constitute an effective barrier from Fe and C diffusion during diamond deposition.

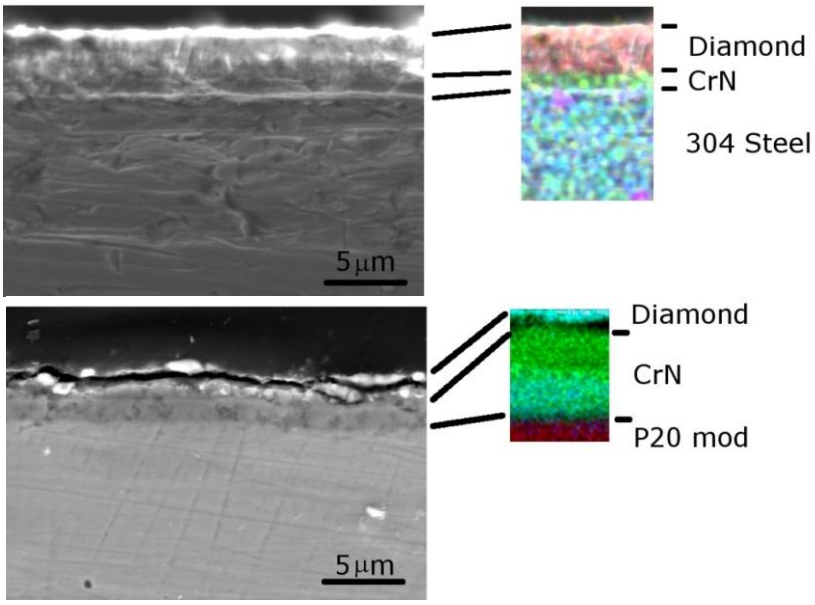

Figure 38 - Cross-section SEM images and EDS maps of diamond deposition onto AISI 304 steel with chromium nitride interlayer using DEP4 (up) and onto AISI P20 modified steel with chromium nitride interlayer using DEP1 (down)

Influence of CrN interlayer thickness on the deposition of diamond on steel

The relative influence of the interlayer thickness on the growth, quality and adhesion properties of diamond films growth on AISI P20 modified steel was also studied and is here reported.

A number of CrN coatings on steel with thicknesses in the range of 1.3 to 2.4 µm (see table 14) were coated by a random arc evaporation PVD system and then submitted to time-modulated CVD process.

Table 14 - Interlayer thickness

Sample	CrN layer (µm)
DC1	~1.3
DC2	~1.5
DC3	~1.8
DC4	~2.4

The samples, with 10 x 10 x 2 mm, were prepared out of AISI P20 modified steel. Prior to the diamond deposition, all samples were subjected to a 2h30 ultrasonic bath in 0.25 µm polycrystalline diamond solution, followed by a 2 minutes cleaning with isopropyl alcohol.

The deposition, carried out in the hot filament CVD reactor, started with a high flow of methane (3% $CH_4/\ H_2$ rate) for 10 minutes, followed by an 80 minute low flow (1% $CH_4/\ H_2$ rate), and again a new high and low concentration, for 10 and 80 minutes, respectively, for a total deposition time of 3h00. The diamond deposition conditions can be seen in table 15.

Table 15 - Diamond deposition conditions

Parameter	Value
Pressure (Torr)	30
Substrate Temperature (°C)	700
Filament Temperature (°C)	2100
Filament-Substrate Distance (mm)	10
H2 flow (sccm)	200
CH4 flow (low – high) (sccm)	2 – 6
High CH4 flow time (minutes)	10
Low CH4 flow time (minutes)	80
Deposition time (minutes)	180

Figure 39 shows the surface of the as-deposited diamond film on samples DC1, DC2, DC3 and DC4. It can be seen that the coating is composed mainly by (111) oriented crystallites and with an averaged crystal size of around 500 nm. Nevertheless, a closer observation of the SEM

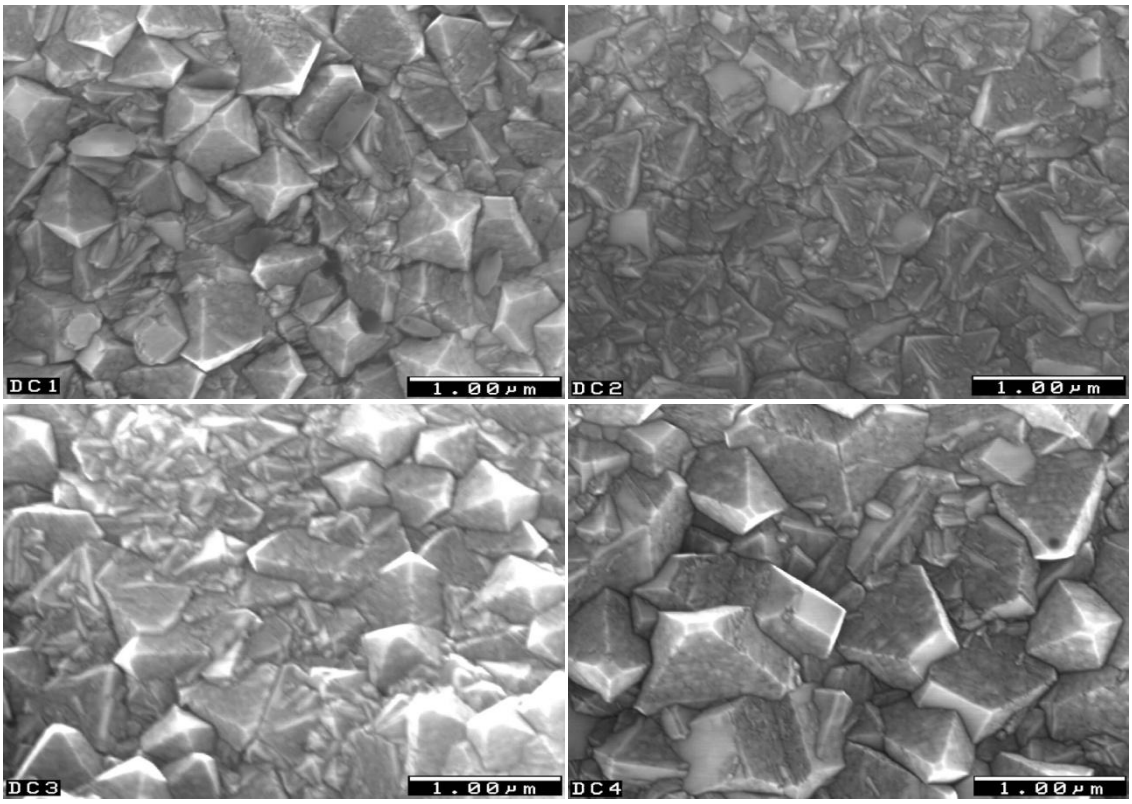

Figure 39 - SEM images of as-deposit diamond film on samples DC1, DC2, DC3 and DC4

images, can reveal some morphological differences, such as some (110) crystal in the sample with the higher interlayer thickness (DC4). The diamond thickness is estimated to be around 1.5 µm in all four samples.

From the Raman spectra of the diamond coating, shown in figure 40, the quality of the film can be assessed, in terms of diamond carbon-phase purity and the Raman shift of the diamond peak (residual stress of the coating) can be measured.

The measurement of the quality of the diamond film can be calculated from:

$$Q = \frac{I_{diamond}}{I_{diamond} + \sum I_{non-diamond}} \quad (11)$$

where Q is the quality factor of the diamond film, $I_{diamond}$ is the intensity of the Raman diamond peak (at 1333 cm^{-1}), and $I_{non\text{-}diamond}$ is the intensity of the non-diamond peaks or bands.

The calculated quality factor values for the diamond coatings are between 50 and 52% and can be seen in table 16.

It is known that CVD diamond typically exhibits a Raman peak centered at 1333 cm^{-1}, although this scattering center may shift to the right or to the left of the spectrum depending on the

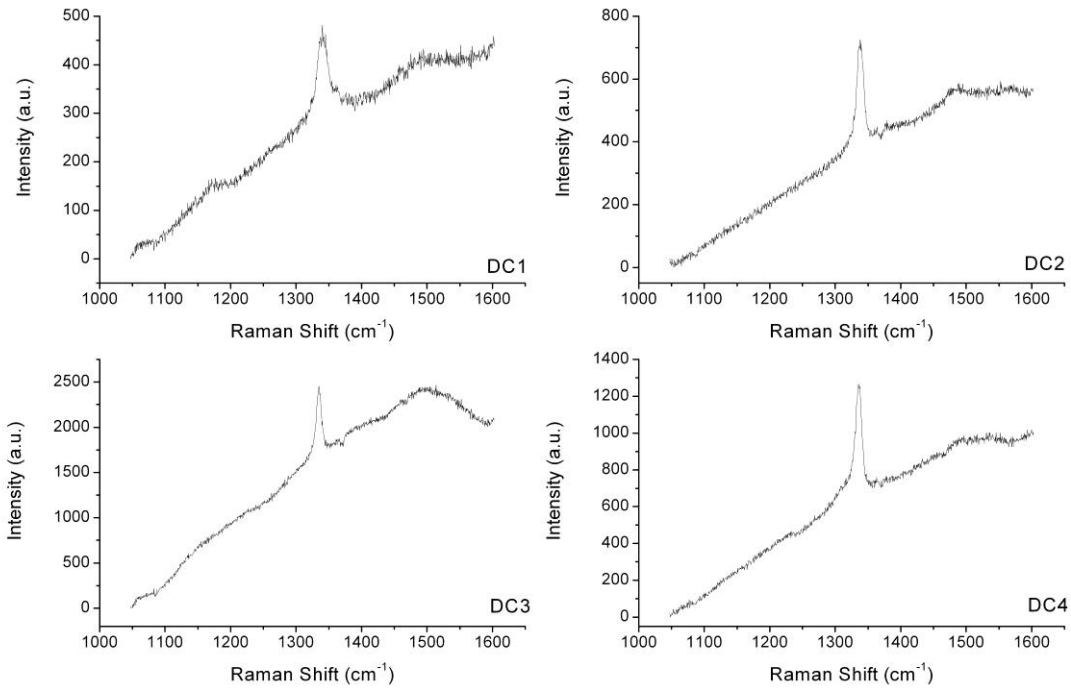

Figure 40 - Raman spectrum of the diamond coatings of samples DC1, DC2, DC3 and DC4

residual stress imposed by the difference in thermal expansion coefficients of the substrate and the film, or to the intrinsic stress due the columnar growth of the crystals [36].

The Raman peak shift can be transformed on an estimation of the residual stresses (σ), by:

$$\sigma = -0.567(\varphi_m - \varphi_0) \quad (15)$$

where φ_0 is the polycrystalline typical peak center and φ_m is the observed peak position.

The calculated residual stress values for the diamond coatings can be seen in table 16. It can be stated, from the results obtained, that the residual stresses are inversely proportional to the thickness of the interlayer.

Table 16 - Raman shift of the diamond peak, calculated residual stress and Raman quality factor

Sample	Raman shift (cm^{-1})	Residual stress (GPa)	Quality factor (%)
DC1	1340.44	-4.2	50
DC2	1338.14	-2.9	51
DC3	1335.38	-1.3	50
DC4	1335.84	-1.6	52

Figure 41 presents the acquired SIMS depth profiles for Fe^+, Cr^+ and C^+. Since the sample were analyzed in different days, the erosion speed was hardly kept constant. Therefore, no depth scale is plotted. Moreover, the erosion is much faster when the beam is sputtering the carbon layer due to its very light mass, when compared with Fe or Cr.

It is clear in all spectra, the desired blocking effect produced by the CrN interlayer. The surface carbon does not diffuse to the bulk, as planned. The decay of the carbon signal is very steeply showing very small layer interpenetration. No matter the interlayer thickness the result is very similar with a clear blockage effect.

In the first profile (DC1) it is also plotted the profile for C_2^+. This ion is attributed for carbon coming from hydrocarbon contaminants, typically from oil used in vacuum pumps. The small peak in the interface CrN-Fe is a strong indication of such contamination. Other typical hydrocarbon peaks (not plotted) were found with a similar behavior. The profile from DC1 sample also suggests an outer surface contamination. It may have occurred during film processing or during film analysis but it is irrelevant for the purpose of this work.

Figure 42 presents the EDS spectra of sample DC1, DC2, DC3 and DC4. EDS is used here as a complimentary tool of the SIMS data. EDS traces the constitutive elements in the near surface region (~1 μm depth). Carbon – the diamond base element – and Cr, are the main elements detected, nevertheless, small traces of Fe can be detected, mainly in the thinner interlayer sample.

Finally, figure 43 presents the Rockwell C hardness measured values for sample DC1, DC2, DC3 and DC4. The as delivered steel substrate presents a HRC value of 30. After the diamond deposition on the different studied samples, the measured HRC values are between 51.4 and 52.9.

After the hardness tests, the indention spots and boundaries were observed by SEM. All samples have shown cracks perpendicular to the indention spot. The latter seemed more pronounced in the thinner interlayer sample, but becoming less noticed as the thickness increased.

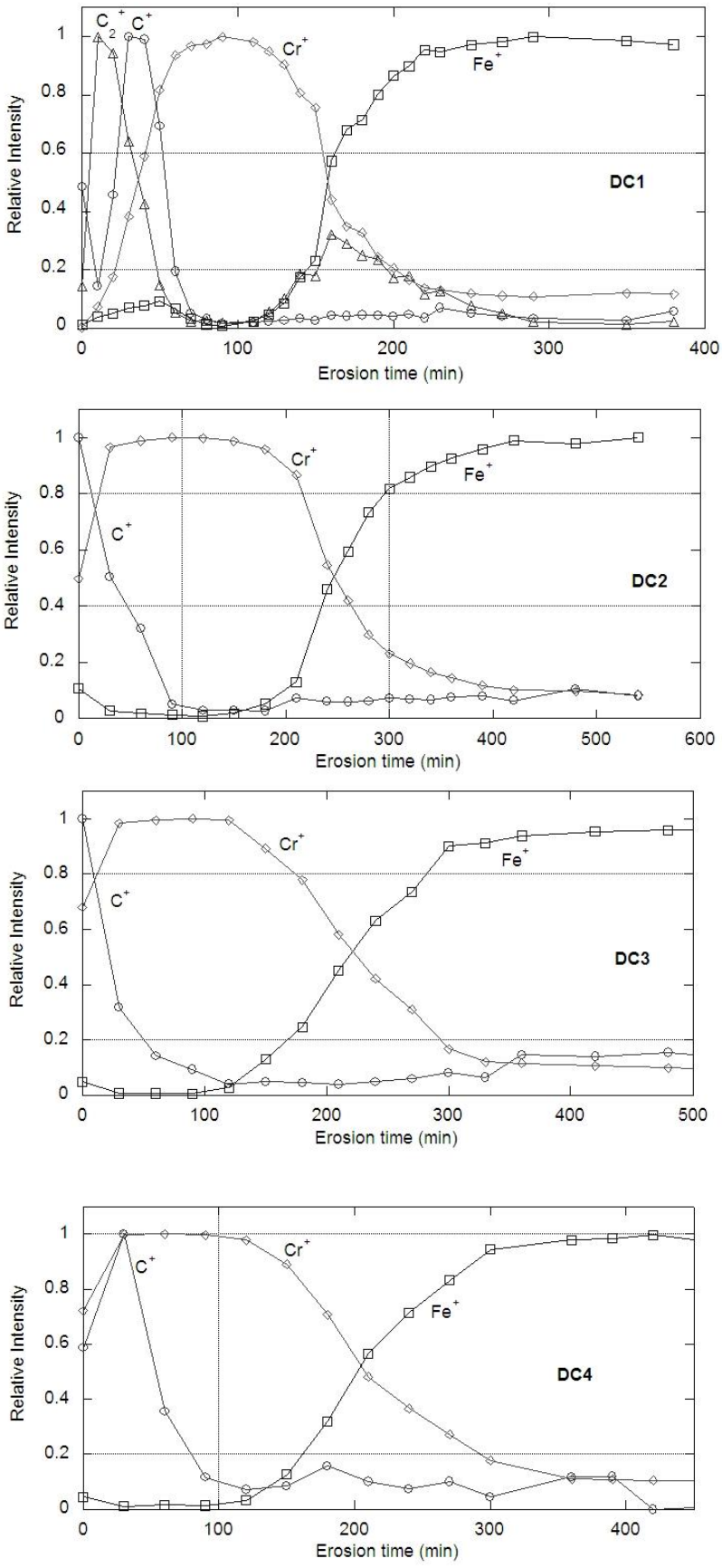

Figure 41 - TOF-SIMS depth profile of sample DC1, DC2, DC3 and DC4

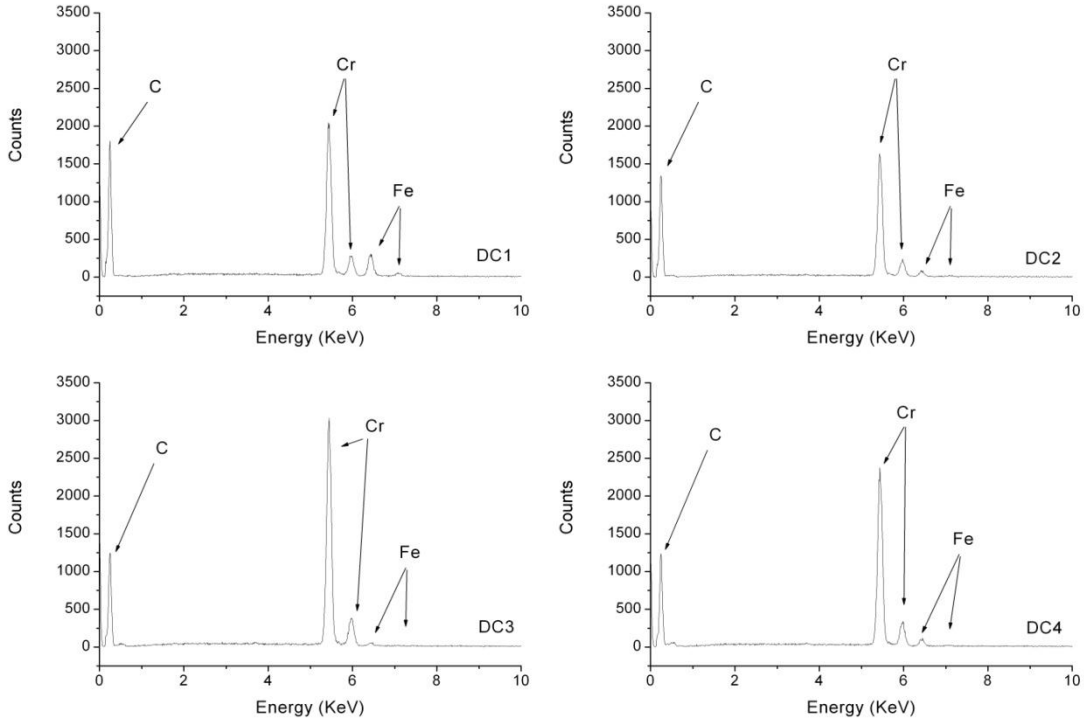

Figure 42 - EDS of samples DC1, DC2, DC3 and DC4

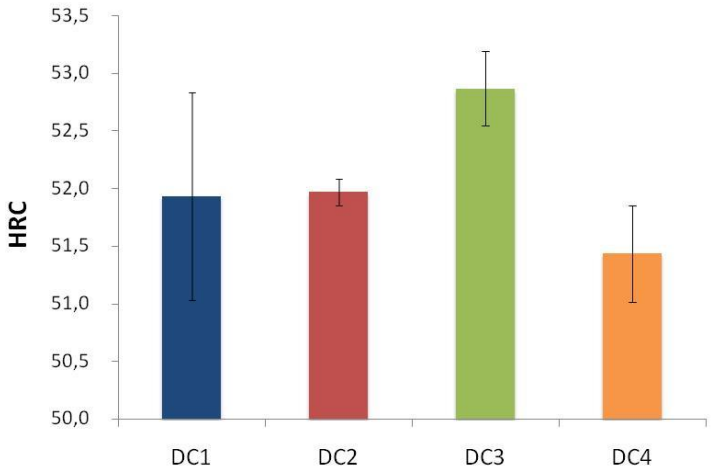

Figure 43 - Rockwell C hardness measured values for samples DC1, DC2, DC3 and DC4

Adhesion assessment of the diamond coated systems

The adhesion strength was assessed by the measurement of the deformation due to a load applied by an indenter, necessary to induce delamination and fracture of the diamond films.

A series of Brinell indentations with loads ranging from 10 to 187.5 kgf was performed. SEM images from indentation at various loads of samples AISI P20 modified coated system and AISI 304 coated system, are presented in figure 44 and figure 45, respectively.

Note that, as presented in chapter 3, Brinell hardness is determined by forcing a hard steel sphere of a specified diameter under a load into the surface of a material and measuring the diameter of the indentation left after the test. The Brinell hardness number (HB) is obtained as presented in equation 20:

$$HB = \frac{2P}{\pi D\left[D-\sqrt{D^2-d^2}\right]} \tag{20}$$

Where P is the applied load in kgf (1 kgf = 9.80665 N), D is the ball diameter and d is the indentation diameter, both in millimeter units. The ball diameter used in these tests was 1 mm.

The depth, h, in mm, of a Brinell indentation can also be calculated from the equation 21:

$$h = \frac{P}{\pi D[HB]} \tag{21}$$

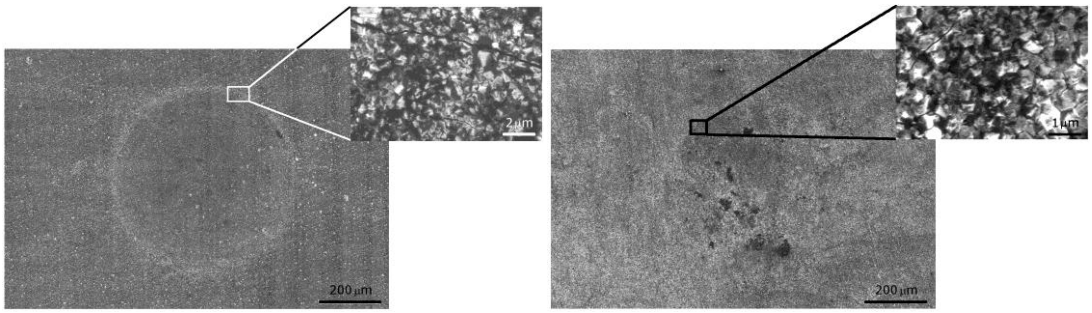

Figure 44 - SEM images from Brinell indentations at 187.5 kgf on AISI P20 modified samples after cycle DEP2 (left) and DEP3 (right)

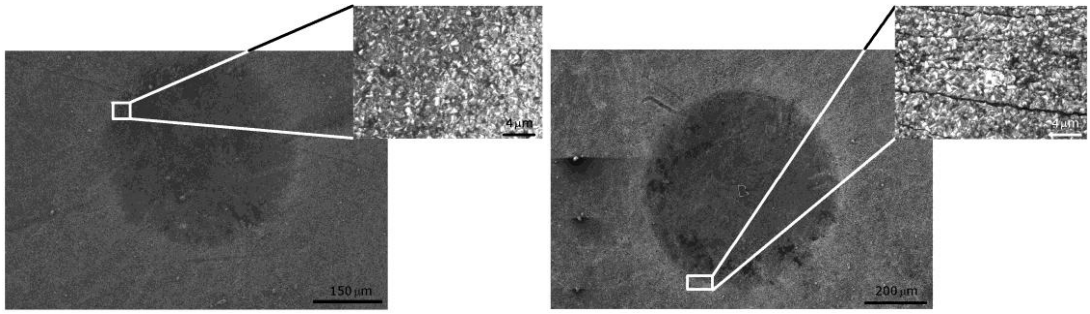

Figure 45 - SEM images from Brinell indentations of a sample of AISI 304 after cycle DEP4 at 20 kgf (left) and at 50 kgf (right)

From these two equations, the deformation can be evaluated as a function of Brinell hardness, indentation diameter and depth. The determined values of Brinell hardness, indentation depth, indentation diameter-depth ratio determination and observable cracks for the studied samples are presented in table 17.

Table 17 - Brinell hardness, indentation depth, indentation diameter-depth ratio determination and observable cracks

Sample	Applied load (kgf)	Indenter diameter (mm)	Indentation diameter (mm)	Brinell hardness (HB)	Indentation depth (mm)	Indentation diameter – depth ratio	Cracks
P20 mod. after DEP2	187.5	1	0.542	748	0.0798	0,1473	Yes
P20 mod. after DEP3	187.5	1	0.386	1540	0.0388	0,1004	Yes
304 after DEP4	20.0	1	0.383	167	0.0381	0,0995	No
304 after DEP4	50.0	1	0.570	178	0.0892	0,1565	Yes

The AISI P20 modified samples after cycle DEP2 presented a hardness of 748 HB and the AISI P20 modified samples after cycle DEP3 (a thicker film) presented a hardness of 1540 HB. The results show no visible delamination occurring up to a load of 125 kgf for AISI P20 modified coated systems. After indentation, it becomes visible a white spallation area around the indentations. This feature demonstrates that after indentation, the film is detached from the substrate [116]. At 125 kgf load, it could be observed small intergranular concentric cracks in both samples. According with Novikov and Dub [117], the absence of radial cracks emanating from the concentric cracks, could be explained with a high level of internal compressive stresses in the diamond film.

At a superior load-deformation, more pronounced concentric cracks are present and the films delamination is evident. From the images of the surface region near the boundary of the indentation, it is visible either inter and intragranular cracks.

SEM images from indentation at various loads demonstrate evidence that the samples deformed to the shape of the indenter. This could be explained by the expected plastic deformation of the steel substrates during indentation.

AISI 304 diamond coated samples presents a lower hardness (average of 173 HB) than the AISI P20 modified coated samples. The deformation due to the loads of 10 and 20 kgf didn't result in any crack or delamination of the diamond film. SEM observations of the indented regions reveal that the film begins to delaminate between 20 and 50 kgf of the applied load. From the images of the surface region near the boundary of the 50 kgf indentation load, it is visible either inter and intragranular fine concentric cracks.

Due to the columnar growth characteristic of polycrystalline diamond films, when a crack occurs on the surface of the film, it tends to propagate through the columnar particles, leading to a decrease in toughness [119]. Although, in the case of multilayered films, as the ones resulting from time-modulated CVD, the interfaces formed in this structures are expected to minimize the crack propagation.

Comparing the results obtained from the different sample substrates, it is possible to say that the formation of cracks in the diamond film, which results in adhesion losses, depends on the deformation imposed but also on the film thickness. Thicker films stand a lower value of deformation.

5. Non-ferrous substrate materials

A group of silicon (100) wafers, with 5 x 5 x 0.5 mm, were tested for diamond growth by conventional CVD and by TMCVD. The sample were hand polished with diamond powder (2–4 µm) for 2 minutes and then cleaned in acetone using ultrasound for 5 minutes.

The TMCVD was carried out for 2h00, with 5 and 2% CH_4/H_2 rate, with high pulses of 10 minutes and low pulses of 50 minutes, as presented previously in figure 22. The conventional deposition was performed at 2% CH_4/H_2 rate, for 2h00. The common parameters for this set of experiments have been presented previously in table 9. The substrate temperature was kept around 700 °C, in order to prevent important steel structural modifications.

Both, conventional and time-modulated depositions were successful in producing diamond layers, as it can be seen in figure 46. It is also clear that crystal density of the two samples is quite different. The conventional CVD resulted in an almost close film, with greater size

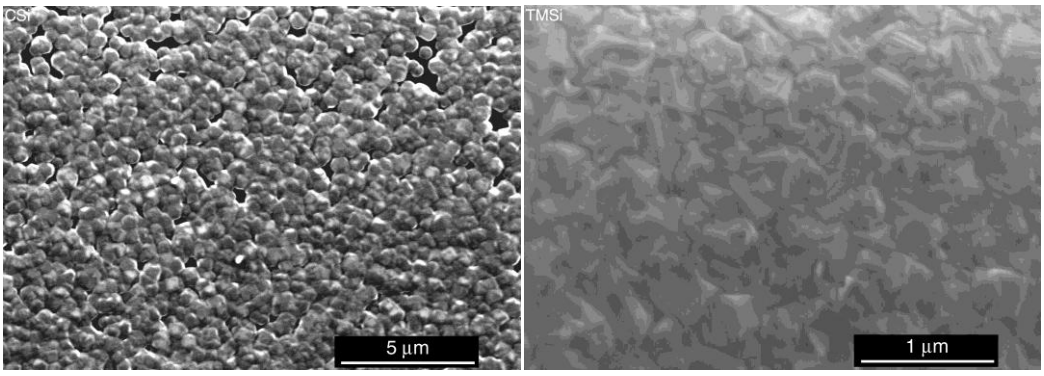

Figure 46 - SEM images of diamond deposition on silicon wafers using conventional CVD (left) and TMCVD (right)

crystals than those obtained on the film produced by TMCVD. Average crystal sizes are 0.7 ± 0.1 μm and 0.4 ± 0.1 μm, for the conventional and TMCVD films, respectively.

Extensive diamond depositions on silicon was performed on the hot filament reactor of the research unit and characterized previously [83].

Chapter 5

Performance of diamond coated mold tools

1. Introduction

As presented in the former chapter, diamond coatings were successfully obtained on AISI P20 modified steel substrates, with the assistance of a chromium nitride interlayer, and also on silicon wafers.

This chapter highlights the work undertaken concerning the usage and evaluation of polycrystalline diamond as a surface engineering coating on molding inserts for thermoplastic injection molding.

First, some preliminary tests will be presented. Second, further experiments are conducted, namely the evaluation of microcrystalline and sub- microcrystalline diamond films, three-dimensional featured coated mold tools and also the behavior of non-ferrous coated materials.

2. Preliminary tests

In this study, a small steel plate has been diamond coated, mechanically characterized and tested under service conditions, to produce high-density polyethylene (HDPE) components.

A 50 × 50 × 5 mm AISI P20 modified plate, was diamond coated in a hot-filament CVD reactor, described previously. Prior to the diamond coating, a chromium nitride (CrN) interlayer was deposited onto the steel plate, in a PVD system. In order to enhance the diamond nucleation, the sample was subjected to a 3h00 ultrasonic bath in 0.25 µm polycrystalline diamond solution, followed by a 2 minutes cleaning with isopropyl alcohol.

Diamond deposition parameters were optimized considering the nature of the interlayer and the steel substrate, as presented in table 18 and in figure 47. It was used CH_4 modulations with respect to deposition time, as shown in figure 47, to enhance the nucleation density in the beginning of the deposition and to promote secondary nucleation during the film growth, resulting in denser and homogeneous coating.

The deposited diamond film, as it can be seen in figure 48, presents a ~30 mm diameter spot centered in the square substrate, where the film has an homogeneous growth, as it can be seen in figure 49. Outside this spot, the film loses its crystallinity and just amorphous carbon is present. This is probably due to the limitations of CVD equipment used which has a theoretical 50 × 50 mm deposition area.

As it can be depicted from figure 49, the as-deposited diamond surface, the film presents a predominant (111) and (100) crystallite orientation, which is typical for the used deposition temperatures. The latter has been confirmed by X-ray diffraction. It can also be depicted from the high amplification shown in figure 49, from measurements, that the predominant crystal size is under 500 nm. The film thickness is estimated to be within 1.5 to 2.0 µm and the measured average roughness is 0.14 µm.

Table 18 - Diamond deposition conditions

Parameter	Value
H_2 flow (sccm)	200
CH_4 flow (sccm)	2 – 6
Base pressure (Torr)	2×10^{-2}
Deposition pressure (Torr)	30
Substrate temperature (°C)	800
Number of filaments	3
Filament temperature (°C)	2100
Filament-substrate distance (mm)	8

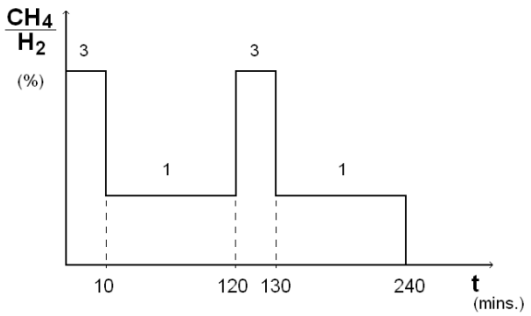

Figure 47 - Time-modulation of the CH_4 gas related to H_2

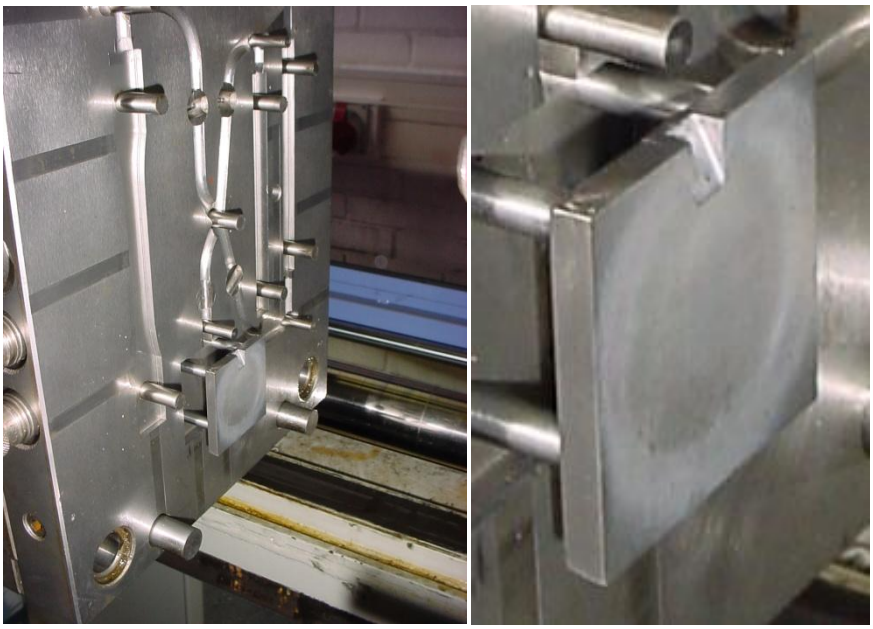

Figure 48 - Mould cavity (left) and close-up of the diamond-coated insert plate (right)

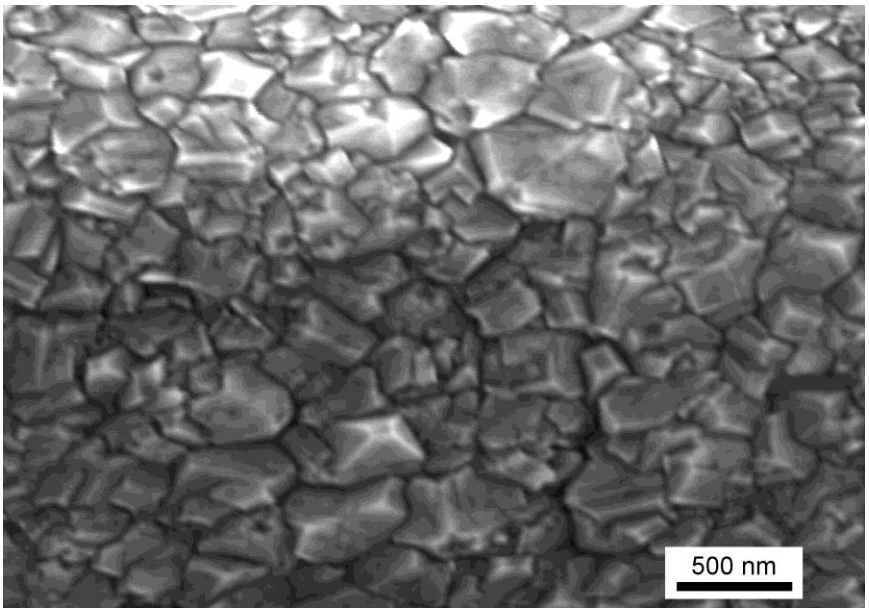

Figure 49 - SEM image of the as-deposited diamond film

After the preliminary analyses of the as-deposited diamond film, the coated steel plate was tested for polymer molding, using a mold tool specially designed to accommodate the insert (figure 48) and mounted in an “Inautom EuroInj D65” injection molding machine to perform a cycle of 250 high-density polyethylene (HDPE) sample plates, as presented in figure 50. The injection molding processing conditions are presented in table 19.

Figure 50 - High-density polyethylene (HDPE) injected plate

Table 19 - Cycle injection moulding processing conditions

Parameter	Value
Injection pressure (bar)	50
Melt temperature (°C)	200
Hold pressure (bar)	30
Hold pressure time (s)	5
Cooling time (s)	22

The first injected samples presented a few small dark spots, as the result of the pealing of the amorphous carbon. After 10 cycles, the injected objects were perfectly clear of any coating contamination.

After the 250 injection cycles, the insert was again removed from the mold tool and re-analyzed in order to evaluate wear and degradation of the polycrystalline diamond coating.

It is common knowledge that a 250 injection cycle is not representative of a routine mold production. Nevertheless, for the purpose of assessing the characteristics of the diamond film after injection molding and the suitability of the coating for this type of application, it is here considered. An increased injection routine will have to be considered in order to fully asses wear resistance of the inserts and the improvement of molding release.

Figure 51 presents SEM images of the diamond film after the routine injection cycle at high magnification (top) and low magnification (bottom). Some darker spots, that may be small amounts of plastic attached to the diamond film, can be seen in the high magnification image. From the lower amplification image, it can be seen that the film is quite homogeneous.

Comparing the diamond surface presented in figure 51 with the as-deposited diamond surface shown in figure 49, no relevant morphological changes are detected.

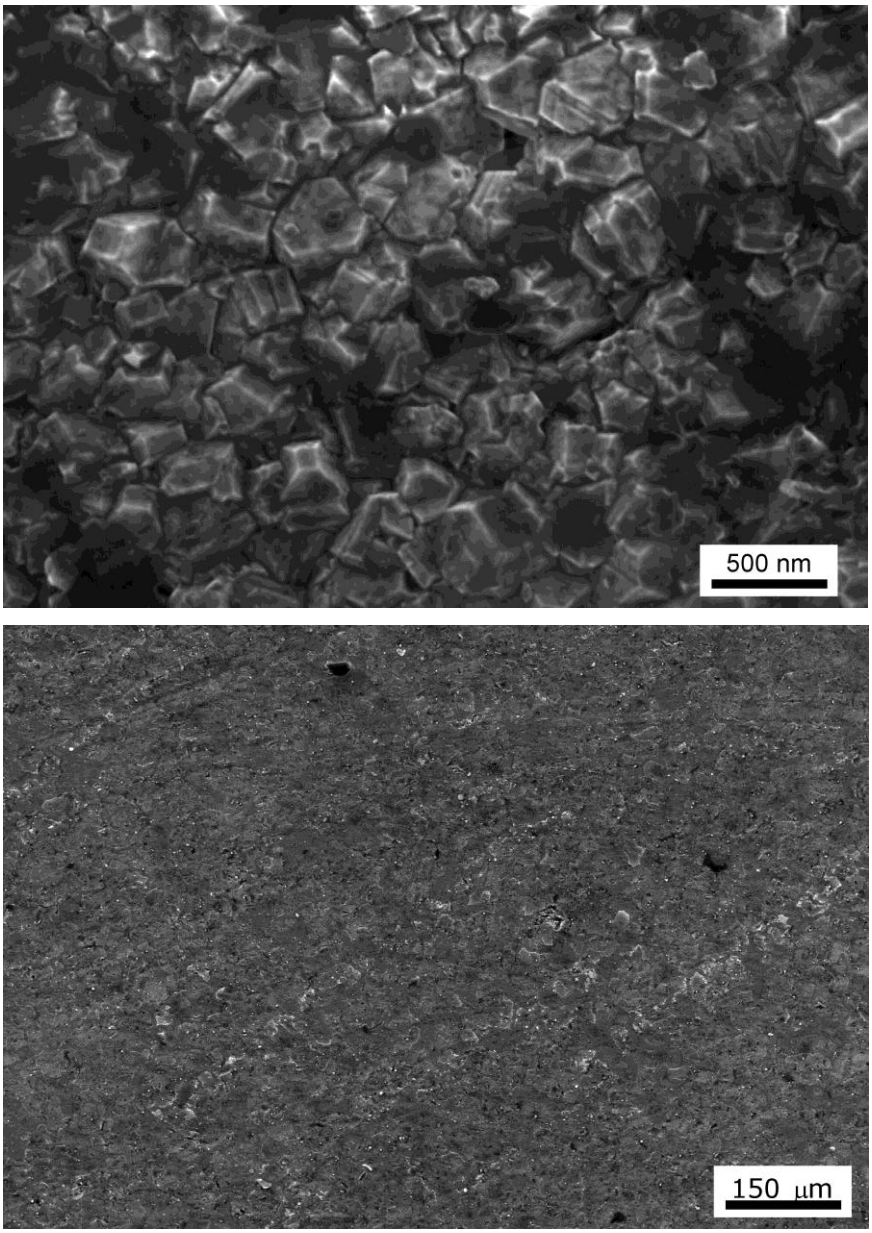

Figure 51 - SEM images of the diamond film after the routine injection cycle at high magnification (top) and low magnification (bottom)

Energy dispersive X-ray spectroscopy was performed on the diamond coated sample, before and after injection. From figure 52, it can be seen that the elements exhibited are carbon, probably from the diamond and enhanced form HDPE residues on the after injection spectrum, chromium from the interlayer, and iron from the substrate matrix. The EDS spectra of the coated plates, before and after injection, are very similar, indicating that no significant modification occurred during the injection cycles.

After the injection molding cycles were carried out, a series of indentation tests were performed in a hardness tester with a 2.5 mm steel Brinell indenter, employing a range of loads between 153.2 N and 613 N. Vickers micro-hardness of the coated samples where measured using a micro-hardness tester, with a range of loads from 0.49 N to 1.96 N.

The measured Brinell hardness, presented in figure 53, for the coated system was determined to be 226 HB, presenting a decrease of 27.9% in hardness when compared with the steel–CrN system (289 HB). The steel substrate coated with CrN also presents a decrease of 8.3% of Brinell hardness compared with the bare steel substrate (313 HB). These reductions on the hardness of the coated systems are probably due to steel and CrN phase transformations occurred when the CrN and diamond films are formed. Diamond growth, as shown in table 18, was performed at a substrate temperature of 800 °C, above the α → γ transformation temperature[16, 108]. The PVD-arc CrN coating, although performed at low temperature, involves high kinetic energy (material leaving the cathode at a velocity of around 10 km/s).

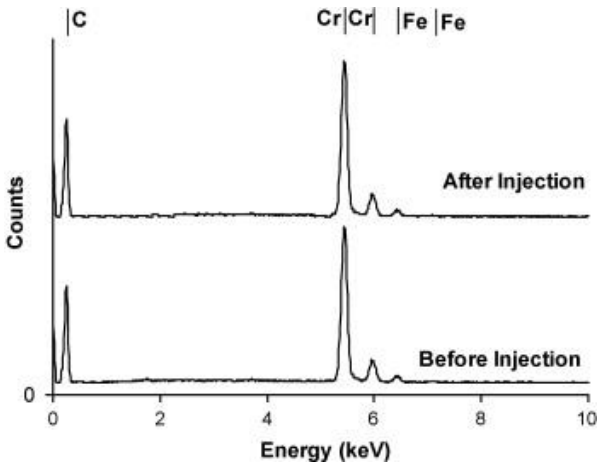

Figure 52 - EDS of the diamond film

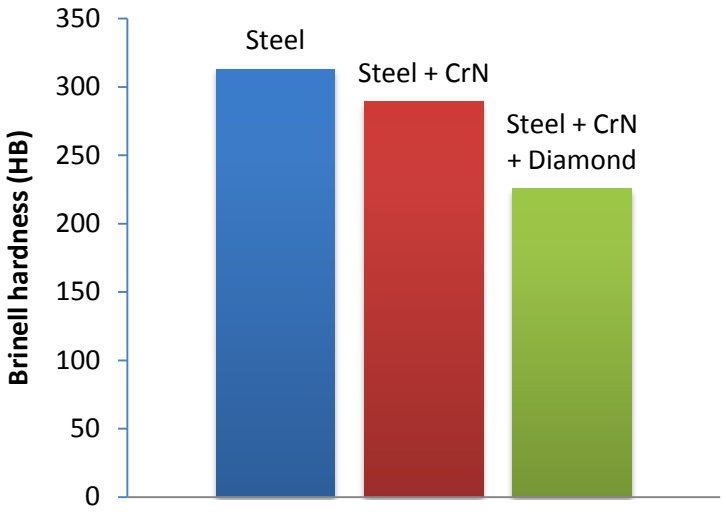

Figure 53 - Brinell hardness of the steel substrate, of the steel substrate-coated with CrN and the steel substrate with CrN interlayer and diamond coated

The Brinell hardness indentations serve also to qualitatively analyze the coatings adhesion. Figure 54 and figure 55 show the effect of the 2.5 mm steel ball indenter with applied loads of 613 N, 490 N, 306.5 N and 153.2 N. It can be observed that no significant delamination occurred, even at the maximum tested load. The coated film deformed to the shape of the Brinell indenter tip. The deformation of the coating to the shape of the indenter and in a synchronized form with the more plastic steel and CrN system, without slating, is an indication of the good adhesion of the diamond film.

Concentric cracks around the indentation spots can be observed in the 613 N, 490 N and 306.5 N indentations, more noteworthy on the highest load and decreasing with smaller loads. The cracks may be due to the external stress imposed onto the film during indentation loading that may force the film to crack in order to dissipate stress and/or energy.

Raman spectroscopy was used to assess the diamond Raman quality, as proposed by Kulisch et al. [98] and to estimate the residual stresses of the diamond film according to Ralchenko et al. [36]. To verify the changes in the coatings residual stress, Raman spectroscopy was performed before and after the indentation tests for different loads.

Raman quality was determined to be around 51%.

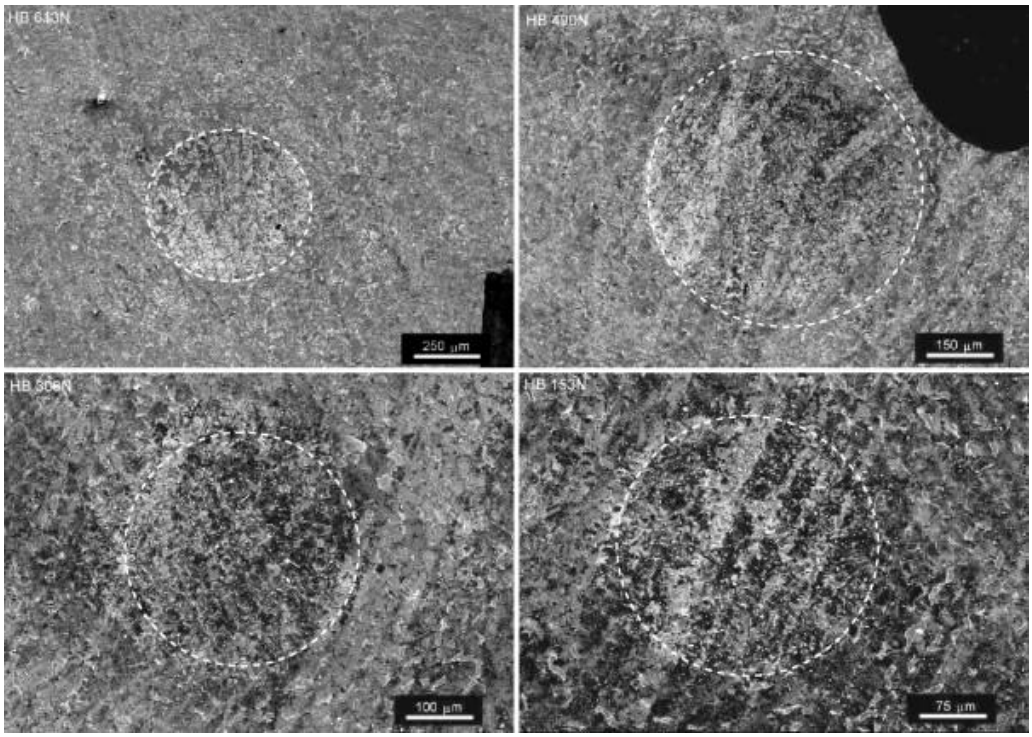

Figure 54 - SEM images of Brinell hardness indentations, using a 2.5 mm steel sphere and loads of 613 N, 490 N, 306.5 N and 153.2 N

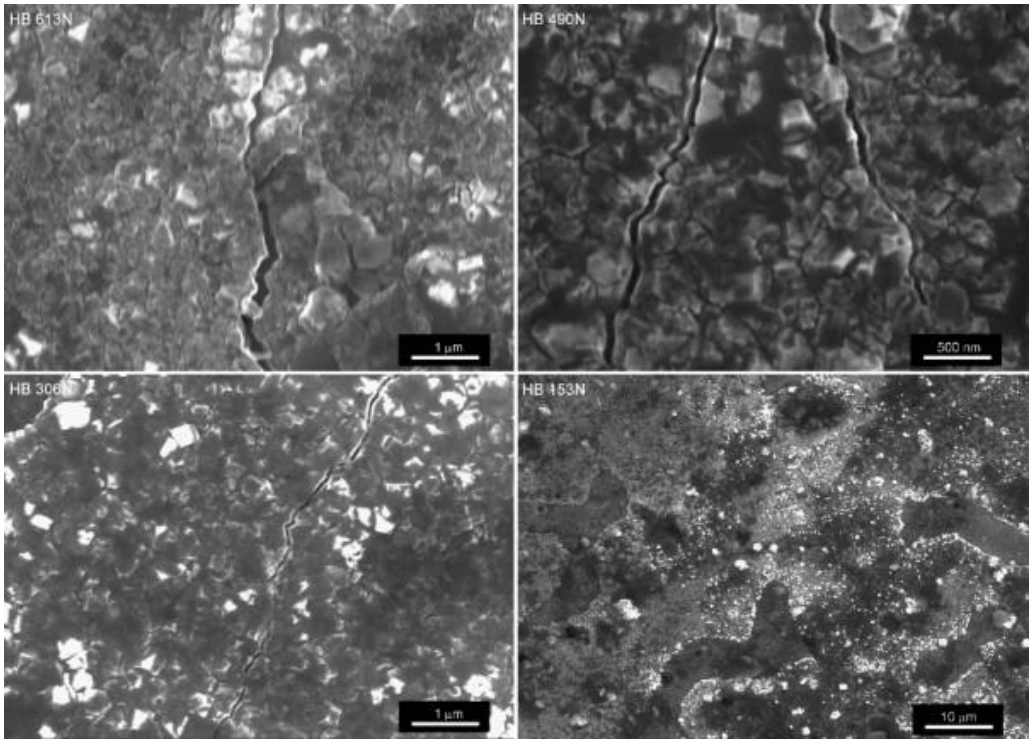

Figure 55 - SEM images of Brinell hardness indentations boundary zone, using a 2.5 mm steel sphere and loads of 613 N, 490 N, 306.5 N and 153.2 N

As it can be observed in figure 56, the as-deposited film has a spectrum shift of 14 cm^{-1}, which corresponds to 7.9 GPa of compressive stress, not very different from the one determined by Ralchenko et al. [36] on a diamond film growth on steel, at similar conditions as the ones presented in this work.

The Raman spectra acquired in the 613 N indentation area, presents a slightly superior compressive stress, decreasing from the boundary of the indentation ($\Delta\varphi = 21cm^{-1} \rightarrow \sigma = 11.9\ GPa$) to its center $\Delta\varphi = 18cm^{-1} \rightarrow \sigma = 10.2\ GPa$).

Complimentary to the Brinell hardness measurements, Vickers micro-hardness indentations, using 0.49 N (50 g), 0.98 N (100 g) and 1.96 N (200 g) and a holding time of 10 s and 5 s, were performed. The measured micro-hardness stabilized at 483 HV (±10%) for the set of measurements performed at 0.98 and 1.96 N for both the holding times. The 0.49 N load, held for 10 s, presented 270 HV. For the 5 s holding time, at the above-referred load, it was not possible to measure the hardness value accurately. Figure 57 shows the SEM images of the micro-indentations zones. All indented spots present surface modifications, in what seems to occur a reduction of the adhesion of the diamond film to the substrate.

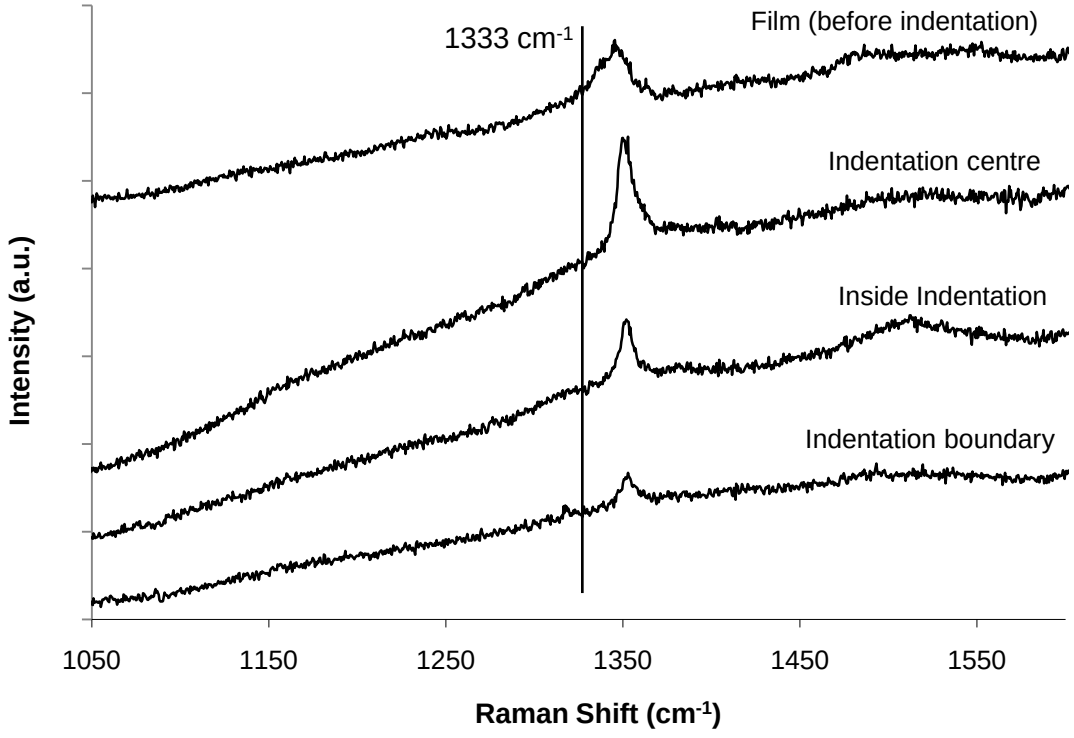

Figure 56 - Raman spectrum of the diamond coating before and after Brinell indentation at 613 N (in the centre, in the middle and in the boundary of the indentation)

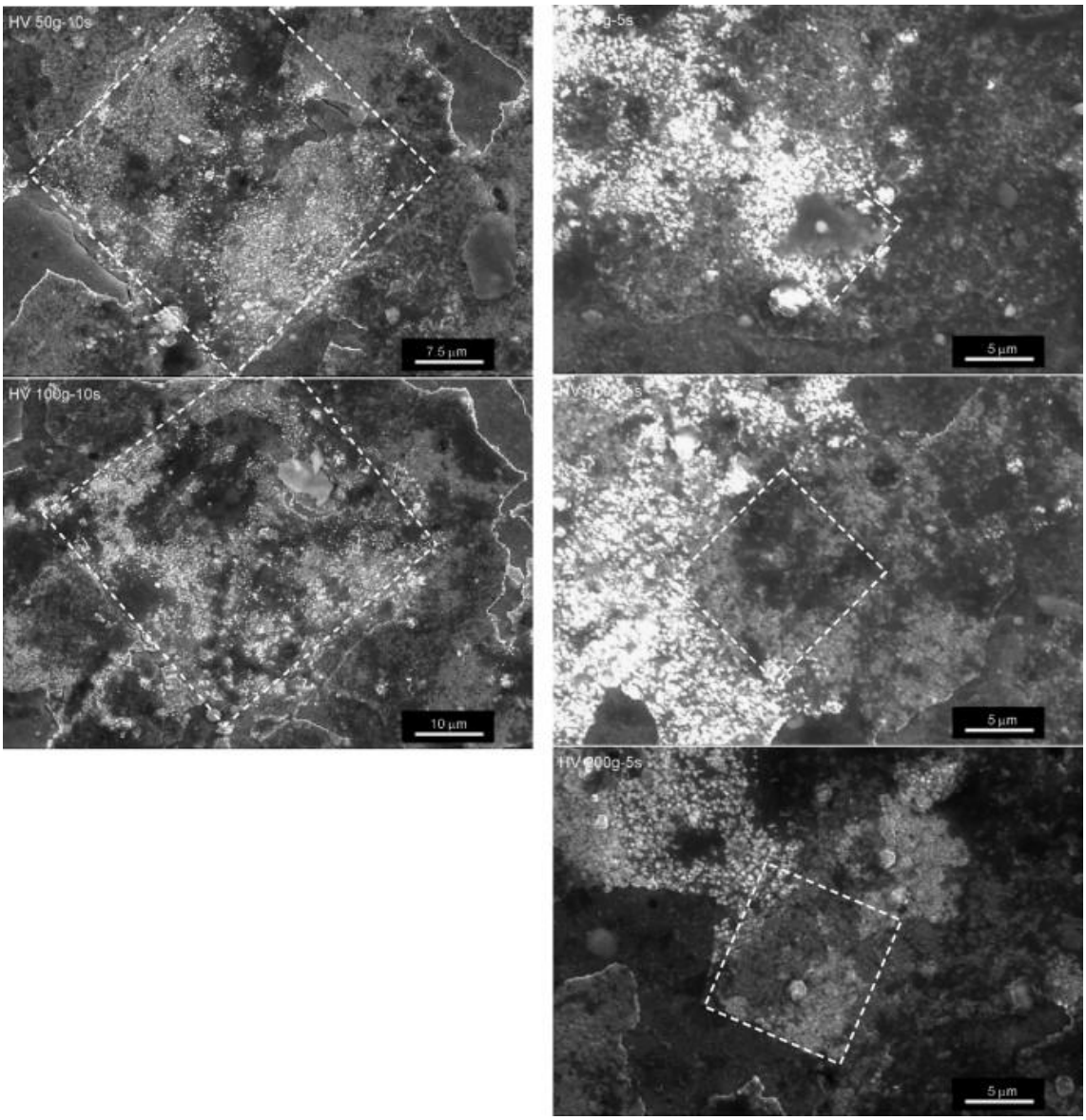

Figure 57 - SEM images of Vickers micro-hardness indentations using a load of 0.49 N, 0.98 N and 1.96 N for 10 s and 5 s

3. Microcrystalline films

Four AISI P20 modified steel molding inserts with 10 × 10 × 3 mm were prepared with different surface engineering treatments, as shown in table 20. The molding surfaces of all the inserts were polished with Silicon Carbide paper till grit # 2000. Samples AC1 and AC2 were coated with a PVD chromium nitride (CrN) film of ~2 µm thickness. Sample AC3 was also coated with the same CrN film in order to compare its performance with the diamond coated inserts.

Table 20 - Description of the different insert mold tools

Insert	Description
AC1	~2 µm diamond film - ~2 µm CrN film - Steel system
AC2	~5 µm diamond film - ~2 µm CrN film - Steel system
AC3	~2 µm CrN film - Steel system
AC4	Bare steel

Prior to the diamond coating, samples AC1 and AC2 were ultrasonic abraded with diamond solution (0.25 µm grain size) for 2h30 and then cleaned for 5 minutes in an ultrasonic bath with isopropyl alcohol.

Diamond growth was performed in a hot-filament CVD reactor, described in chapter 3, using time-modulated CVD. The deposition conditions employed are shown in table 18. Sample AC1 was submitted to 4h30 of deposition (2 modulated cycles) and sample AC2 was submitted to 9h00 of deposition (4 modulated cycles), as it can be seen in figure 58.

Figure 59 shows the SEM images of inserts AC1, AC2, AC3 and AC4 before injection molding and figure 60 presents the X-ray diffraction spectra of the same samples.

Both diamond coated samples exhibited diamond crystallites mainly displaying (111) crystal orientation, although (100) oriented crystals were also observed. These growth directions are typical for the processing temperatures employed in this investigation. The measured average crystal size of these films was 1.74 and 1.25 µm, and the measured average roughness was 0.18 and 0.16 µm, for samples AC1 and AC2, respectively. Inserts AC3 and AC4 presented an average roughness of 0.10 and 0.11 µm, respectively.

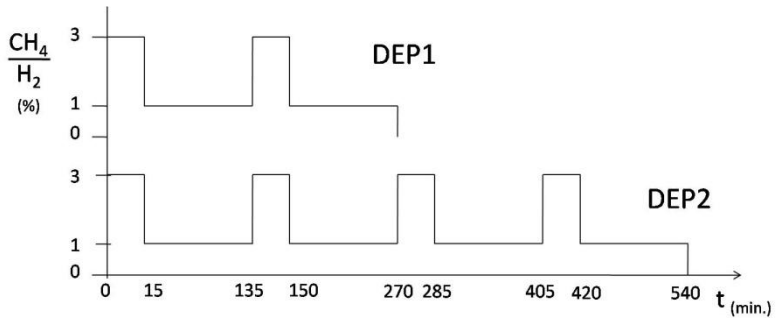

Figure 58 - Time-modulated CVD conditions used

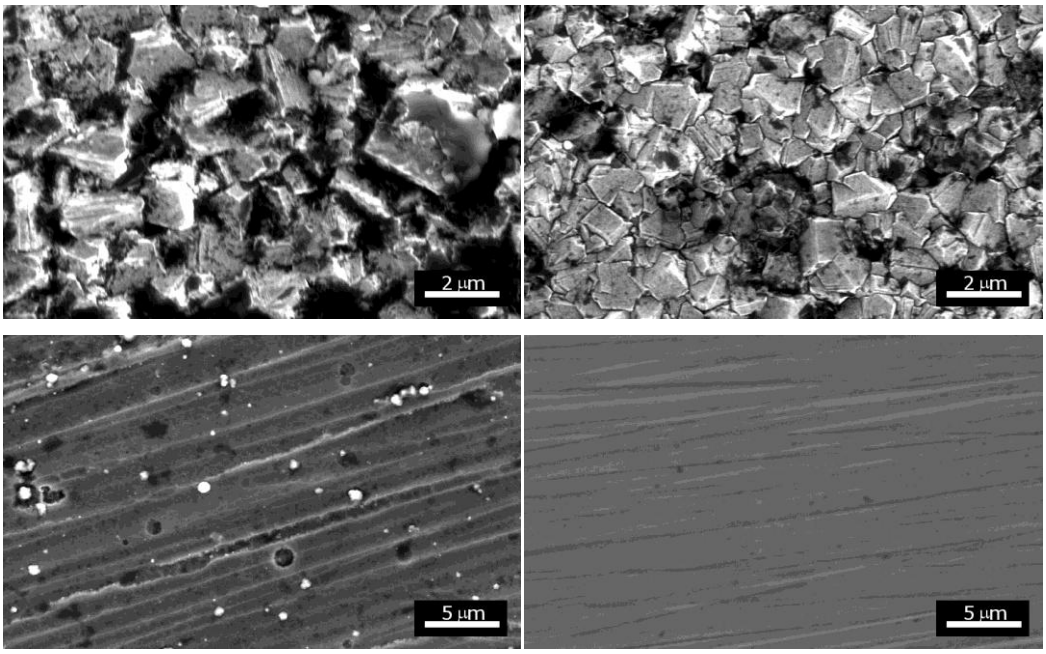

Figure 59 - SEM images of inserts AC1 (top left), AC2 (top right), AC3 (bottom left) and AC4 (bottom right) before injection molding

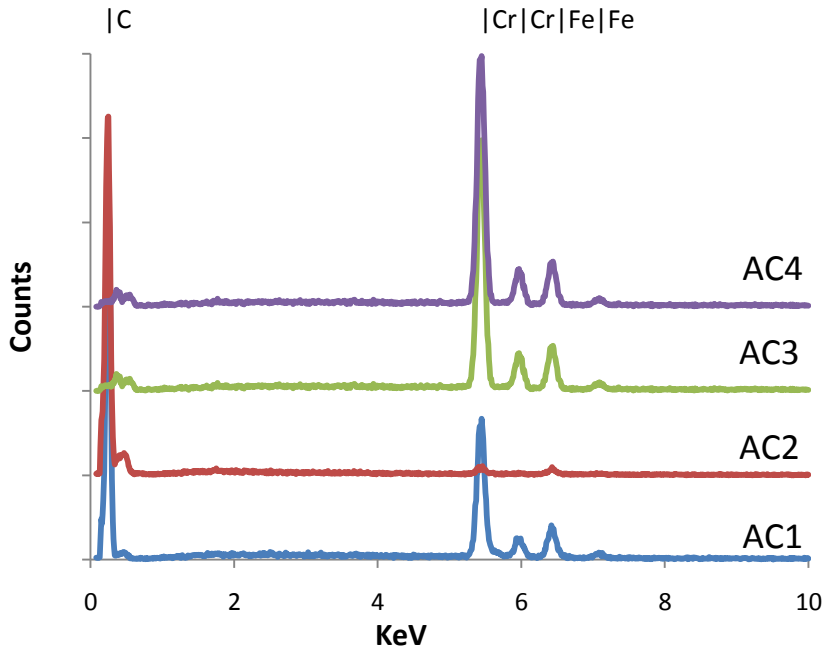

Figure 60 - EDS of the molding inserts

From the X-ray diffraction spectrum presented in figure 60 it may be observed that the ~5 µm diamond film (sample AC2) is the only material being stimulated by the X-ray beam. In samples AC1, AC3 and AC4 it is visible the presence of both iron (Fe) and chromium (Cr), beside carbon

(C). The presence of chromium on the steel substrate is believed to be due to the 2% that is included in the composition of AISI P20 modified.

Raman spectroscopy was used to assess the diamond Raman quality, on the diamond coated samples, as proposed by Kulisch et al. [98] and to estimate the residual stresses of the diamond film according to Ralchenko et al. [36].

Calculated quality factor values for the diamond coatings are 56.0 and 58.3%, for samples AC1 and AC2, respectively.

Samples AC1 and AC2 presented diamond peak shifts ($\Delta\varphi$) of 11 and 13 cm^{-1}, respectively. Calculated residual stress (σ) values for the diamond coatings are 6.2 and 7.4 GPa, for samples AC1 and AC2, respectively.

After this preliminary analysis to the molding inserts, they were placed in a mold tool specially designed to accommodate the 10 x 10 x 3 mm inserts and mounted in an "Inautom EuroInj D65" injection molding machine to perform a cycle of 500 high-density polyethylene (HDPE) sample plates, at the conditions presented in table 19.

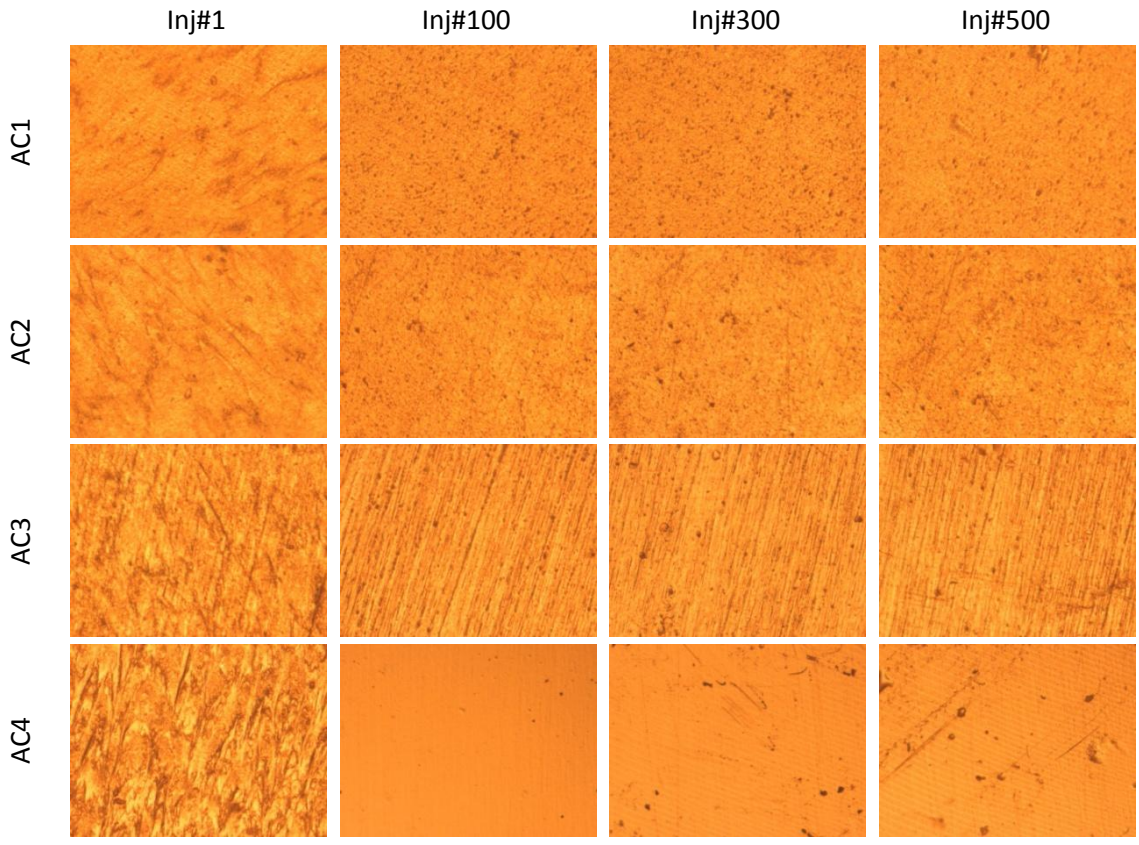

Figure 61 - Optical microscopy images of the HDPE molded surfaces

The molded samples were analyzed using optical microscopy. Figure 61 displays 150 times magnified images of HDPE objects from the run number 1, 100, 300 and 500. Whatever the type of insert surface, the first injected object presents more heterogeneous surface than the objects injected in cycles 100, 300 or 500. After the first set of injections, the polymeric objects molded with both diamond coating are very alike. The molded pieces by AC3 and AC4, present some surface scratches, but maintain the optical brightness (observed at the naked eye). The samples molded with the diamond coated inserts presented a slightly more tarnished surface than the samples molded with bare steel or with the CrN coating. This may be due to the slight increased roughness that the diamond coated inserts present, compared with the non-diamond coated samples, and also due to the crystalline nature of the diamond coatings. It is also worth of mention that the injected samples 100 by the bare steel insert is very clean, but as the number of injections are increased, the surface of the plastic sample becomes heterogeneous.

The diamond coating was again observed by SEM, after the injection process, and as it can be seen in figure 62, apparently no morphological change occurred.

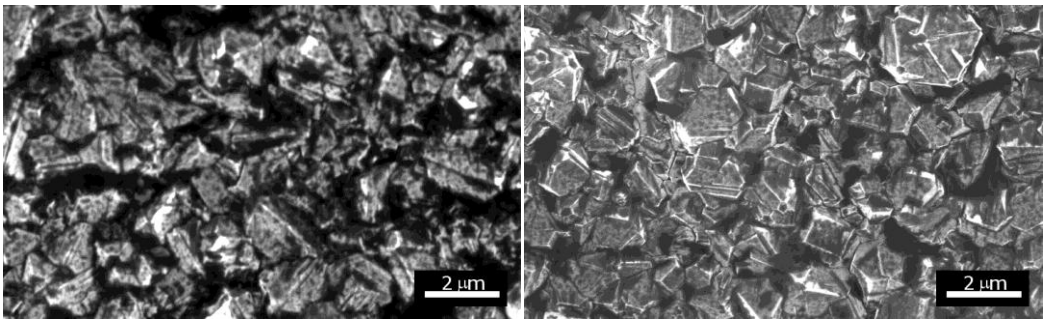

Figure 62 - SEM images of inserts AC1 (left) and AC2 (right) after 500 injection molding

4. Sub-microcrystalline films

In the previous sub-chapter, it was referred that the samples molded with the diamond coated inserts presented a slightly more tarnished surface than the samples molded with bare steel or with CrN coating. This may be due to the slighty increased roughness that the diamond coated inserts present, compared with the non-diamond coated samples, and also due to the crystalline nature of the diamond coatings. Nevertheless, it is expected that if the average roughness and crystal size of the diamond film is reduced, this problem may be overcome.

Diamond average roughness and crystal size reduction may be accomplished by the deposition of sub-microcrystalline or nanocrystalline diamond [97].

In this study, a similar work to the one performed in previous sub-chapter will be presented, but using sub-microcrystalline diamond coatings.

A set of steel samples made out of AISI P20 modified steel, with the dimensions of 5 × 5 × 0.5 mm were used in this investigation. The steel samples were pre-coated with PVD chromium nitride (CrN) ~2 µm thick film, in order to block the mutual diffusion between the ferrous substrate and the diamond growth atmosphere. The steel plates had the molding surface polished with Silicon Carbide paper till grit #2000.

Prior to the diamond deposition, the samples coated with CrN were ultrasonic abraded with diamond solution (0.25 µm grain size) for 2h30 and then cleaned for 5 minutes in an ultrasonic bath with isopropyl alcohol.

Diamond growth was conducted in a hot-filament CVD reactor, described in chapter 3, using time-modulated CVD. The deposition conditions employed are shown in table 18 and figure 63.

In order to obtain homogeneous coatings with an average crystal size of about 1 µm, cycles of 15 minutes were employed for high methane pulses, followed by a low methane stage of 120 minutes.

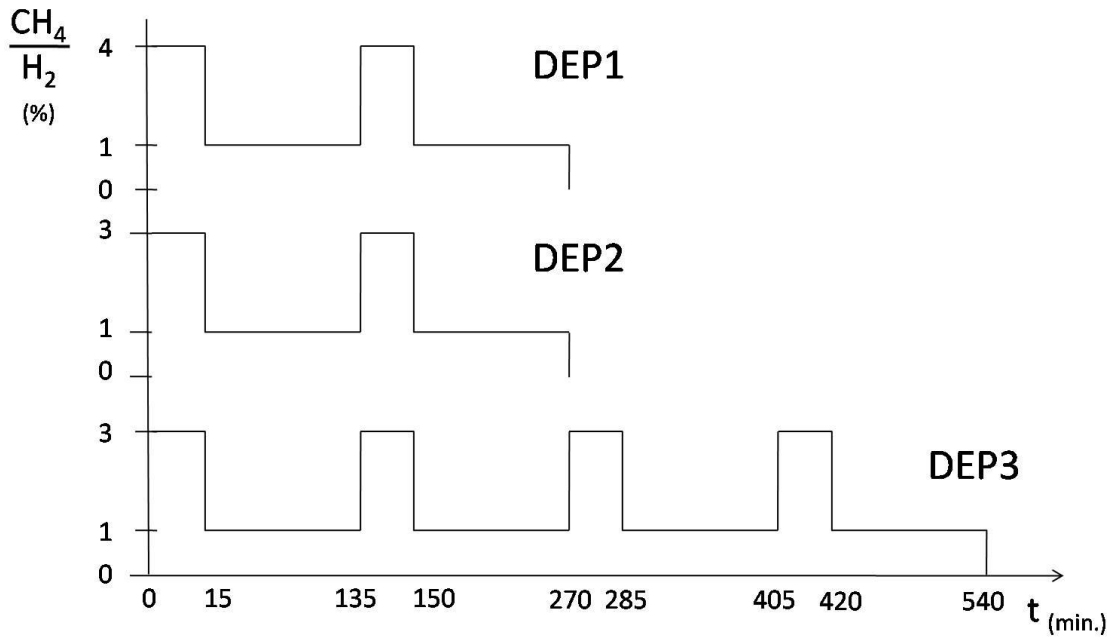

Figure 63 - Diamond deposition conditions

Diamond deposition under conditions DEP1, DEP2 and DEP3, as shown in figure 63, was carried out using 2 and 4 cycles, which corresponds to a total deposition time of 4h30 and 9h00, respectively. Conditions DEP1 and DEP2 differ from one another on the high-pulse methane concentration. Higher methane concentration promotes the increase of diamond nucleation density [80] and consequently changes in the diamond film morphology, namely crystal size can be reduced, but at the expense of diamond quality. In order to illustrate the latter conditions, DEP1 and DEP2 were used to observe the effect of those morphology changes.

The deposition conditions DEP1, DEP2 and DEP3 were used to produce samples FD1, FD2 and FD3, respectively, as shown in table 21. A bare steel plate (sample F1) was also used in the adapted mold, to serve as a reference sample.

After the deposition of diamond coatings on all samples, the morphology of the as grown films were characterized using scanning electron microscopy (SEM) and the intrinsic stress state and quality of the diamond coatings was characterized using Raman 514.5 nm Ar^+ ion laser spectroscopy.

Figure 64 shows microscopic images of the diamond coatings. All the as-grown films exhibited sub-micron diamond crystallite size, mainly displaying (111) crystal orientation, but (100) crystal orientation was also observed. These growth directions are typical for the processing temperatures employed in this investigation (700 – 800 °C). The average diamond crystallite sizes of the deposited films are 0.61, 0.71 and 0.83 µm, for sample FD1, FD2 and FD3, respectively.

Figure 65 displays Raman spectra of the as-deposited samples. Raman spectroscopy was used to assess the diamond Raman quality and to estimate the residual stresses of the diamond film as deposited.

The quality factor of the diamond coatings was calculated to be 50.9, 55.9 and 58.3%, for samples FD1, FD2 and FD3, respectively. The calculated residual stress (σ) values for the diamond coatings are 4.5, 6.2 GPa, for samples FD1 and FD2, respectively. The longer deposition time sample, FD3, exhibited a residual stress of 7.4 GPa.

Table 21 - Description of the different insert mold tools

Insert	Description
FD1	Steel plate diamond coated (DEP1)
FD2	Steel plate diamond coated (DEP2)
FD3	Steel plate diamond coated (DEP3)
F1	Bare steel plate

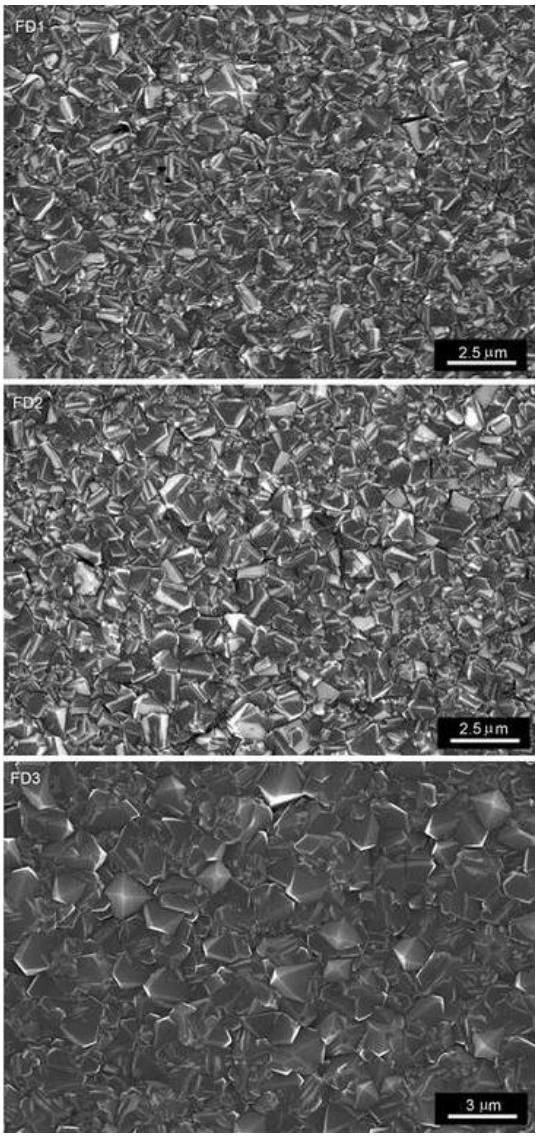

Figure 64 - SEM images of diamond coatings on steel substrates
Sample FD1 (top), FD2 (middle) and FD3 (bottom)

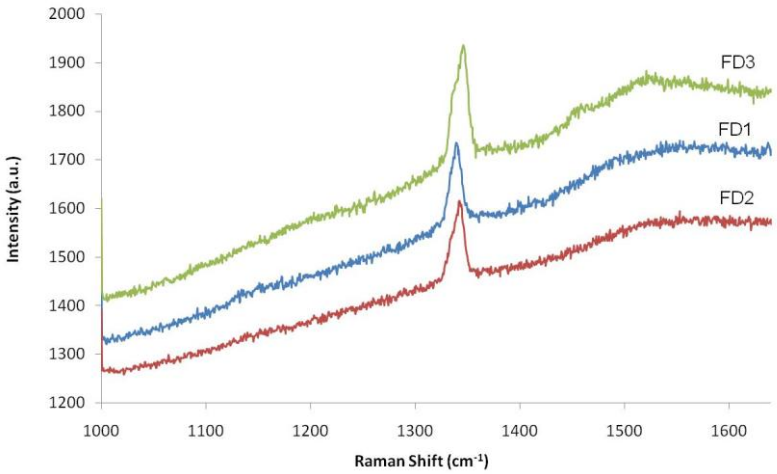

Figure 65 - Raman spectra of the diamond-coated steel plates

Steel linear thermal expansion coefficient largely differs from the coefficient value displayed by CVD diamond [36]. Time-modulated CVD process helps to attenuate the direct time dependence of the residual stress of diamond films growth on steel substrates, but does not eliminate it.

The four inserts, described in table 21, were tested for polymer injection molding, using a mold tool specially designed to accommodate the inserts and mounted in an injection molding machine to perform a cycle of 80 high-density polyethylene (HDPE) sample components at the conditions presented in table 19

Figure 66 displays micrographs of the polymeric molded surface by the different inserts, in run number 1, 50 and 80. Apart from the first set of samples, that present marks of the demolding spray used in the beginning of the processing work, the injected parts are identical.

All samples presented a good finishing surface, not showing the tarnished surface that the diamond coated insert of the previous sub-chapter originated.

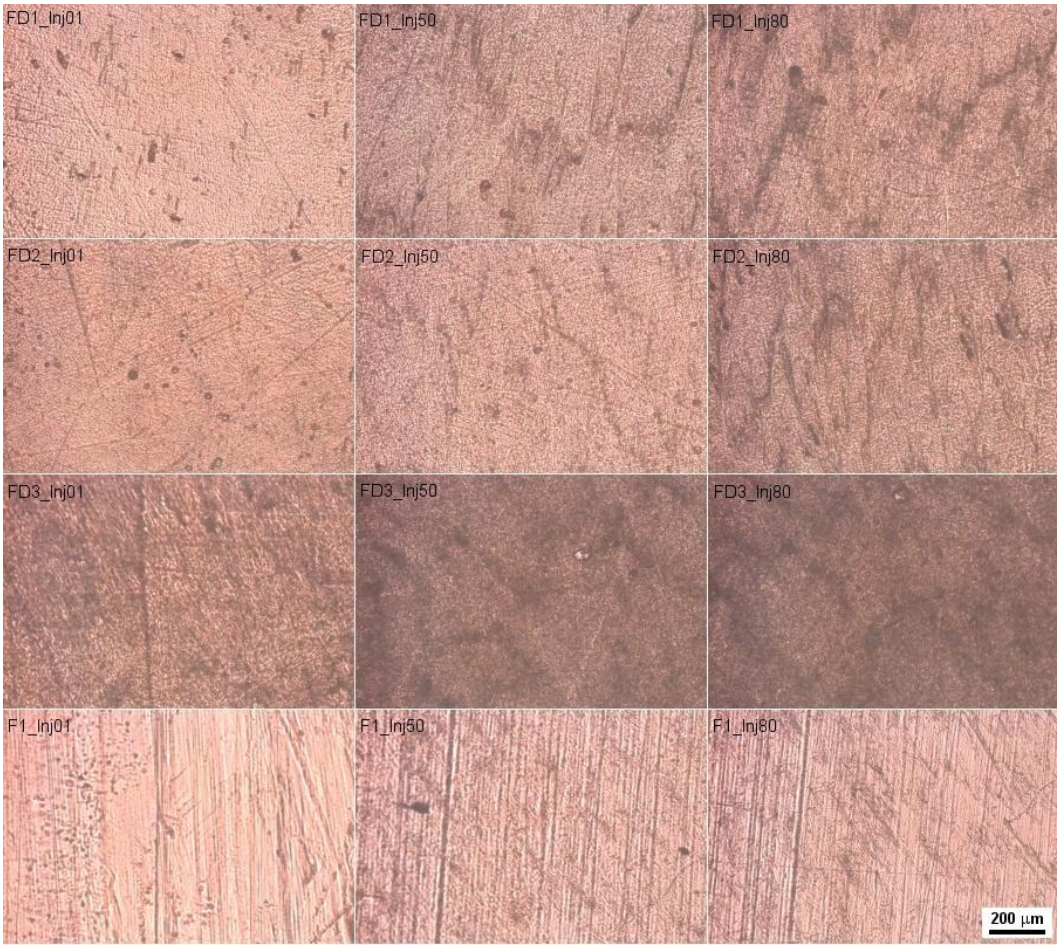

Figure 66 - Optical microscopic images of the HDPE-injected plate surface, by the different inserts, in run number 1, 50 and 80

From the images presented in figure 66, it is evident that the molded objects with the diamond-coated inserts, present more homogeneous surfaces than the ones molded by the insert without coating. It should be noted that insert F1 has the same or better surface finish than the samples that were used to deposit diamond, because their surface was not diamond abraded as the ones pre-treated for diamond coating. The initial steel samples were not surface polished to achieve a mirror surface, in order to obtain optical smooth surfaces and, hence, good quality plastic components/parts. Therefore, the results indicate that polishing time may be saved when using diamond-coated surfaces.

Figure 67 shows SEM micrographs of diamond-coated steel after the injection routine cycles were carried out.

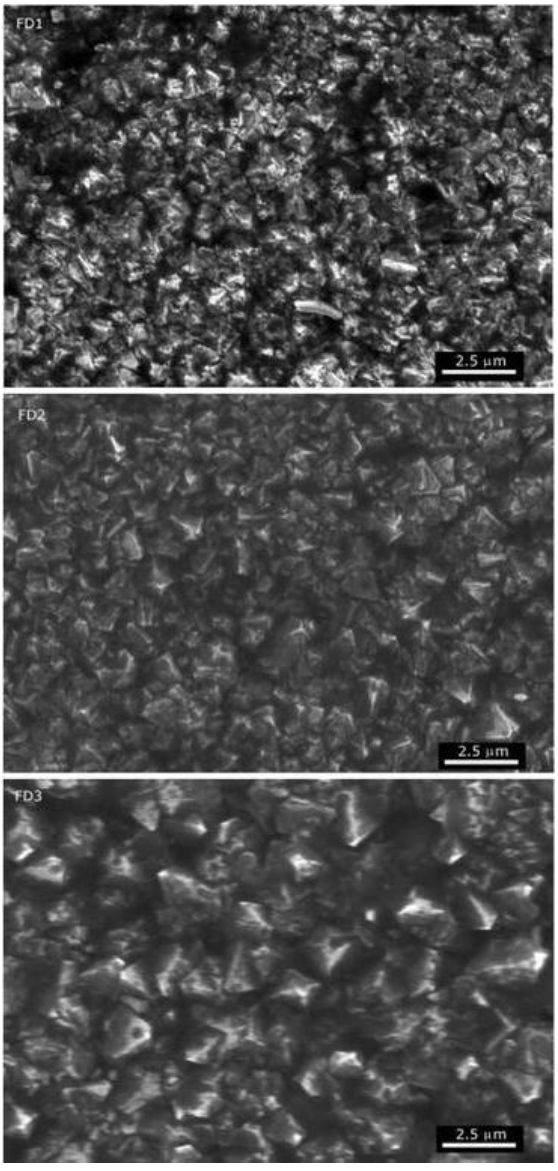

Figure 67 - SEM images of diamond coatings on steel substrates after HDPE moulding injection Sample FD1 (top), FD2 (middle) and FD3 (bottom)

Once again, it should be referred that a reduced number of molding cycles were carried out. Nevertheless this study has a relative importance since the suitability of the technique is being evaluated in laboratory conditions prior to full industrial assessment. Therefore, by comparing SEM images prior to injection (figure 64), with post-injection (figure 67), it can be stated that no degradation is observed.

5. Three-dimensional featured coated mold tools

In this sub-chapter, it will be presented work focusing the deposition of diamond coatings onto three-dimensional (3D) structured steel substrates using interlayer systems and its usage as a surface coating to thermoplastic injection molding functional systems.

The samples considered for the analysis were obtained by injection molding of high density polyethylene (HDPE) on an "Inautom EuroInj D65" injection molding machine, at the conditions presented in table 19, using an adapted mold plate, where 4 different 3D mold inserts were installed. The injection molding cycle was then repeated 500 times.

All molding inserts had 10 × 10 × 3 mm and a center cross in the surface, with ~0.5 mm deep, as it can be seen in the schematic drawings of figure 68 and the picture of figure 69. AISI P20 modified steel was used to produce the 3D molding inserts and each tool was prepared with different surface engineering treatments, as shown in table 22. Samples AD1, AD2 and AD3 were coated with a film of chromium nitride (CrN) ~2 µm thick.

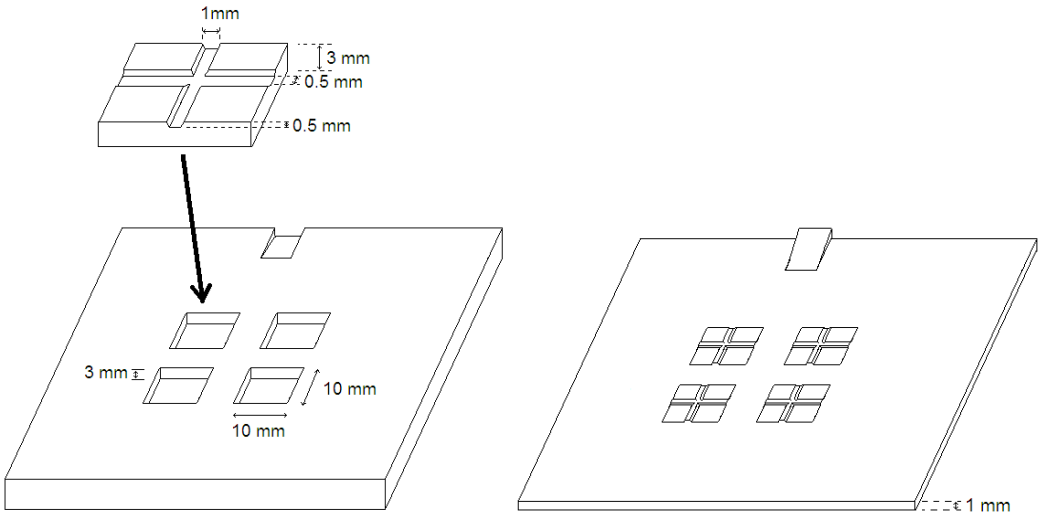

Figure 68 - Schematic drawings of the adapted mold tool (left) and the molded polimeric part (right)

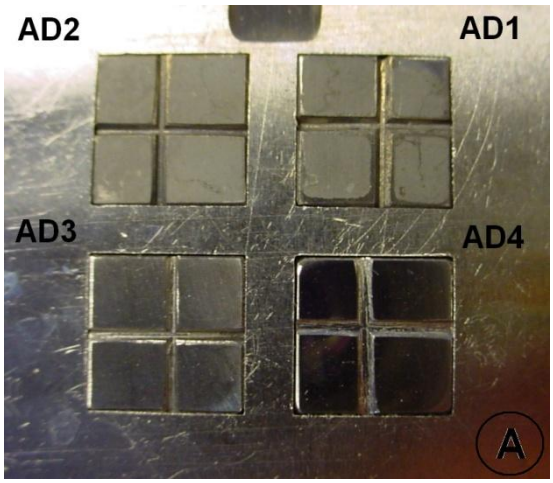

Figure 69 - Image of the 3D inserts on the mold tool

Table 22 - Description of the different insert mold tools

Insert	Description
AD1	~2 µm diamond film - ~2 µm CrN film - Steel system
AD2	~5 µm diamond film - ~2 µm CrN film - Steel system
AD3	~2 µm CrN film - Steel system
AD4	Bare steel

The pre-deposition and deposition process of samples AD1 and AD2 were simultaneous and identical to the process applied in samples AC1 and AC2, presented in chapter 5. Low magnification images of the diamond coated samples are presented in figure 70.

Figure 71 shows SEM images of three close-up views of the diamond film on the surface, on the valley and on the slope of each of the featured steel inserts. Samples AD1 and AD2 exhibit great morphological similarity, with respect to the diamond coatings. All the as-grown films exhibited diamond crystallite size of about 1 µm, mainly displaying (111) crystal orientation, nevertheless (100) oriented crystals were also observed.

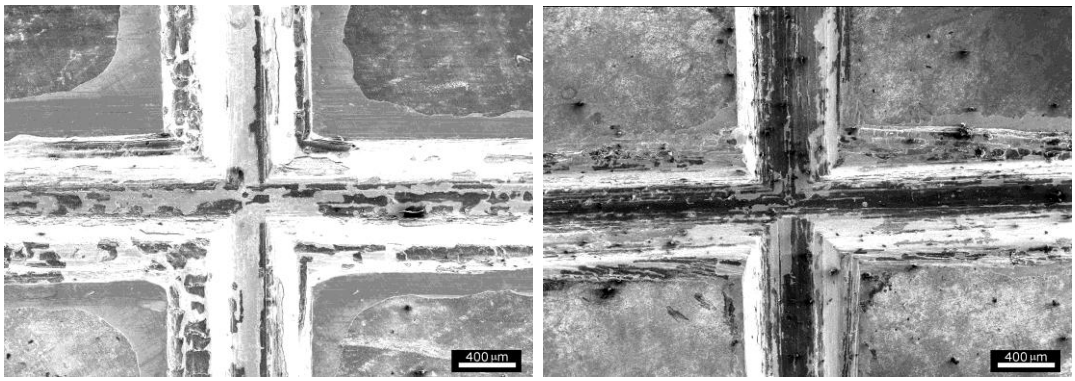

Figure 70 - SEM images of inserts AD1 (left) and AD2 (right) as diamond coated

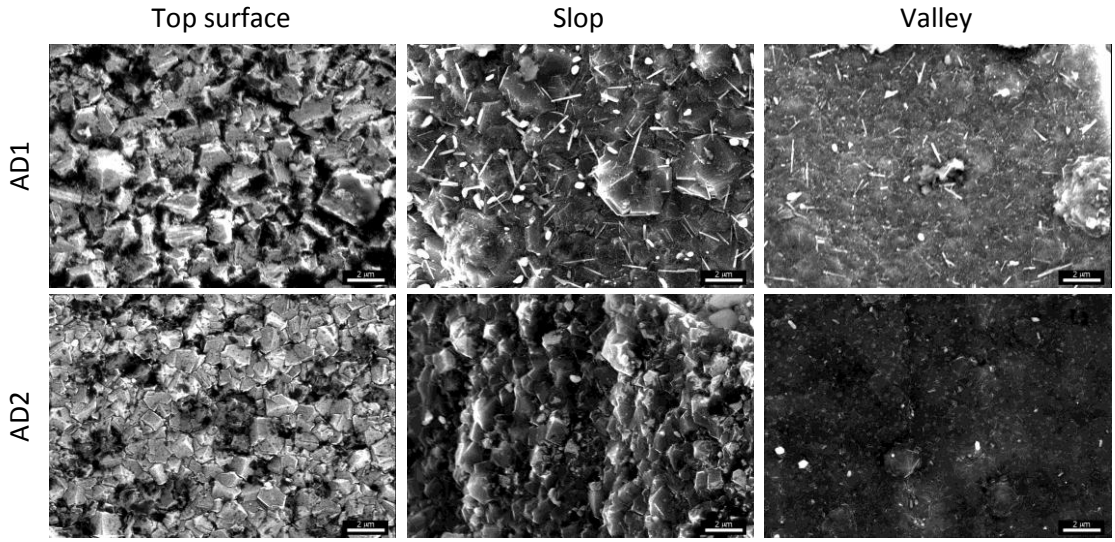

Figure 71 - SEM image of the different regions of the 3D features on inserts AD1 and AD2, as-deposited

The measured average roughnesses of these films, at the top surface, are 0.16 and 0.15 µm, for samples AD1 and AD2, respectively. Inserts AD3 and AD4 presented an average roughness of 0.10 and 0.11 µm, respectively.

The edges of the 3D cross are not fully covered with diamond, nor the slope and the valley of the feature. The irregular shape of the 3D cross does not allow a good seeding on it, inducing an heterogeneous coating. Nevertheless, most of the surface of the 3D feature is coated with diamond film. It can be observed that the diamond film crystal size decreases when going from the top surfaces of the samples, passing throw the slop, and getting to the valley, as it can be seen in figure 71.

Calculated quality factor values for the diamond coatings are 55.9 and 58.3%, and the calculated residual stress values are 6.2 and 7.4 GPa, for samples AD1 and AD2, respectively. These parameters were only measured from the top surface films.

After the preliminary evaluation of the two diamond coated inserts, the system was installed in a molding plate, together with two other inserts, one coated with commercial grade ~2 µm CrN (identical to the coating used as interlayer for the diamond growth) and one bare steel insert, as described in table 22 and shown in figure 69.

The inserts were then subjected to 500 injections of HDPE, at the conditions presented in table 19. Figure 72 presents the injected plate number 400.

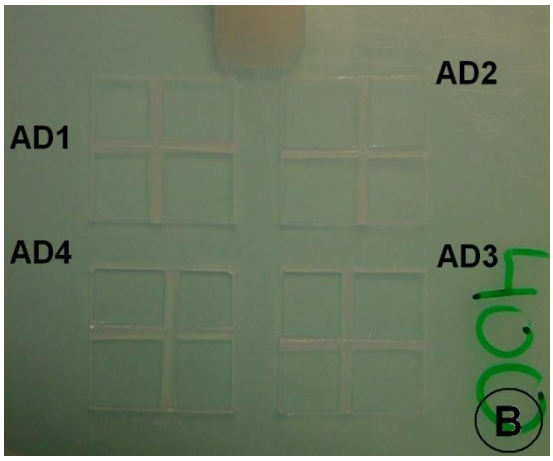

Figure 72 - Molded plastic plate on run 400

The dimensional stability of the molding insert and that of the polymeric object is of utmost importance, in order to guaranty the molded parts quality and to comply with customer requisites. In this investigation, the dimensional trend is only shown for the polymeric injected objects. Nevertheless, the dimensional stability of the molding insert and of the polymeric objects is directly related to one another.

A set of injected plates were analyzed for dimension degradation by a coordinate measuring machine and the results are presented in figure 73. Samples molded by inserts AD1 and AD2 show a degradation trend of − 0.0001 mm/injection, with a correlation coefficient of 0.9782 and 0.9287, respectively. Samples molded by inserts AD3 and AD4 show a degradation trend of − 0.0004 mm/injection, with a correlation coefficient of 0.9095 and 0.7936, respectively. It is assumed that this is due to polymer aggregation to the cavity.

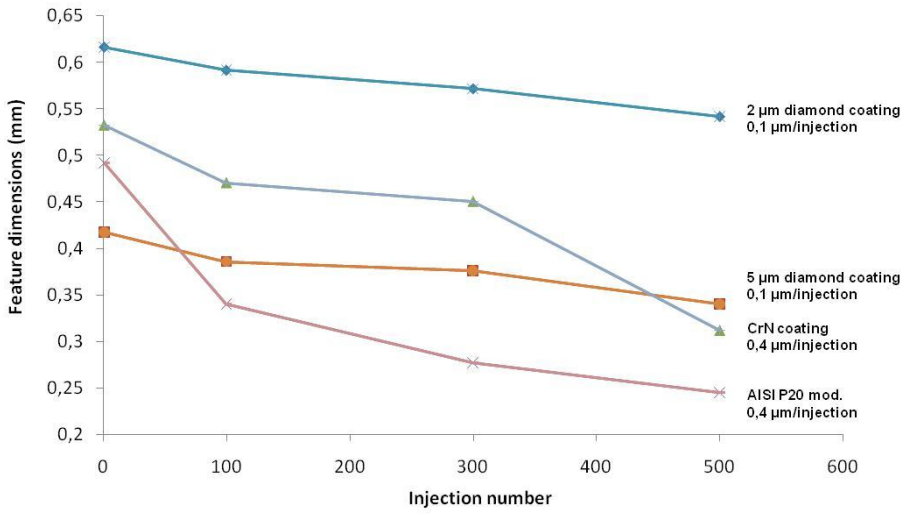

Figure 73 - Degradation of the feature height

The diamond coating was again observed by SEM, after the injection process. Figure 74 presents the SEM images of inserts AD1 and AD2 after 500 injections, and figure 75 shows SEM images of close-up views of the diamond film on the surface, on the valley and on the slope of each of the featured steel inserts, after injection molding. Apparently no morphological change occurred.

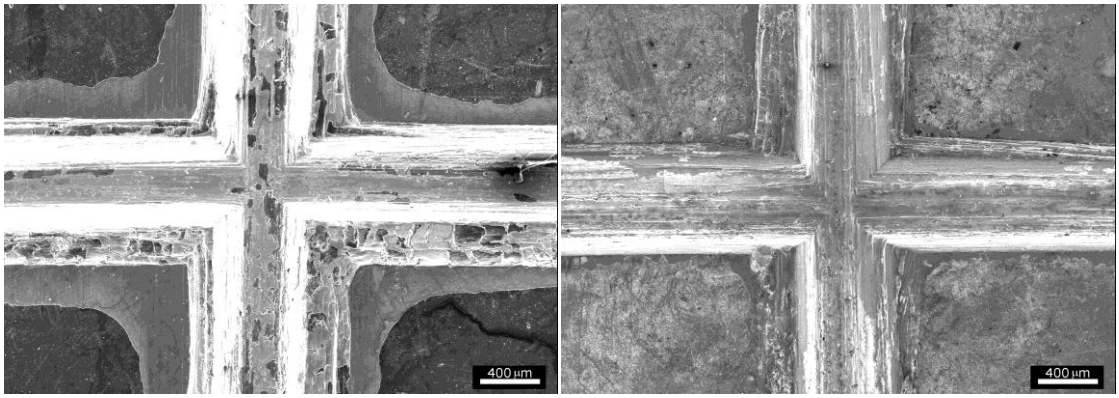

Figure 74 - SEM images of inserts AD1 (left) and AD2 (right) after 500 injection molding

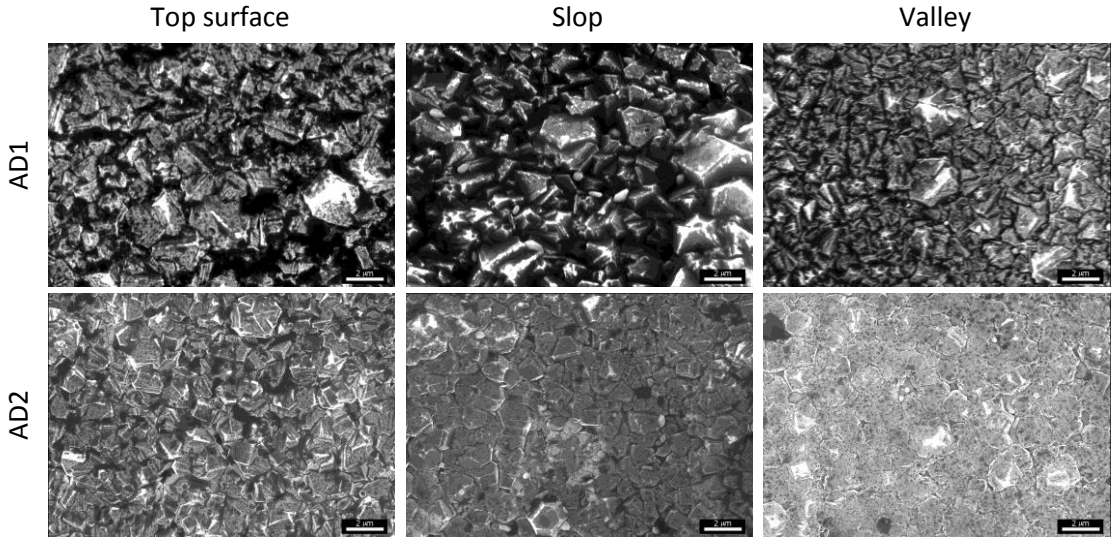

Figure 75 - SEM image of the different regions of the 3D features on inserts AD1 and AD2, after injection molding

6. Non-ferrous substrates materials coated mold tools

Hybrid molds or multi-material molds are currently used for injection molding prototyping or to enhance mold heat extraction effectiveness.

Nevertheless, as the demand for smaller devices continues to increase, current manufacturing processes will find it more challenging to meet cost, quantity, and dimensional requirements.

While microfabrication technology processes can create electronic devices in vast quantities with increasingly smaller dimensions, they are challenged to do so for mechanical devices at low cost and in large quantity. More traditional manufacturing processes such as machining or injection molding can more easily meet cost and quantity requirements, but are unable to currently match the dimensional challenges of microfabrication processes.

By merging microfabrication, namely applied to silicon technology, and traditional injection molding techniques, the benefits of both technologies can be combined to produce parts to meet all three requirements. [123-125]

The objective of the work here presented is to investigate the possibilities of injection molding polymer parts with silicon diamond coated inserts.

A set of silicon wafers, with the dimensions of 5 × 5 × 0.5 mm were used. Prior to the diamond deposition, silicon wafers were scratched with diamond powder (2–4 µm grain size) for approximately 2 minutes, in order to enhance the subsequent diamond nucleation density, and then cleaned for 5 minutes in an ultrasonic bath with isopropyl alcohol.

Diamond growth was conducted in a hot-filament CVD reactor, described in chapter 3, using time-modulated CVD. The deposition conditions employed are shown in table 18 and figure 63 and are the same as the conditions employed for the sub-microcrystallinity study, performed earlier as described in chapter 5.

The deposition conditions DEP1, DEP2 and DEP3 were used to produce samples SD1, SD2 and SD3, respectively, as shown in table 23. A bare silicon plate (sample S1) was also used in the adapted mold, to serve as a reference sample.

Table 23 - Description of the different insert mold tools

Insert	Description
SD1	Silicon plate diamond coated (DEP1)
SD2	Silicon plate diamond coated (DEP2)
SD3	Silicon plate diamond coated (DEP3)
S1	Bare silicon plate

After the deposition of diamond coatings on all samples, the morphology of the as grown films was characterized using scanning electron microscopy (SEM) and the intrinsic stress state and quality of the diamond coatings was characterized using Raman 514.5 nm Ar^+ ion laser spectroscopy.

Figure 76 shows microscopic images of the diamond coatings. All the as-grown films exhibited sub-micron diamond crystallite size, mainly displaying (111) crystal orientation, but (100) crystal orientation was also observed. The average diamond crystallite sizes of the deposited films are 0.62, 0.68 and 0.85 μm, for sample SD1, SD2 and SD3, respectively.

Figure 77 displays Raman spectra of the as-deposited samples. Raman spectroscopy was used to assess the diamond Raman quality and to estimate the residual stresses of the diamond film.

The quality factor of the diamond coatings was calculated to be 51.6, 66.2 and 67.1%, for samples SD1, SD2 and SD3, respectively. The calculated residual stress (σ) values for the diamond coatings are 0.6, 1.1 GPa, for samples SD1 and SD2, respectively. The longer deposition time sample, SD3, exhibited a residual stress of 0.6 GPa. As expected, diamond on the silicon plates presented higher quality and comparatively lower residual stress, once diamond linear thermal expansion coefficient is similar to the one presented by silicon [126].

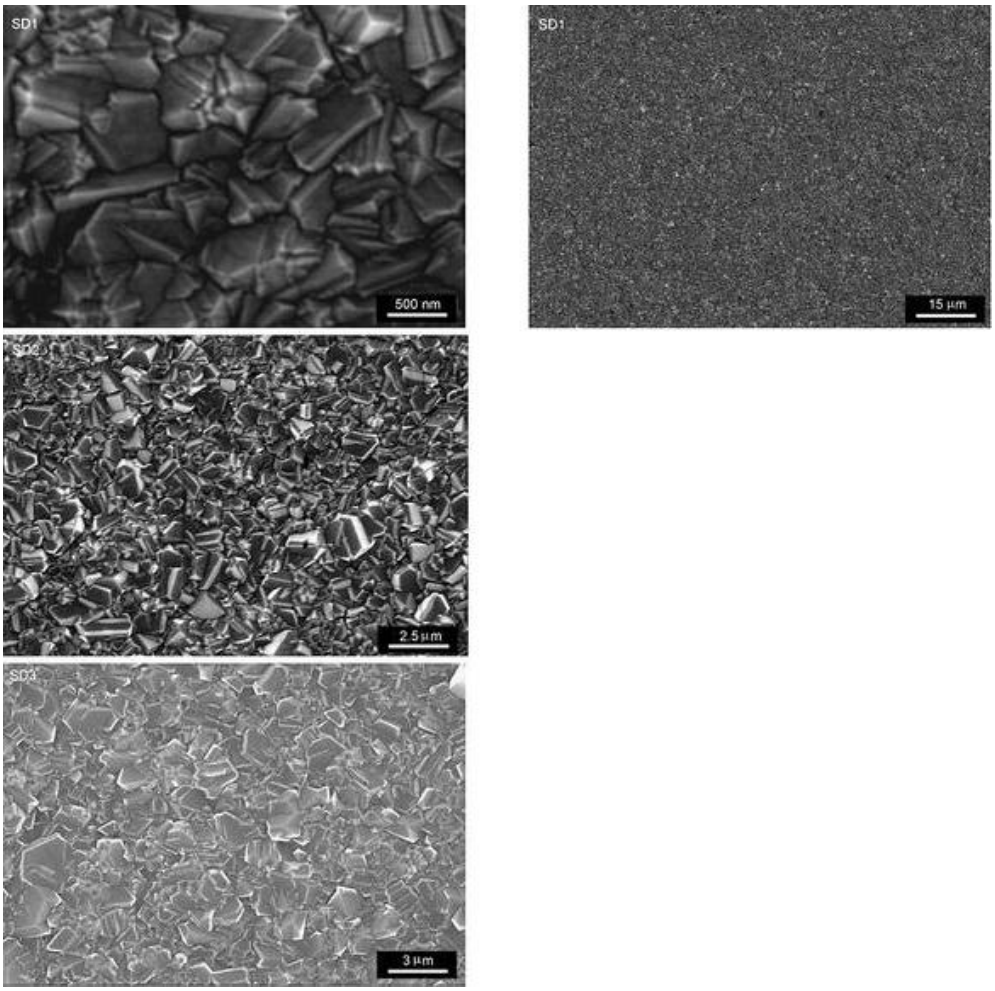

Figure 76 - SEM images of diamond coatings on silicon substrates
Sample SD1 (top), SD2 (middle) and SD3 (bottom)

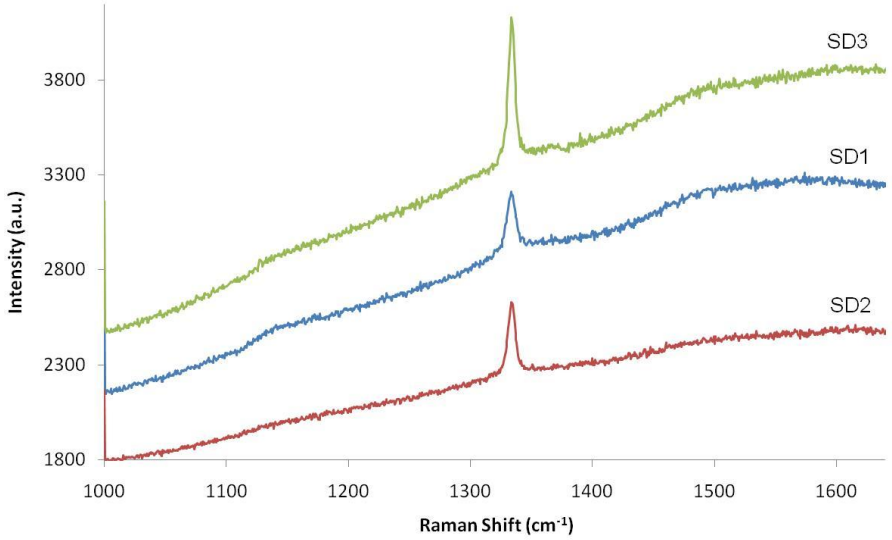

Figure 77 - Raman spectrum of the silicon-coated steel plates

The four inserts were tested for polymer injection molding, using a mold tool specially designed to accommodate the inserts and mounted in an injection molding machine to perform a cycle of 80 high-density polyethylene (HDPE) sample components at the conditions presented in table 19.

Figure 78 displays micrographs of the polymeric molded surface by the different inserts, in run number 1, 50 and 80. Apart from the first set of samples, that present marks of the demolding spray used in the beginning of the processing work, the injected parts is very identical. All samples presented a good finishing surface.

From the images presented in figure 78, it is evident that the molded objects with the diamond-coated inserts, present more homogeneous surfaces than the ones molded by the insert without coating. It should be noted that insert S1 has a mirror surface finish and that the diamond coated samples were abraded with diamond powder to enhance the diamond nucleation process.

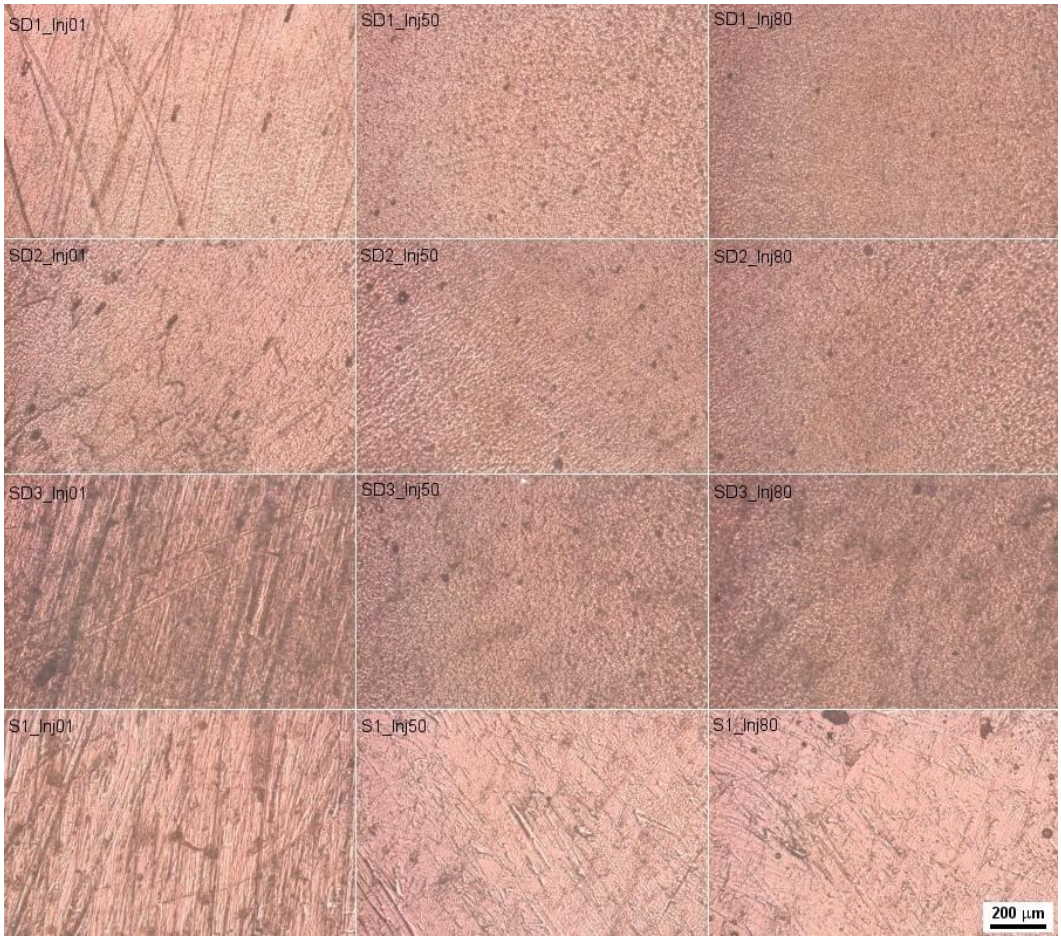

Figure 78 - Optical microscopic images of the HDPE-injected plate surface, by the different inserts, in run number 1, 50 and 80

Figure 79 presents SEM micrographs of diamond-coated silicon after the injection routine cycles were carried out.

Although in this work a reduced number of molding cycles were carried out, it is also important to assess the characteristics of the diamond films after the injection period. Therefore, by comparing SEM images prior to injection (figure 76), with post-injection (figure 79), it can be stated that no degradation is observed.

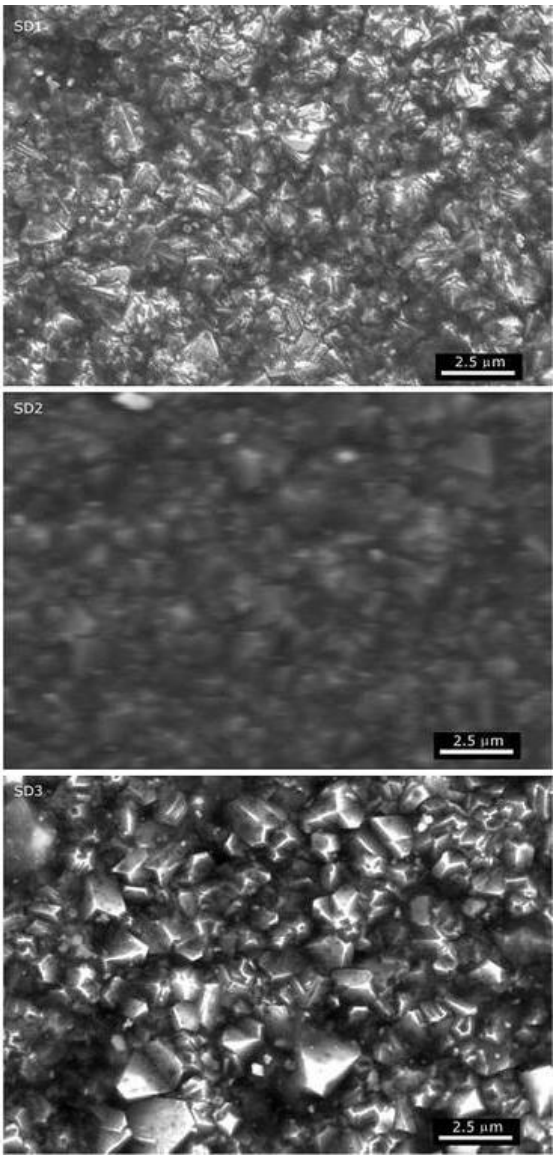

Figure 79 - SEM images of diamond coatings on silicon substrates after HDPE molding injection Sample SD1 (top), SD2 (middle) and SD3 (bottom)

Chapter 6

Conclusions and further work

1. Conclusions

Thermoplastic injection molding is a manufacturing technique that enables high production rates at low cost.

Portuguese mold makers detain a considerably good reputation worldwide and therefore are responsible for a significant percentage of the worlds mold production. Portugal is also one of the world's principal producers of precision molds for the plastic industry. Nevertheless, the Portuguese mold making industry, as the European, is coming under increasing economic pressure. To reverse the decline in the Small and Medium based EU tooling industry, processes that offer mold makers a competitive advantage over non-EU imports are required.

Microsystems-based products will be an important contributor to industrial and economic future. Moreover, plastic microinjection molding tools, with a high complexity and top pioneering and engineering solution requirements, can clearly be seen as an added value to industry and to increase competitiveness.

Despite the above mentioned, there are still some problems on the downstream to plastic microinjection molding tools that must be overcome. It is necessary to overcome technological problems such as wear rates due to high aspect ratios, complex geometries and aggressive polymer and additives, releasing problems due to static charges and complex featured requirements.

Chemical vapor deposited diamond films present a set of properties that point it as an ideal candidate to surface engineer molding tool. It detain an extreme mechanical hardness and wear resistance, one of the highest bulk modulus, the lowest compressibility, the highest room temperature thermal conductivity, a very low thermal expansion coefficient at room temperature and is very resistant to chemical corrosion.

The growth of diamond on carbide-forming materials usually leads to the production of adherent diamond coatings. Silicon is a widely used material for depositing diamond films using CVD processes. On the other hand, diamond grown directly on strong carbon-dissolving materials, such as steel, or on non-carbon affinity materials, yields poor adhesion. Also, iron is known to diffuse out from the bulk steel material towards the substrate surface during the growth process, promoting the growth of sp^2 carbon specimens, instead of diamond. Furthermore, the difference in the thermal expansion coefficients of diamond and steel is large, which results in the incorporation of residual stresses in the deposited diamond films and influences negatively the adhesion of the diamond coating.

A possible solution to overcome these problems is to use an interlayer that will block both inward carbon and outward Fe vapor diffusions, and provide a mutual good adhesion medium.

From the state-of-the-art review and the preliminary tests performed with the use of chromium nitride (CrN), titanium (Ti) and silicon (Si) as interlayer, physical vapor deposited chromium nitride (CrN) was selected as the interlayer material to coat diamond on steel substrates in this study.

A group of different steel substrates was also tested, namely stainless steels – austenitic chromium-nickel alloys AISI 304, 310 and 316, and the common steel used for mold tool production – AISI P20 modified. The best performer was AISI P20 modified. On AISI 304 steel with CrN interlayer, fully closed and homogeneous film was obtained for more than 6h00 of deposition. On AISI 310 and 316 steel samples not even the longer deposition conditions yielded good results. This performance of the stainless steels maybe due to the high contents of nickel, a strong carbon-dissolving material [29-34].

AISI P20 modified samples with a 9h00 deposited diamond film presented a Brinell hardness of 1540 HB and did not present delamination up to a load of 125 kgf. AISI 304 diamond coated samples presented a Brinell hardness of 173 HB and withstand a load of at least 20 kgf without any cracking or delamination of the diamond film.

In all the diamond coatings, Raman quality factor is above 50% and the coatings stress is lower than the predicted theoretical values.

Worth of mention is that diamond films were grown using a recently developed time-modulation chemical vapor deposition (TMCVD) process. TMCVD consists on the modulation of the CH_4 gas flow during the deposition time. The sort high pulses of CH_4 enriches the reactor atmosphere with methyl specimens, which at the nucleation stage enables a higher nucleation density and during the growth process it is believed to inhibit further growth of diamond crystallites and promote a new nucleation site on top of the growing crystals.

Finally, the usage and evaluation of polycrystalline diamond as surface engineering coatings on molding inserts for thermoplastic injection molding was performed.

Different coated systems were tested to reproduce high-density polyethylene (HDPE) components, namely microcrystalline and sub-microcrystalline diamond films, and three dimensional featured inserts.

Each coated system was tested for a number of injection cycles in order to evaluate the polymeric produced parts and also the degradation of the coated inserts. All coated samples presented good stability at least till 500 runs (the maximum that a single diamond coated insert was subjected to, under laboratory conditions).

The HDPE thermoplastic molded objects presented good quality and reproduced well the molding surface. Microcrystalline diamond coated inserts produced slightly tarnished plastic parts. The latter, seems to be considerably dimmed with the use of sub-microcrystalline films.

The three dimensional featured steel inserts presented a good performance and a reduced degradation trend comparatively to the non-coated surfaces.

By merging microfabrication, namely applied to silicon technology, and traditional injection molding techniques, the benefits of both technologies can be combined to produce parts to meet low cost, high quantity, and complex dimensional requirements. With this approach in mind, it was investigated the suitability of polymer injection molding with silicon diamond coated inserts.

Diamond on silicon is rather simpler than diamond on steel, so the diamond films coated on silicon substrates presented superior characteristics than the similar grown films on steel.

The HDPE molded objects, by the silicon diamond coated inserts, presented good quality and reproduced well the molding surface.

2. Further work proposals

The research work here undertaken has highlighted the need for further work. Therefore it is here considered the need for subjecting the diamond coatings to extensive run cycles in industrial environment and the evaluation of nanocrystalline diamond coatings performance.

Extensive run cycles in industrial environment

The maximum number of injection molding cycles carried out for each coated insert was 500. The latter, was considered to be representative of batch production [1] and therefore suitable for the type of analysis intended throughout this study. Nevertheless, extensive run cycles in industrial environment are desirable in order to establish the performance of the diamond coatings during service.

Nanocrystalline diamond coatings performance

The technology process of depositing nanocrystalline diamond films has achieved considerable advancement in the recent years [127]. Similarly to the work accomplished here for microcrystalline and sub-microcrystalline diamond films, it should be of interest to evaluate nanocrystalline films which may present some surface advantages over microcrystalline films, namely the surface roughness.

References

1. Rosato, D.V., D.V. Rosato, and M.G. Rosato, *Injection molding handbook*. 2000, Massachusetts, USA: Kluwer Academic Publishers.
2. Mossman, S., *Early plastics - Perspective 1850-1950*. 1997, London: Lencaster University Press and Science Museum.
3. Wikipedia. *Injection molding*. [cited; Available from: http://en.wikipedia.org/wiki/Injection_molding.
4. CEFAMOL, *Situação Actual da Indústria Portuguesa de Moldes*. 2006, CEFAMOL - Associação Nacional da Industria de Moldes: Marinha Grande.
5. USITC, *Tools, Dies, and Industrial Molds: Competitive Conditions in the United States and Selected Foreign Markets*. 2002, United States International Trade Commission: Washington.
6. AICEP. *Case Studies*. [cited; Available from: http://www.investinportugal.pt/.
7. CEFAMOL. *History - The Portuguese moulds Industry*. [cited; Available from: http://www.cefamol.pt.
8. Henriques, E., *Modelos de negócio nos moldes*, in *Inovar-te – a revista de inovação*. 2007.
9. Menezes, J., in *Diário de Noticias*. 2004.
10. Dimov, S.S., *Multi-Material Micro Manufacture (4M): Challenges and Opportunities*, in *Micromanufacturing*. 2008. p. 12-15.
11. Manser, P., *An Overview of Micro Moulding*, in *Micromanufacturing*. 2008. p. 14-19.
12. Whynott, J., *Micro Moulding: A cost Effective Alternative to Micro Machining*, in *Micromanufacturing*. 2008. p. 18-22.
13. Martins, G., *Apostilas Técnicas – Tecnologia Básica de Construção e Projecto de Moldes para Injeção de plásticos*. 2007, Brasil: Instituto Avançado do Plástico.
14. Gibbons, G.J. and R.G. Hansell, *Thermal-sprayed coatings on aluminium for mould tool protection and upgrade.* Journal of Materials Processing Technology, 2007: p. in press.
15. Lee, S.T., Z. Lin, and X. Jiang, *CVD diamond films: nucleation and growth.* Materials Science and Engineering: R: Reports, 1999. **25**(4): p. 123-154.
16. William D. Callister, J. and D.G. Rethwisch, *Fundamentals of Material Science and Engineering - An integrated Approach*. 3rd. ed. 2008, Asia: Wiley.
17. *Diamond At Work*. [cited; Available from: http://www.diamondatwork.com.
18. *Element Six*. [cited; Available from: http://www.e6.com.
19. Spears, K.E. and J.P. Dismukes, eds. *Synthetic diamond: emerging CVD science and technology*. The Electrochemical Society. 1994, Wiley Inter-Science: New York. 688.
20. Haubner, R. and B. Lux, *Diamond growth by hot-filament chemical vapor deposition: state of the art.* Diamond and Related Materials, 1993. **2**(9): p. 1277-1294.
21. Kittel, C. and H. Kroemer, *Thermal Physics*. 1980: W. H. Freeman and Company.
22. Reif, F., *Fundamentals of Statistical and Thermal Physics*. Physics Series. 1985: McGraw-Hill International Editions.
23. Markov, I.V., *Crystal Growth for Beginners – Fundamentals of Nucleation, Crystal Growth and Epitaxy*. 1995: World Scientific.
24. *MatWeb - Online Materials Information Resource*. [cited 2008 26 May 2008]; Available from: MatWeb.
25. May, P.W., *Diamond thin films: a 21st-century material.* hilosophical Transactions of the Royal Society A, 2000. **358**: p. 473.
26. Gruen, D.M. and I. Buckley-Golder, eds. *Diamond Films: Recent Developments* MRS Bulletin, ed. MRS. Vol. 23. 1998, MRS.

27. Field, J.E., *The properties of diamond*. Academic Press ed. 1979.
28. Field, J.E., *The properties of natural and synthetic diamond*. Academic Press ed. 1992.
29. Nesladek, M., et al., *Improved adhesion of CVD diamond films to steel and WC---Co substrates.* Diamond and Related Materials, 1994. **3**(1-2): p. 98-104.
30. Ong, T.P. and R.P.H. Chang, *Properties of diamond composite films grown on iron surfaces.* Applied Physics Letters, 1991. **58**(4): p. 358-360.
31. Weiser, P.S., et al., *Carbon diffusion in uncoated and titanium nitride coated iron substrates during microwave plasma assisted chemical vapor deposition of diamond.* Journal of Applied Physics, 1992. **72**(10): p. 4643-4647.
32. Ashfold, M.N.R., et al., *Thin film diamond by chemical vapour deposition methods.* Chemical Society Reviews, 1994. **23**(1): p. 21-30.
33. Hartsell, M.L. and L.S. Plano, *Growth of diamond films on copper.* Journal of Material Research, 1994. **9**: p. 921.
34. Fan, Q.H., A. Fernandes, and J. Gracio, *Diamond coating on steel with a titanium interlayer.* Diamond and Related Materials, 1998. **7**(2-5): p. 603-606.
35. Haubner, R. and B. Lux, *Diamond deposition on steel substrates using intermediate layers.* International Journal of Refractory Metals and Hard Materials, 2006. **24**(5): p. 380-386.
36. Ralchenko, V.G., et al., *Diamond deposition on steel with CVD tungsten intermediate layer.* Diamond and Related Materials, 1995. **4**(5-6): p. 754-758.
37. Fan, Q.H., J. Grácio, and E. Pereira, *Preparation of freestanding diamond films by a two-step-growth method.* Journal of Material Research, 1998. **13**(10): p. 2787.
38. Chen, H., et al., *Growth of diamond films on stainless steel.* Thin Solid Films, 1992. **212**(1-2): p. 169-172.
39. Fenker, M., et al., *Deposition of CVD diamond onto ion beam modified ASP 23 cutting tools.* Surface and Coatings Technology, 1998. **98**(1-3): p. 1053-1059.
40. Buijnsters, J.G., et al., *The applicability of ultra thin silicon films as interlayers for CVD diamond deposition on steels.* physica status solidi (a), 2003. **195**(2): p. 383-395.
41. Klages, C.P., et al., *Diamond coatings and cBN coatings for tools.* International Journal of Refractory Metals and Hard Materials, 1998. **16**(3): p. 171-176.
42. Schäfer, L., et al., *Chemical vapour deposition of polycrystalline diamond films on high-speed steel.* Surface and Coatings Technology, 1999. **116-119**: p. 447-451.
43. Fan, Q.H., *Diamond Growth on Metals*, in *Department of Physics*. 1999, University of Aveiro: Aveiro.
44. Fan, Q.H., et al., *Adhesion of diamond coatings on steel and copper with a titanium interlayer.* Diamond and Related Materials, 1999. **8**(8-9): p. 1549-1554.
45. Weiser, P.S. and S. Prawer, *Chemical vapour deposition of diamond onto iron based substrates--The use of barrier layers.* Diamond and Related Materials, 1995. **4**(5-6): p. 710-713.
46. Lorenz, H.P., *Investigation of TiN as an interlayer for diamond deposition on steel.* Diamond and Related Materials, 1995. **4**(8): p. 1088-1092.
47. Silva, F.J.G., et al., *Microwave plasma chemical vapour deposition diamond nucleation on ferrous substrates with Ti and Cr interlayers.* Diamond and Related Materials, 2002. **11**(9): p. 1617-1622.
48. Polini, R., et al., *Effects of Ti- and Zr-based interlayer coatings on the hot filament chemical vapour deposition of diamond on high speed steel.* Thin Solid Films, 2006. **494**(1-2): p. 116-122.
49. Lin, C.R. and C.T. Kuo, *High adhesion and quality diamond films on steel substrate.* Diamond and Related Materials, 1998. **7**(6): p. 903-907.
50. Sikder, A.K., et al., *Chemical vapour deposition of diamond on stainless steel: the effect of Ni-diamond composite coated buffer layer.* Diamond and Related Materials, 1998. **7**(7): p. 1010-1013.
51. Shang, N.G., et al., *Effect of ion beam nitriding on diamond nucleation and growth onto steel substrates.* Diamond and Related Materials, 2001. **10**(8): p. 1506-1510.
52. Borges, C.F.M., E. Pfender, and J. Heberlein, *Influence of nitrided and carbonitrided interlayers on enhanced nucleation of diamond on stainless steel 304.* Diamond and Related Materials, 2001. **10**(11): p. 1983-1990.
53. Bareiβ, C., et al., *Diamond coating of steel at high temperatures in hot filament chemical vapour deposition (HFCVD) employing chromium interlayers.* Diamond and Related Materials, 2006. **15**(4-8): p. 754-760.
54. Schwarz, S., et al., *High temperature diffusion chromizing as a successful method for CVD-diamond coating of steel.* Diamond and Related Materials, 2002. **11**(3-6): p. 757-762.

55. Schwarz, S., et al., *High temperature diffusion chromizing as a successful method for CVD-diamond coating of steel--Part II.* Diamond and Related Materials, 2003. **12**(3-7): p. 701-706.
56. Fayer, A., O. Glozman, and A. Hoffman, *Deposition of continuous and well adhering diamond films on steel.* Applied Physics Letters, 1995. **67**(16): p. 2299-2301.
57. Glozman, O., et al., *Influence of Cr---N interlayer properties on the initial stages of CVD diamond growth on steel substrates.* Diamond and Related Materials, 1998. **7**(2-5): p. 597-602.
58. Glozman, O., et al., *Study of the wear behavior and adhesion of diamond films deposited on steel substrates by use of a Cr-N interlayer.* Diamond and Related Materials, 1999. **8**(2-5): p. 859-864.
59. Glozman, O. and A. Hoffman, *Adhesion improvement of diamond films on steel subtrates using chromium nitride interlayers.* Diamond and Related Materials, 1997. **6**(5-7): p. 796-801.
60. Avigal, Y., et al., *[100]-Textured diamond films for tribological applications.* Diamond and Related Materials, 1997. **6**(2-4): p. 381-385.
61. Buijnsters, J.G., et al., *CVD diamond deposition on steel using arc-plated chromium nitride interlayers.* Diamond and Related Materials, 2002. **11**(3-6): p. 536-544.
62. Buijnsters, J.G., et al., *The adhesion of hot-filament CVD diamond films on AISI type 316 austenitic stainless steel.* Diamond and Related Materials, 2004. **13**(4-8): p. 848-857.
63. Silva, F.J.G., et al., *A new interlayer approach for CVD diamond coating of steel substrates.* Diamond and Related Materials, 2004. **13**(4-8): p. 828-833.
64. Silva, F.J.G., et al., *Tribological behaviour of CVD diamond films on steel substrates.* Wear, 2003. **255**(7-12): p. 846-853.
65. Silva, F.J.G., et al., *Unstressed PACVD diamond films on steel pre-coated with a composite multilayer.* Surface and Coatings Technology, 2005. **191**(1): p. 102-107.
66. Kreines, L., et al., *Fretting wear of thin diamond films deposited on steel substrates.* Diamond and Related Materials, 2004. **13**(9): p. 1731-1739.
67. Gowri, M., et al., *Direct deposition of diamond films on steel using a three-step process.* Diamond and Related Materials, 2006. **15**(4-8): p. 498-501.
68. RAMADA. [cited; Available from: http://www.ramada.pt/.
69. Ramada, *Aços Especiais*. 2008, F. Ramada, Aços e Indústrias, S.A.
70. Cerqueira, M.F., et al., *Macrocrystalline silicon thin films prepared by RF reactive magnetron sputter deposition.* Vacuum, 1995. **46**(12): p. 1385-1390.
71. GALOL. [cited; Available from: http://www.galol.com/.
72. PRIREV. [cited; Available from: http://www.prirev.com.
73. Avigal, Y. and A. Hoffman, *A new method for nucleation enhancement of diamond.* Diamond and Related Materials, 1999. **8**(2-5): p. 127-131.
74. Rotter, S.S., *Applications of Conformal CVD Diamond Films.* Israel Journal of Chemistry, 1998.
75. Sumant, A.V., et al., *Surface composition, bonding, and morphology in the nucleation and growth of ultra-thin, high quality nanocrystalline diamond films.* Diamond and Related Materials, 2007. **16**(4-7): p. 718-724.
76. Mehta Menon, P., et al., *Filament metal contamination and Raman spectra of hot filament chemical vapor deposited diamond films.* Diamond and Related Materials, 1999. **8**(1): p. 101-109.
77. Tsutsumoto, T., *Improvement of Ta filament for diamond CVD.* Thin Solid Films, 1998. **317**(1-2): p. 371-375.
78. Ali, N., et al., *Deposition of polycrystalline diamond films using conventional and time-modulated CVD processes.* Thin Solid Films, 2002. **420-421**: p. 155-160.
79. Ali, N., et al., *Role of substrate temperature during diamond film growth using the newly developed time-modulated chemical vapor deposition process.* Journal of Materials Science Letters, 2003. **22**(14): p. 1039-1042.
80. Ali, N., V.F. Neto, and J. Grácio, *Promoting secondary nucleation using methane modulations during diamond chemical vapor deposition to produce smoother, harder, and better quality films.* Journal of Materials Research, 2003. **18**(2): p. 296-304.
81. Ali, N., et al., *Optimisation of the new time-modulated CVD process using the Taguchi method.* Thin Solid Films, 2004. **469-470**: p. 154-160.
82. Fan, Q.H., et al., *Novel time-modulated chemical vapor deposition process for growing diamond films.* Journal of Materials Research, 2002. **17**(7).
83. Neto, V.F.S., *Investigation on the film properties of advanced diamond coatings deposited using time-modulated CVD*, in *Department of Physics and Department of Mechanical Engineering*. 2004, University of Aveiro: Aveiro. p. 112.
84. Cahn, R.W., *Concise encyclopedia of materials characterization*. 1993: Pergamon Press.

85. Watt, I.M., *The principles and practice of electron microscopy*. 1997: Cambridge University Press.
86. Wilson, M.J., *Clay Mineralogy: Spectroscopic and Chemical Determinative Methods*. 1995: Chapman & Hall.
87. Rubbi, C.P., *Light Microscopy*. 1994, Chichester: John Wiley.
88. Nikon, *Nikon Eclipse LV150 microscope user manual.*
89. Ferraro, J.R., *Introductory Raman spectroscopy*. 1994: Academic Press.
90. Schrader, B., *Infrared and Raman spectroscopy : methods and applications*. 1995: VCH.
91. Gupta, S., et al., *Ultraviolet and visible Raman spectroscopic investigations of nanocrystalline carbon thin films grown by bias-assisted hot-filament chemical vapor deposition.* Journal of Raman Spectroscopy, 2003. **34**(3): p. 192-198.
92. Ferrari, A.C. and J. Robertson, *Raman spectroscopy of amorphous, nanostructured, diamond-like carbon, and nanodiamond.* Philosophical Transactions of the Royal Society A: Mathematical, Physical and Engineering Sciences, 2004. **362**(1824): p. 2477-2512.
93. Pereira, L., *Propriedades optoelectrónicas de diamante crescido a partir da fase gasosa*, in *Department of Physics*. 2000, University of Aveiro: Aveiro.
94. Das, D., et al., *Low surface temperature synthesis and characterization of diamond thin films.* Diamond and Related Materials, 2006. **15**(9): p. 1336-1349.
95. Ager, J.W. and M.D. Drory, *Quantitative measurement of residual biaxial stress by Raman spectroscopy in diamond grown on a Ti alloy by chemical vapor deposition.* Physical Review B, 1993. **48**(4): p. 2601.
96. Jackman, R.B., J. Beckman, and J.S. Foord, *The growth of nucleation layers for high-quality diamond CVD from an r.f. plasma.* Diamond and Related Materials, 1995. **4**(5-6): p. 735-739.
97. Popov, C., S. Bliznakov, and W. Kulisch, *Influence of the substrate nature on the properties of nanocrystalline diamond films.* Diamond and Related Materials, 2007. **16**(4-7): p. 740-743.
98. Kulisch, W., L. Ackermann, and B. Sobisch, *On the Mechanisms of Bias Enhanced Nucleation of Diamond.* Physica Status Solidi (a), 1996. **154**(1): p. 155-174.
99. Silva, F., et al., *Control of an MPACVD reactor for polycrystalline textured diamond films synthesis: role of microwave power density.* Diamond and Related Materials, 1996. **5**(3-5): p. 338-344.
100. Shroder, R.E., R.J. Nemanich, and J.T. Glass, *Analysis of the composite structures in diamond thin films by Raman spectroscopy.* Physical Review B, 1990. **41**(6): p. 3738.
101. Rats, D., et al., *Crystalline quality and residual stresses in diamond layers by Raman and x-ray diffraction analyses.* Journal of Applied Physics, 1995. **78**(8): p. 4994-5001.
102. Fayette, L., et al., *Local order in CVD diamond films : Comparative Raman, x-ray-diffraction, and x-ray-absorption near-edge studies.* Physical Review B, 1998. **57**(22): p. 14123.
103. Hammond, C., *The basics of crystallography and diffraction*. 2nd ed. 2001, Oxford: Oxford University Press.
104. *X'Pert HighScore*. 2007, PANalytical.
105. *TOF-SIMS- Introduction, Basic Principles, Application Presentation*. [cited 2008-07-17]; Available from: http://www.eaglabs.com.
106. Davim, J.P. and J.J. Grácio, *Tecnologias dos Materiais Metálicos*. 1999: Universidade Aberta.
107. *Frank hardness tester Frankoskop 38180 Manual*, Frank.
108. *Metals Handbook*. Formerly Ninth Edition ed. ASM Handbook. Vol. 8. 1985.
109. Ashfold, M.N.R., et al., *Thin film diamond by chemical vapour deposition methods.* Chemical Society Reviews, 1994: p. 21-30.
110. Cabral, E.G.S.d.S., *Development and application of diamond coatings onto cutting tools to machine EDM electrodes for mould industry*, in *Department of Mechanical Engineering*. 2006, Univeristy of Aveiro: Aveiro.
111. Li, Y.S., et al., *Effect of various alloying elements on diamond growth on Fe-Cr steels.* Thin Solid Films, 2008. **516**(10): p. 3089-3093.
112. Michler, J. and E. Blank, *Analysis of coating fracture and substrate plasticity induced by spherical indentors: diamond and diamond-like carbon layers on steel substrates.* Thin Solid Films, 2001. **381**(1): p. 119-134.
113. Nesládek, M., et al., *Adhesion of diamond coatings on cemented carbides.* Thin Solid Films, 1995. **270**(1-2): p. 184-188.
114. Vaz, R.M.A., *Growing and Characterisation of Diamond Coatings on Steel Substrates*, in *Department of Mechanical Engineering*. 2008, Univeristy of Aveiro: Aveiro.
115. Xie, Z.H., et al., *Contact damage evolution in a diamond-like carbon (DLC) coating on a stainless steel substrate.* Thin Solid Films, 2007. **515**(6): p. 3196-3201.

116. Ali, N., et al., *Characterization of diamond adhesion on micro-grain WC-Co substrates using Brinell indentations and micro-Raman spectroscopy.* Journal of Physics: Condensed Matter, 2004. **16**: p. 6661-6674.
117. Novikov, N.V. and S.N. Dub, *Hardness and fracture toughness of CVD diamond film.* Diamond and Related Materials, 1996. **5**(9): p. 1026-1030.
118. Fan, Q.H., et al., *Quantitative evaluation of adhesion of diamond coatings.* Journal of Materials Research 1999. **14**(3): p. 1142-1147
119. Takeuchi, S., S. Oda, and M. Murakawa, *Synthesis of multilayer diamond film and evaluation of its mechanical properties.* Thin Solid Films, 2001. **398-399**: p. 238-243.
120. Crank, J., *The mathematics of diffusion*. 2nd ed. 1979, Oxford: Clarendon Press.
121. Haubner, R. and B. Lux, *Deposition of ballas diamond and nano-crystalline diamond.* International Journal of Refractory Metals and Hard Materials, 2002. **20**(2): p. 93-100.
122. Bareiβ, J.C., et al., *CVD diamond coating of steel on a CVD-TiBN interlayer.* Surface and Coatings Technology, 2006. **201**(3-4): p. 718-723.
123. Gourgon, C., et al., *Uniformity across 200 mm silicon wafers printed by nanoimprint lithography.* Journal of Physics D: Applied Physics, 2005(1): p. 70.
124. Guo, L.J., *Nanoimprint Lithography: Methods and Material Requirements.* Advanced Materials, 2007. **19**(4): p. 495-513.
125. Lohner, K.A., et al. *Microfabricated silicon carbide microengine structures*. in *Materials Research Society Symposium*. 1998.
126. Xu, C.H., et al., *Theory of the thermal expansion of Si and diamond.* Physical Review B, 1991. **43**(6): p. 5024.
127. Marina, B. and V. Alexander, *New prospects and frontiers of nanodiamond clusters.* Journal of Physics D: Applied Physics, 2007(20): p. 6300.